Catalysis Reviews
Publication details, including instructions for authors and subscription information:
http://www.tandfonline.com/loi/lctr20

Electrocatalytic Activity and Stability of Pt clusters on State-of-the-Art Supports: A Review

Sujan Shrestha [a], Ying Liu [a] & William E. Mustain [a]
[a] Department of Chemical, Materials and Biomolecular Engineering, University of Connecticut, Storrs, CT, USA

Available online: 10 Aug 2011

To cite this article: Sujan Shrestha, Ying Liu & William E. Mustain (2011): Electrocatalytic Activity and Stability of Pt clusters on State-of-the-Art Supports: A Review, Catalysis Reviews, 53:3, 256-336

To link to this article: http://dx.doi.org/10.1080/01614940.2011.596430

Catalysis Reviews: Science and Engineering, 53:256–336, 2011

ISSN: 0161-4940 print / 1520-5703 online
DOI: 10.1080/01614940.2011.596430

Taylor & Francis
Taylor & Francis Group

Electrocatalytic Activity and Stability of Pt clusters on State-of-the-Art Supports: A Review

Sujan Shrestha, Ying Liu, and William E. Mustain

Department of Chemical, Materials and Biomolecular Engineering, University of Connecticut, Storrs, CT, USA

Instability of supported Pt clusters due to limited bonding with conventional carbon supports and carbon dissolution leads to significant cathode performance losses with time, impeding the development of commercial proton exchange membrane fuel cells. One approach that has recently been gaining momentum is the use of the electrocatalyst support to enhance both the stability and activity of Pt clusters for the oxygen reduction reaction. This review article focuses on four support types: advanced carbons, conductive ceramics, metallic underlayers for Pt monolayer catalysts, and the 3M crystalline organic whiskers. Advantages and disadvantages of each support are summarized and promising future directions for research in this area are discussed.

Keywords Oxygen reduction, Catalyst, Support, Fuel cell, Platinum

1. INTRODUCTION

Electrochemical energy conversion devices, fuel cells, have received considerable attention over the past few decades because of their potential to provide high efficiency power since electrochemical processes are not limited by traditional Carnot or Rankine heat cycles. Though several high temperature ($T > 650$ °C) and low temperature (25 °C $< T <$ 200 °C) variants exist (1), perhaps the most widely investigated fuel cell over the past two decades is the proton exchange membrane fuel cell (PEMFC). PEMFCs offer several advantages over these other cell architectures including: (1) a compact, high energy

Received March 20, 2011; accepted May 24, 2011.

Address correspondence to William E. Mustain, Department of Chemical, Materials, and Biomolecular Engineering, University of Connecticut, Storrs, CT 06269, USA. E-mail: mustain@engr.uconn.edu

density design that is facilitated by its solid polymer electrolyte and thin electrodes, (2) low complexity sealing, assembly and handling, (3) straightforward thermal management, (4) fast startup times, (5) microstructural control that allows for high reactant and product mobility in the active layers, (6) relative tolerance to common ambient impurities, and (7) high electrolyte conductivity at low temperature (60–80 °C). On the other hand, the low operating temperature of the PEMFC places a premium on developing sophisticated water management schemes (2–8) and has forced both researchers and manufacturers to rely on expensive Pt-based electrocatalysts for both the hydrogen oxidation reaction (HOR) and oxygen reduction reaction (ORR) (9, 10).

1.1. Operating Principles of the PEMFC

In the PEMFC (Fig. 1), high purity hydrogen is fed to a typically serpentine-structured flowfield that distributes the fuel across the cell. The hydrogen diffuses through a porous carbon layer, which allows it to be distributed evenly over the anode electrode where it is oxidized to protons and electrons (Eq. (1)):

$$H_2 \rightarrow 2H^+ + 2e^-, E^\circ = 0.0\ V \tag{1}$$

The most common, and highly efficient, anode electrocatalyst for the HOR is nanometer-sized clusters of platinum dispersed on high surface area carbon

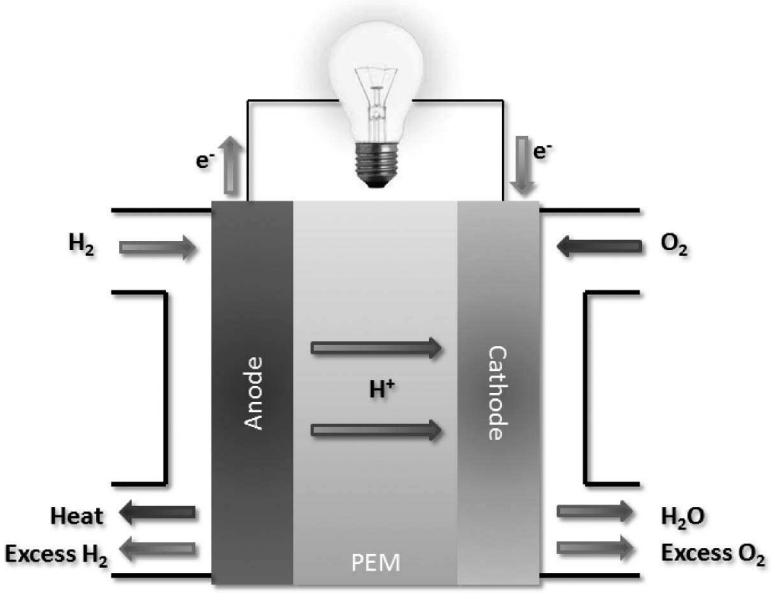

Figure 1: Operational schematic for the PEMFC.

(Pt/C). The resulting electrons travel through an external circuit (i.e., the device being powered), while the protons travel through a cation-conducting polymer electrolyte. The most common electrolyte for the PEMFC is Nafion®, which is manufactured by DuPont. The protons and electrons meet at the cathode where they reduce molecular oxygen (Eq. (2)):

$$O_2 + 4H^+ + 4e^- \rightarrow H_2O,\ E^\circ = 1.23\ V \tag{2}$$

Taking the electron equivalence for each reaction into account, the HOR and ORR allow for the non-combustive redox reaction of two hydrogen molecules and one oxygen molecule, yielding two water molecules (Eq. (3)):

$$2H_2 + O_2 \rightarrow 2H_2O \tag{3}$$

The ORR is the performance limiting reaction in state-of-the art PEMFCs (9). Nanometer Pt_3M (M = Co, Fe, Ni, Pd, etc.) alloy clusters supported on acetylene carbon blacks represent the state-of-the-art electrocatalyst for the ORR in PEMFCs.

Carbon blacks are the most widely used supports in PEMFCs due to their: (i) tolerance to strongly acidic media; (ii) high electronic conductivity; (iii) low cost; (iv) high surface area; and (v) complex microporous structure. These properties allow for efficient mobility of electrons, rapid mass transport of products and reactants within PEMFC electrodes, high specific surface area and fine dispersion of the catalyst in both the anode and cathode active layers.

Unfortunately, conventional Pt/C and Pt_3M/C ORR catalysts are plagued by rapid performance loss with time through several mechanisms that will be detailed in the Sections 1.2–1.4. These degradation mechanisms have combined to significantly hinder the widespread implementation and commercialization of PEMFCs, which are expected to play a critical role in the global 21st century energy portfolio (11). This review article will shed light on the reaction mechanisms that can be either mitigated or eliminated by rethinking the purpose and design of the electrocatalyst support and to highlight current research efforts in this area.

1.2. Role of Catalyst Electronic Structure in ORR Activity

For decades, it has been known that the activity of ORR electrocatalysts is strongly dependent on electronic structure of the surface. Even as early as 1970, Appleby correlated experimental data for the ORR collected on several noble metal electrodes (Pt, Pd, Ir, Os, Au, Rh, etc.) in orthophosphoric acid at 25 °C to the electronic work function of the metal, % d-character, d-band vacancy, and the adsorption enthalpy of molecular oxygen (12). It was found that these transition metal catalysts exhibited a volcano-type behavior for the

ORR as a function of both the d-band vacancy and O_2 adsorption enthalpy, with Pt exhibiting an activity near the projected peak.

Modification of Pt activity for the ORR by alloying was first reported by Jalan and Taylor in 1983 using Pt-Fe electrodes in phosphoric acid (13). A few years later, similar results were reported by Glass et al. (14) and Gottesfeld (15) using PtCr electrodes in phosphoric and sulfuric acid, respectively. In 1990, Beard and Ross reported new PtCo, PtMo, and PtMn electrocatalysts for the ORR and it was found that PtCo was the top performing electrocatalyst (16). Next, Mukerjee and Srinivasan reported several Pt alloys with enhanced electrocatalytic activity in a laboratory scale PEMFC (17). During this time, the prevailing view was that Pt-alloys led to a contraction in the Pt crystal lattice. This contraction was believed to bring the Pt-Pt interatomic distance closer to the length of the O=O bond, leading to preferred adsorption modes and improving the electron transfer. This view was later transformed by seminal papers by Toda et al. (18), and Mukerjee et al. (19), who showed the root cause for the enhancement in the ORR on Pt alloys was a modified electronic structure of Pt surface atoms compared with pure Pt, which validated the hypothesis put forward, but never quite proven by Appleby. This finding ignited a firestorm of experimental investigations into Pt (12, 17, 20–24) and Pd (25–29) alloy electrocatalysts for the ORR and several authors have reported significant enhancements in the mass activity of both metals with alloying.

Theoretical investigations (30–50), utilizing quantum mechanical first principles density functional theory (DFT) calculations have led to a significantly improved understanding of the mechanism for Pt and Pd activity enhancement. The d-band model proposed by Nørskov et al. (51–54), which relates the chemisorption energy of oxygen species directly to the metal d-band center (52–54), has provided the most complete explanation for the root cause of ORR enhancement through alloying to date. While the metal sp band is broad, the d-band is sharp. Reactant interaction with the sp band broadens adsorbate (i.e., O_2) bonding and antibonding orbitals and shifts them down relative to their non-adsorbed form. These broadened orbitals further split when they interact with the metal d-band, forming adsorbate-surface bonding and antibonding states. The empty adsorbate-surface antibonding states above the Fermi level yield an attractive interaction between the adsorbate and the metal surface while the filled adsorbate-surface antibonding states below the Fermi level cause a repulsive interaction between the adsorbate and the metal surface. It was further discovered that the broadened bonding orbitals have little effect on the energy difference caused by the adsorbate-metal interaction as they are already filled. Thus, the closeness of metal d-band center to the Fermi level determines the splitting and filling of the these antibonding adsorbate-metal states; a d-band center close to the Fermi level results

in a larger number of the antibonding adsorbate-metal states to be above the Fermi level and empty, and a smaller number of antibonding adsorbate-metal states to be below the Fermi level and filled. Chemisorption energies of various species on pure transition metals and pseudomorphic overlayers have been well accounted for by this model.

The position of the d-band center also depends on geometric effects due to mismatch in the lattice constant between the overlayers and underlying metal atoms. If the lattice constant of the overlying metal atoms is smaller than that of underlying metal atoms, the lattice of the former expands (tensile strain) and the overlap between its d-orbitals decreases. This narrows the d-band; to maintain constant filling, the d-band shifts upward in its average energy (54, 55). An opposite trend is observed when the lattice of the overlying metals is larger than the underlying metal such that the metal atoms on the surface are under compressive strain, which increases d-band orbital overlap, ultimately decreasing the average energy of the d-states.

Therefore, it is now believed that the most critical parameter in the ORR activity is the binding energy of atomic oxygen to the catalyst surface, which is a linear function of the electrocatalyst d-band center (28, 30, 56, 57). Strong binding energies indicate a higher density of antibonding states above the Fermi level, with significant donation from valence electrons in the oxygen 2p orbitals to the metal d orbitals in the electrocatalyst. This strong interaction with the surface both facilitates facile electron transfer between the surface and reactant oxygen and helps to break the O=O bond. However, these surfaces also favor surface oxidation, which leads to the active site being shielded by high coverage of Pt-O and Pt-OH species, which are significantly less active for the ORR than metallic Pt. On the other hand, weak binding energies produce limited oxygen interaction with the surface, leading to low electron transfer probabilities and difficulty breaking the O=O bond. These two effects combine to yield a volcano-type plot for the ORR on both raw (30) and alloyed metals (57) as a function of the oxygen binding energy. This is shown for the ORR on Pt and Pd alloys in Figs. 2a (56) and 2b (28), respectively.

Though results on both Pt and Pd were promising, the secondary metal, M, in the alloy has almost always been a non-noble transition metal and, thus, these catalysts show low Pourbaix stability in the highly acidic PEMFC cathode. Extensive leaching of the secondary metal has been observed (10, 29, 58), leading to reductions in the cell performance below even Pt/C-cathode PEMFCs since the dissolved metal cations can ion exchange with H^+ in Nafion®, reducing electrolyte conductivity, as well as electrodeposit at the PEMFC anode, reducing the number of active sites there.

Several non-noble metal catalysts have been proposed including Co and Fe porphyrins, macrocycles, and Ru-Se chalcogenides (10, 59–64). In recent

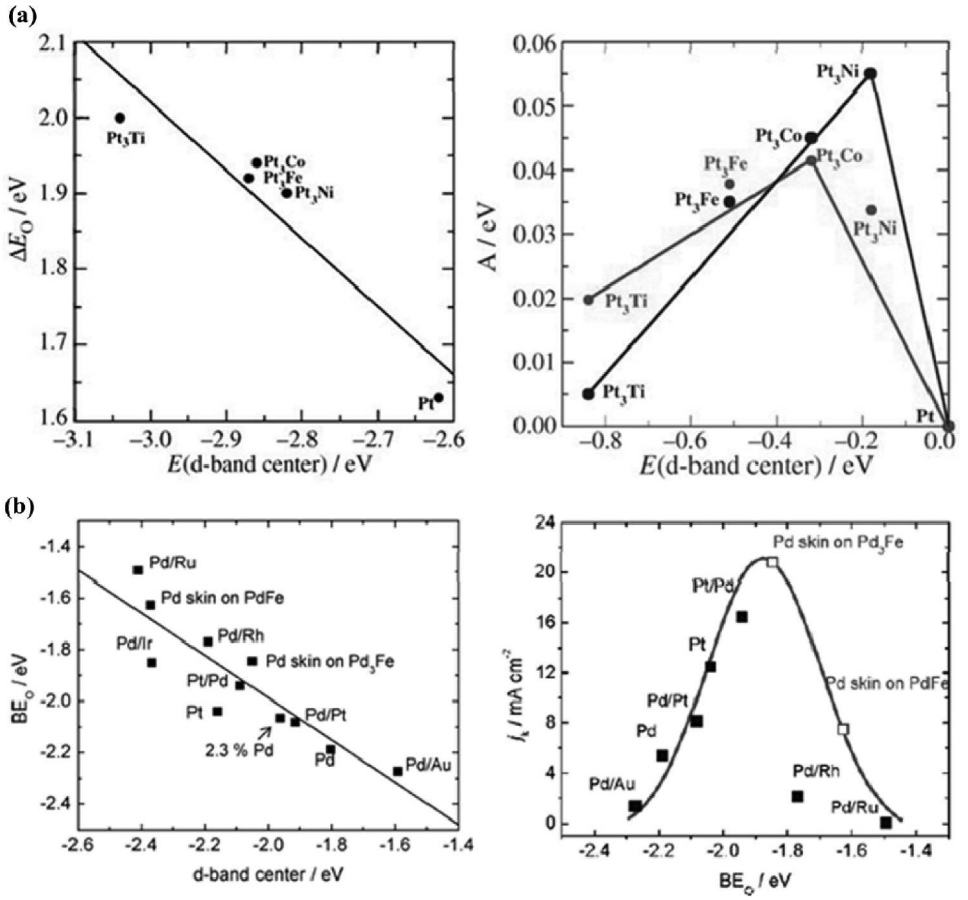

Figure 2: Linear relationship between the d-band center and oxygen binding energies and the resulting volcano-type behavior for ORR activity reported for Pt (a) by Norskov (56) and Pd (b) by Adzic (28).

years, significant advances have been made. Perhaps the most notable study is one by Lefèvre et al., who have shown non-precious metal electrodes with performances similar to that of Pt/C in a PEMFC (65), which has been used to show the promise of non noble catalysts in the literature (9). However, due to low mass and volumetric activities, the catalyst layer for all non-noble metal catalysts is significantly thicker than Pt-based catalyst layers, which has important implications on commercial devices, including water management issues, system weight, high mass transfer overpotentials, and low durability (65, 66). This has led some researchers to doubt that Pt will ever be totally replaced in PEMFCs and call for new approaches to shift the Pt-O binding energy while not introducing intrinsic stability limitations into the catalyst (10).

1.3. Instability of Pt Clusters on Traditional Carbon Supports

One of the most pressing issues in state-of-the-art PEMFCs is the agglomeration of Pt clusters at the cathode, which leads to significant reductions in the electrochemically active area (ECA) during operation. It is believed that there are two primary mechanisms that drive the Pt surface area loss with time: Mechanism I—crystal migration of Pt atoms and clusters on the support surface—and Mechanism II—dissolution of smaller Pt clusters and Pt ion redeposition on larger Pt clusters, which has also been referred to as modified Ostwald ripening. These two mechanisms are illustrated in Fig. 3 (67).

The primary evidence for Mechanism I lies in the particle size distribution after long term chronoamperometric experiments in PEMFCs (68, 69). In both (68) and (69), researchers investigated the average Pt particle size and particle size distribution after exposure to constant load for several thousand hours. It was found that the final Pt particle size distribution was asymptotic, with a distinct tail at large particle sizes. Historically, this shape in the particle size distribution was consistent with growth via crystal migration (70). Unfortunately, this mechanism is not able to explain the potential dependence of Pt particle degradation that has been observed by several researchers (71), and it is generally considered that Mechanism I is a minority contributor to the Pt degradation mechanism in PEMFCs, though it may play a more significant role at elevated temperatures relevant to phosphoric acid fuel cells (72, 73).

The potential dependence of the degradation rate of Pt ORR electrocatalysts in PEMFCs has led most researchers to point toward Mechanism II as the primary cause for performance loss at the cathode. In this mechanism, platinum ions result from the dissolution of metallic and oxidized platinum (74) surface species and are redeposited onto larger particles. Larger particles are thermodynamilcally favored for redeposition because of their lower intrinsic interfacial free energy. Each of the dissolution

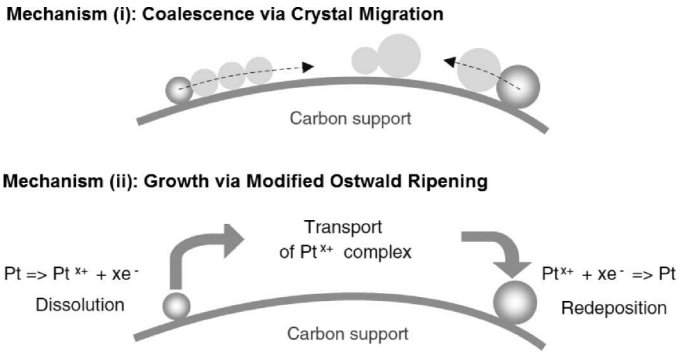

Figure 3: Mechanisms for Pt agglomeration during operation at the PEMFC cathode. Modified from (67).

steps has a Nernstian dependence, where the thermodynamic concentration of Pt^{+2} has a clear potential dependence. This is shown for the dissolution of metallic platinum in Eq. (4):

$$Pt \leftrightarrow Pt^{+2} + 2e^{-}; \log\left[Pt^{+2}\right] = \frac{2F}{2.303RT}\left(E - E^{*}\right) \tag{4}$$

where F is Faraday's constant, R is the ideal gas constant, T is the temperature, E is the electrode potential, and E^{*} is the formal potential for the reaction of interest. The potential dependence for the interaction of Pt^{+2} with other PtO and PtO_2 species have been summarized nicely by Borup et al. (74). The resulting Pt^{+2} ions are then plated either elsewhere within the cathode or even in the proton exchange membrane (75, 76).

Recently, Darling and Meyers developed a simplified model for Pt dissolution in the PEMFC cathode. Three reactions are considered: the dissolution of Pt metal (Eq. (4)) and the oxidation of metallic Pt by water followed by the chemical dissolution of the surface oxide in acidic media (Eqs. (5) and (6)) (77, 78):

$$Pt + H_2O \leftrightarrow PtO + 2H^{+} + 2e^{-} \tag{5}$$

$$PtO + 2H^{+} \leftrightarrow Pt^{+2} + H_2O \tag{6}$$

This model can be used to explain the general trends reported for a host of experimental studies (79–85) that showed that the oxidation of Pt^{+2} is limited at low potentials and Pt dissolution is inhibited by surface oxide species at elevated potentials. However, at intermediate potentials ($0.6 < E < 0.8$ V vs. NHE), which are most relevant for the PEMFC cathode, the intermediate surface coverage of oxide species facilitates the rapid dissolution of clean Pt. Regardless of the dominant mechanism, modification of the catalyst-support interface is desperately needed to both anchor Pt to the support and shift the oxidation of Pt clusters to more positive potentials.

1.4. Thermodynamic Stability Limitations of Carbon Electrocatalyst Supports

Another significant cause for the performance drop in the PEMFC cathode is the oxidation/corrosion of the carbon support itself. Here, surface carbon atoms are activated electrochemically at potentials greater than 0.207 V vs. NHE. Next, the activated carbon species reacts with nearby water molecules, eventually yielding CO_2. This is summarized in Eqs. (7)–(10) (86, 87):

$$C_s \rightarrow C_s^{+} + e^{-} \tag{7}$$

$$C_sO^+ + H_2O \rightarrow C_sO + 2H^+ + e^- \quad (8)$$

$$C_sO + H_2O \rightarrow CO_2(g) + 2H^+ + 2e^- \quad (9)$$

$$\text{Total}: C + 2H_2O \rightarrow CO_2(g) + 4H^+ + 4e^-;\ E^o = 0.207\,\text{vs. NHE} \quad (10)$$

The rate of carbon corrosion is slow, but steady under typical PEMFC operating conditions ($0.6 < E_{cathode}$ (V) < 0.8; $60 < T(^\circ C) < 90$). This consistent support degradation brings the long-term stability of carbon supports into question. Also, it has been shown that Pt most likely acts as a carbon corrosion catalyst (88, 89), which may localize a majority of the carbon loss to areas in direct contact with Pt. This localized degradation orphans Pt particles and expedites their dissolution; both of these mechanisms cause a decrease in the electrochemically active area and PEMFC performance loss with time.

Not surprisingly, the rate of carbon oxidation is a strong function of the electrode potential and cell temperature (90). Though this is not a concern during steady-state operation, it has significant implications on transient cell operation, most notably during startup and shut down. Several researchers (91–93) have suggested that during these transient states, the cell often inadvertently runs at negative currents. This is caused by large gradients in the hydrogen concentration across the anode electrode, which forces a net reduction at that electrode. Under these conditions, water oxidation is the primary reaction at the PEMFC cathode where local potentials may be in excess of 1.5 V. These elevated potentials lead to rapid dissolution of the carbon support. Thus, PEMFC cathode supports must have an electrochemical stability window that exceeds 1.5 to 2.0 V vs. NHE, which is not achieved by conventional carbon supports.

1.5. Using Catalyst-Support Interactions in Chemical Systems to Enhance Activity and Stability

Strong metal-support interaction (SMSI) was first reported by Tauster et al. in 1978 (94) to explain the reduction in chemisorption behavior and increased catalytic activity of noble metals supported on TiO_2. Since then, SMSI has been used as a generic term to describe a host of interactions between the catalyst and the support, mostly on oxide surfaces. In the simplest case, SMSI has been used to describe the contribution of the support to multifunctional reaction mechanisms, where the support adsorbs one or more reactants or allows the spillover of activated intermediates to secondary sites. Secondly, SMSI has been used to describe cases where there is charge transfer between the catalytic metal and the support, leading to a change in the electronic structure of the metal catalyst. Though both of these interactions faciliitate synergistic effects in multicomponent catalyst systems, the main

focus here will be cases where the electronic structure of the metal is affected by the support, which will likely have the most straightforward translation to the electrochemical systems discussed later.

In 2007, Fu and Wagner (95) summarized the known fundamentals for the charge redistribution at the interface between oxide supports and metal overlayers. Here, they discuss experimental and theoretical results on the interaction of both noble and non-noble metals with TiO_2, Al_2O_3, MgO, and SiO_2 supports for various chemical reactions, and it was clearly shown that the electronic structure of the supported metal is affected by the nature of the support. Two of the dominant factors in the enhancement of the catalytic activity of the metal are its electronegativity relative to the support and work function. These two factors dictate both the degree and magnitude of charge transfer between the two materials, which directly affect the oxidation state of surface metal atoms as well as their dispersion and stability.

Differences in the electronic structure of supported and unsupported Pt on titania have been linked to changes in the interaction energy between the Pt clusters and adsorbates (typically CO or H_2) (53), where there is a shift of the local d-band center relative to the Fermi level. This shift is caused by metal-metal bonding between Pt and surface Ti and donation of electrons from Pt to Ti. This was confirmed by Horsley, who used first principle calculations to show significant electron donation to surface Ti from Pt (96). More recently, significant activity and durability improvement of Pt was shown by Vajda and coworkers (97) for subnanometer Pt clusters on alumina for the dehydrogenation of propane. Yoshida et al. (98) have shown that by using LIII-edge XANES, the oxidation state of Pt during propane combustion varied with the support. Support oxides with higher electronegativity increased the oxidation resistance of supported Pt, increasing its mass and specific activity. The same trend was observed by Lemonidou and coworkers (99) for the oxidative dehydrogenation on vanadium oxide catalysts on MgO, ZrO_2, TiO_2, and Al_2O_3.

Enhancement of the behavior of non-Pt noble metals has also been observed. Farrauto et al. (100) reported the oxidation resistance of Pd on zirconia, titania, and ceria. The tailoring of the PdO state was shown to have implications on the catalytic combustion of natural gas and the oxidation of methanol. In their review of supported Au water gas shift catalysts, Ratnasamy and Wagner (101) suggested that on Au/ceria, the metal-support interaction can slow the agglomeration of catalytic particles. Comotti and coworkers (102), looking at Au catalysts for CO oxidation supported on TiO_2, Al_2O_3, ZnO, and ZrO_2, showed that the support directly affected activity, mostly from an adjustment in the Au crystal growth mechanism, where the support influenced the size and dispersion of the Au particles as well as preferential faceting of the clusters. On top of this, Arrii and co-workers (103) saw a negative shift in the Au 4f7/2 binding energy using XPS for the Au

supported on TiO_2, which was correlated with an increase in its activity for the same reaction.

1.6. Extension to Electrochemical Systems

Sections 1.2–1.4 discussed three intrinsic limitations of current Pt/C ORR catalysts: (1) leaching of secondary metals from Pt alloys designed to enhance the ORR; (2) high surface mobility and dissolution of Pt supported on traditional carbons; and (3) insufficient electrochemical stability of raw carbon supports. This suggests that a new approach is needed for high activity, high stability catalysts for the ORR in the PEMFC cathode. As shown in Section 1.5, each of these limitations, to some extent, has been addressed by careful design and development of support materials in non-electrochemical applications for at least 25 years. SMSI between Pt electrocatalysts and next generation support materials, and the resulting rearrangement of the d-electron structure of the supported Pt clusters, has the potential to concomitantly increase cluster dispersion and stability by providing anchoring sites for Pt deposition while also increasing their electrocatalytic activity through an analogous mechanism to that observed by alloying Pt with Co, Cr, Fe, Ni, etc. while removing the intrinsic instability that these metals introduce.

One significant difference between the systems reported in Section 1.5 and electrochemical systems is the added requirements that electrochemical supports must possess high electronic conductivity and stability at potentials greater than their potential of zero charge. Thus, common, near zero cost materials like aluimina cannot be used. Over the past several years, PEM researchers have begun investigating Pt catalysts that undergo SMSI with unconventional supports. This includes new geometries, coordinated and functionalized carbons, as well as electrically conducting carbides, nitrides, oxides, and other chemistries as electrocatalyst supports for the ORR. The purpose of this review article is to summarize this body of work; present the influence of these materials on Pt dispersion, stability, and ORR activity; and to identify the most promising pathways for future research.

2. ADVANCED CARBONS

In response to the instability of acetylene carbon black electrocatalyst supports at potentials relevant for the ORR, researchers have recently tried several approaches to alter the nature of the carbon support to improve stability. Many of these studies have focused on supports with a higher level of graphitization, such as nanotubes and graphene. The higher level of graphitization is thought to yield higher stability due to a lower density of edge and defect sites, whose oxidation and subsequent corrosion is kinetically more facile than incorporated sp^2 carbon. Other groups have focused on supports where both the

level of graphitization and support microstructure can be tailored. Candidate supports here include nanofibers, hierarchical carbon, aerogels, and ordered mesoporous carbon. Finally, surface functionalized carbon has been getting increased attention over the past few years. It is thought that not only can surface functional groups help to stabilize the carbon structure, intelligent selection of the surface group can also provide a bonding site for Pt, increasing its dispersion and stability.

2.1. Carbon Nanotubes (CNTs)

Both single-walled carbon nanotubes (SWNTs) and multi-walled carbon nanotubes (MWNTs) (104) have received considerable attention in recent years. The theoretical specific surface area of SWNTs is 1315 $m^2\ g^{-1}$ (105). However, SWNTs tend to form bundles, leading to reduced surface areas in practice. Due to the greater radius of curvature of its outer tubes, MWNTs have lower specific surface area than SWNTs and their surface area is a strong function of the number of annular layers; e.g., 580–880 $m^2\ g^{-1}$ for double walled CNTs and 295–430 $m^2\ g^{-1}$ for five walled CNTs (105). Nanotubes can be classified as arm-chair, zigzag, or chiral depending on the arrangement of carbon bonds on the curved graphene surface. Also, SWNTs can be metallic or semiconducting depending on the direction that the graphene sheet is rolled. The wall diameter also determines its electronic properties (106). Since their structure is similar to turbostratic graphitic materials (with a graphene-graphene spacing of 3.4 Å), MWNTs have similar electronic properties to metallic SWNTs (104, 106). However, CNTs often come with both defects and impurities and different synthesis procedures often result in CNTs with variant electronic properties, which are very difficult to isolate.

Because of the tunability in their structure, high graphitic character and high electronic conductivity, CNTs have been the most popular alternative carbon support material for Pt in electrochemical systems. Britto et al. (107) suggested the use of CNTs as a catalyst support for the ORR. On clean (non-platinized) CNTs, they showed that the ORR onset occurred at higher potentials than that of Pt supported on carbon black. From ab initio DFT and molecular dynamics (MD) simulations, they concluded that the ORR activity was enhanced by facile charge transfer from the catalyst to atomic oxygen. More experimental results in a PEMFC showed improved performance over commercial Pt/C when CNTs were used as the Pt support (108–112). Even at ultralow Pt loading on Pt/MWNT (6 $\mu g_{Pt}\ cm^{-2}$), the fuel cell exhibited markedly better performance than one empolying higher loading Pt/VulcanXC-72 (0.12 $mg_{Pt}\ cm^{-2}$) and Pt/NSTF (26 $\mu g_{Pt}\ cm^{-2}$) (113).

Even early on, the importance of surface functionalization in the dispersion and platinization of CNTs was realized as pristine CNTs are nearly inert towards metal deposition due to their extensive sp^2 structure (114). Therefore,

several surface treatment techniques and modifications have been attempted to facilitate Pt deposition. The surface functionalization not only provides sites for metal deposition but also influences their wettability and allows Van der Waals bundled CNTs to break apart and disperse in solution. Pt supported on surface functionalized CNTs was shown to have very high dispersion with a narrow Pt size distribution resulting in high ECA (114, 115). Besides refluxing CNTs with HNO_3 or HNO_3/H_2SO_4, different functionalization methods have been studied (116), such as sonochemical treatment and KOH activation (117, 118). Surface oxidation through such chemical modification creates oxygen functionalities, such as carboxyl (COOH), hydroxyl (COH), and carbonyl (C=O), and various surface defects (119). Hernández-Fernández et al. showed that the Pt dispersion, size, and mass activity of Pt/MWNT depends on the preparation conditions. Hence, surface oxidation conditions must be optimized for maximum boost in ORR activity. This can be accomplished through selection of proper chemical reagents (e.g., H_2SO_4 + HNO_3 rather than HNO_3) (114), technique (e.g., sonochemical) (117), and severity of treatment (mild rather than severe) (119).

Centi et al. created physical defects in MWNTs through ball-milling and studied the effect of physical defects on Pt deposition (120). The Pt cluster size was found to have a narrower distribution on the MWNTs with induced physical defects than raw MWNTs without such physical defects. However, the physical defects created by ball-milling exist on a much larger length scale than those created by surface oxidation. On mildly oxidized MWNTs, Xu and Lin clearly observed clusters of Pt nanoparticles growing as large as 123 nm on the open ends of the MWNTs when Pt nanoparticles were selectively deposited using electrodeposition methods (121). It has been well established that these surface defects are active sites for Pt nucleation. From, DFT calculations, Wang et al. found that Pt binding energy on these defect sites are greater than defect free CNTs, implying that these sites bond Pt clusters directly (122). The stronger binding energy is due to stronger orbital hybridization between Pt and C at the vacancy sites, which intensifies charge transfer.

Even on Pt-free, mildly oxidized MWNTs, Matsubara and Waki have reported that onset of the ORR shifts to higher potential facilitating the reduction of O_2 to H_2O_2 (123). These results suggest that surface functionalities and defects may play a role in their electrocatalytic activity. These studies signify that CNTs affect the ORR not just by having high conductivity and improving Pt dispersion, but there exists a more fundamental influence, such as higher binding energy between Pt and C, or improved charge transfer, or co-catalyst activity on defect sites. On the other hand, creation of surface oxides and defect sites decreases conductivity and significantly increases the reaction rates of support oxidation and corrosion.

The Pt deposition method also influences the extent to which the surface functionalities are utilized. As suggested above (121), selective deposition of Pt

can be made on CNT defects and functional groups with methods such as electrodeposition and ion-exchange (124–126). Nonselective deposition methods can produce bimodal or a wide Pt size distribution. Thus, a suitable deposition method is necessary to fabricate supported Pt catalysts with ultralow loadings with greater utilization (22). Good reviews of different methods used for Pt deposition have been presented by Lee et al. (127) and Wee et al. (22). Selective deposition allows for more deliberate Pt placement, where defects sites are specifically targeted. This allows researchers to make greater use of the surface defect sites, which can be anchor sites for Pt and/or allow for a synergistic enhancement in the ORR.

The ion-exchange method targets H atoms in the oxygen functional groups. Here, Pt^{+4} ions attack the oxygen group, replacing H^{+}. Through electrodeposition, Pt should locate on the surface centers with optimum ionic and electronic conductivity, leading to higher Pt utilization. Of course, each method has several critical control parameters to optimize Pt cluster size and dispersion. The uniformity of the surface defects created by oxidative treatment can be increased by sonochemical treatment (127). The Pt size can be controlled independent of the CNT surface using stabilizing surfactants or viscous reducing/stabilizing agent (i.e., ethylene glycol) (109, 128, 129). Also, the synthesis time can be decreased by microwave irradiation (130–132). Other Pt deposition methods, such as supercritical deposition, (133, 134) atomic layer deposition (ALD), (135) microemulsion (129), and freeze drying (136), have been shown as promising for fuel cell applications. Pt deposition methods and their effect on fuel cell performance have been studied by a number of authors (109, 128, 137). These studies underscore the effect of smaller size and streamlined Pt distribution depending upon the preparation method and its enhancing effect on fuel cell performance. These studies suggest that optimized ORR catalysts will have a small Pt cluster size with very narrow size distribution even at high Pt loading (>50 wt %) with wide, regular spacing. This could allow researchers to drastically decrease the carbon loading in fuel cell electrodes and reduce the catalyst layer thickness significantly, which will circumvent many problems that are caused by current porous electrodes. This should be possible on CNTs due to their high surface area to volume ratio, though, to date, highly effective ultrathin electrodes utilizing Pt/CNT catalysts have not been reported.

Ordered Pt/CNT films have shown greater Pt utilization than Pt/C by increasing the catalyst-electrolyte-oxygen triple phase boundary. Aligned CNTs have been grown directly onto carbon substrates (138–140) or externally grown and applied to the solid electrolyte (141–143). Clearly, the ability to grow preferentially oriented CNTs shows their versatility, though their length, diameter, and MEA preparation technique will play a key role in electrode performance. Generally, improved or comparable performance to Pt/C has been reported. Pt/CNT paper (0.42 mg_{Pt} cm^{-2}) electrodes prepared by Saha et al.,

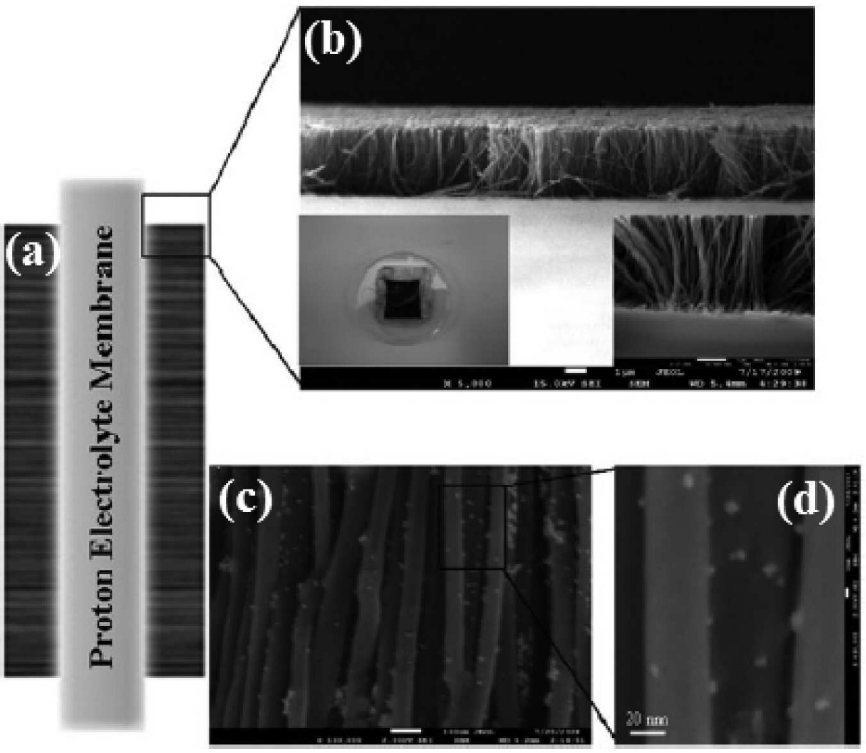

Figure 4: Membrane-electrode-assembly showing platinized free standing vertically aligned carbon nanotubes (ACNT) (143): (a) Schematic of the MEA; (b) SEM image of the ACNT/Nafion membrane; (c) and (d) SEM image of Pt nanoparticles on ACNT.

had higher specific activity and higher mass activity than Pt/C (0.5 mg_{Pt} cm^{-2}) (139). Zhang et al. also had similar results when vertically aligned CNTs were used as both anode and cathode supports in a PEMFC (143). They were also successful in maintaining vertical alignment of the CNTs even after hotpressing at 5000 psi (Fig. 4). At 0.65 V, they reported nearly twice the power density compared to Pt/C catalyst at identical Pt loading. The improved performance was attributed to the three dimensional CNT structure, which improved both the ECA and reactant mass transport in the catalyst layer. They also showed that the fuel cell with vertically aligned CNTs had lower charge transfer resistance (R_{CT}) than Pt/C while the Ohmic resistance was similar (143). Rao and Xing performed semi-empirical modeling on CNTs covered by a Nafion film and aligned perpendicular to the electrolyte surface as cathodes in PEM fuel cells. They found that spacing between the nanotubes is important because it affects the oxygen concentration gradient in the electrode. At very small spacing, Knudsen diffusion dominates and imparts mass transfer resistance (142). In such aligned systems, the height of the CNT dictates the limit of Pt loading depending upon Pt size and packing on the CNT surface.

Surprisingly, few reports have compared Pt/CNT electrodes with commercial Pt/C electrodes with regard to parameters that signify real gains in ORR activity in PEMFCs (i.e., higher exchange current density, decreased overpotentials, or higher specific activity). PEMFCs are highly complex systems and their performance depends on various parameters. Although it is possible to dissect polarization curves into Ohmic, activation, and concentration overpotentials (144), in a comparative study it is very difficult to control all variables between two different systems. Thus, ex-situ studies on rotating disk electrodes (RDE) are typically used to extract pure kinetic data and compare catalysts. On Pt/SWNT catalysts, Kongkanand et al. (145) demonstrated that the onset potential for Pt/SWNT is 10 mV higher than Pt/C, though the specific surface area of Pt/SWNT was 17.8 $m^2\ g_{Pt}^{-1}$; this was lower than the specific surface area of Pt/C, 33.5 $m^2\ g_{Pt}^{-1}$. On the contrary, Li et al. and Hasché et al. (115, 136) observed no appreciable difference between Pt/MWNT and Pt/C regarding onset potential. Alexeyeva et al. (129) showed that when Pt was deposited through the same method, Pt nanoparticles on SWNTs had higher ECA and half-wave potential than that of MWNT, but lower specific activity. Although Alexeyeva et al. did not weigh their result against that of Pt/C, their specific activity reported for Pt/SWNT and Pt/MWNT (330 $\mu A\ cm^{-2}$ to 1280 $\mu A\ cm^{-2}$) was higher than that of Pt/C (53 $\mu A\ cm^{-2}$) reported in the literature in 0.5 M H_2SO_4, though the Pt loading on the former is not clear (129, 146). Such high specific activity is really astonishing and needs further confirmation.

In-situ electrochemical impedance spectroscopy (EIS) was conducted by Tang and Chua (147) at 0.4 V, 0.6 V, and 0.8 V. These three voltages were chosen to focus on regions in the polarization curve where concentration, Ohmic and activation polarization, respectively, are dominant. Here, they compared three different catalysts, Pt/CNT, 20 wt % Pt/C (ETEK), and 40% Pt/C (Johnson Matthey), with identical Pt loading (0.04 $mg_{Pt}\ cm^{-2}$) at the cathode with the same Pt/C anode. The polarization curves obtained using Pt/CNT showed improved performance to Pt/C. The high frequency intercept from the EIS was identical for all three catalysts at different voltages, which was expected as it depends mainly on the electrolyte. However, the R_{CT} correlated well with the fuel cell performance and Pt/CNT had the lowest R_{CT}. This was also confirmed by Zhang et al. for vertically aligned CNTs (143). The authors also concluded that the mass transport of O_2 and H_2O were better in Pt/CNT electrodes.

The durability of Pt/CNT has been studied by several authors ex-situ under simulated PEMFC conditions (136, 148–154). Accelerated degradation tests (ADT), such as potentiostatic hold at high potential and potential cycling, are used to replicate fuel cell performance under repeated use or start-up/shutdown. Though ex-situ conditions do not quite recreate the PEM environment where Pt degradation depends on various factors, such as fuel starvation,

reduction by H_2 crossover, etc., they are mostly reliable in studying performance losses due to Pt agglomeration. Many authors have shown that Pt/CNT has higher resistance against carbon corrosion and Pt agglomeration than Pt/C (136, 148–154). High resistance against carbon corrosion has been attributed to the highly ordered graphitic layers in CNTs. Furthermore, Wang et al (152), based on increases in the hydroquinone-quinone (HQ-Q) redox peak, concluded that MWNTs are more stable than SWNTs as the HQ-Q indicates formation of surface oxides which are active sites for carbon corrosion. In MWNTs, the surface oxidation is limited to the top few layers, which act as a protective sheath for the inner basal planes, resulting in fewer defects than the top layers, which are formed during oxidative pretreatment (150).

Li and Xing studied the corrosion of platinum supported on carbon black and MWNTs (150). Both with and without Pt, the surface oxidation of the CNTs was found to be greatly reduced compared to carbon black. Support corrosion after platinization was accelerated for both types of carbon. Interestingly, after several cycles, the specific charge due to surface oxides (HQ-Q complex) on the MWNTs was stable unlike carbon black, which showed continuous increase with time. This was attributed to the protection and stability of the inner basal plane in MWNTs and high aspect ratio of the support. Also, carbon oxidation at the open end of the CNTs was not observed. On the contrary, carbon black is turbostratic, and the amorphous carbon and disordered graphitic planes allow for deep oxidation. When the MWNTs were heated to a very high temperature (2800 °C) in inert atmosphere prior to surface functionalization and Pt deposition, Pt agglomeration after electrochemical treatment decreased slightly (153). Hasché et al. subjected Pt/MWNT and Pt/C to 10,000 potential cycling between 0.5 to 1.0 V and 2000 cycles between 0.5 to 1.5 V to examine lifetime and transient startup/shutdown stability testing (136). The percentage increase in Pt size was remarkably greater and ECA significantly lower following the transient stability test. They credited the decrease in ECA between 0.5 and 1.0 V mostly to Ostwald ripening and carbon corrosion, while Pt dissolution in acid and carbon corrosion dominated during the startup/shutdown tests. Enhanced support corrosion resistance (especially for MWNTs) and stability of supported Pt clusters seemed to be a direct result of specific interaction and electron transfer between the Pt nanoparticles and CNTs.

2.2. Graphene

Graphene is a freestanding single atomic layer of sp^2 carbon. The 2010 Nobel prize in Physics was awarded to Andre Geim and Konstantin Novoselov just 6 years after they isolated graphene from highly ordered pyrolytic graphite (HOPG) (155). In graphene, the carbon *s* orbitals make strong σ bonds while *p* orbitals form a half-filled π band, which when combined

with its virtue of being single atom thin, imparts it with unique electronic properties such as the electrons traveling on its surface have zero effective mass, conductivity even at zero charge carrier density, very high intrinsic mobility (250,000 $cm^2\ V^{-1}\ s^{-1}$), and little scattering over micrometer distances (156). It also has very impressive physical properties, such as extremely high breaking strength ($\sim$40 $N\ m^{-1}$) and very high Young's modulus ($\sim$1.0 TPa) (157).

Graphene is also a very promising support for catalytically active platinum nanoparticles. The theoretical specific surface area of graphene is 2630 $m^2\ g^{-1}$ (105). It also has a very high conductivity; air-dried graphene paper has shown electronic conductivity of 7200 $S\ m^{-1}$ (158). First principles DFT studies have shown that instead of weak Van der Waals bonding, there is strong electrostatic interaction between Pt and graphene due to transfer of electrons from its π orbitals to the d-orbitals of Pt (159). Furthermore, during ozone decomposition, superoxide and hydroxyl radical formation, graphene enhances Pt activity by regulating its electronic structure. Hence, graphene not only has a very high surface area and high conductivity, it may have the ability to impact the ORR activity and stability of supported Pt particles. Also, its preparation is less complex than CNTs, making it attractive from a processing perpective.

However, in practice, exploiting its properties fully has proven challenging. The most common method of obtaining graphene in bulk is by chemical oxidation and exfoliation of graphite (158). Such exfoliated graphenes are decorated with mostly hydroxyl and epoxide groups, though some carboxyl and carbonyl groups exist at the edges. Thus, the materials that have been tested to date are referred to as graphene oxide (GO). These oxygen functionalities form sp^3 bonds with the carbon atoms thereby disrupting their π band and increasing the band gap, leading to very low electronic conductivity for highly oxidized GO (160). The conductivity can be increased by reducing the oxide content; however, fully reducing GO is not possible from most preparation methods. Full realization of Pt/graphene catalysts is important if the high conductivity, surface area, and Pt interaction are to be used to our advantage.

Hence, GO is used as a substrate for Pt deposition instead of graphene. GO has good wetability and disperses quite well in solution due to its hydrophilic oxygen functionalities, though aggregation is difficult to fully avoid due to Van der Waals forces and GOs are usually a few layers thick. As they aggregate, the electronic structure varies greatly; at a stack of 10 layers, GO loses its 2D properties and acts similar to a thin sheet of 3D graphite (156). Also, the edge-plane of a graphene sheet has a heterogeneous electron transfer (HET) rate constant of $\sim$0.01 $cm\ s^{-1}$ while the basal plane has a rate constant of lower than 10^{-9} $cm\ s^{-1}$ (161), which forces Pt nanoparticles to preferentially deposit onto the graphene edges over the sp^2 hybridized lattice. Si and Samulski (162) deposited 3–4 nm Pt clusters onto GO in solution. Pt nanoparticles helped to inhibit stacking and the BET surface area of Pt/GO was 862 $m^2\ g^{-1}$ compared to 44 $m^2\ g^{-1}$ for raw GO. Alternatively, Zhu et al.

(163) functionalized GO with 1-(3-aminopropyl)-3-methylimidazolium bromide ionic liquid (G-IL) making it positively charged and complexed Pt particles with citrate giving them a negative charge. Thin film electrodes having alternate layers of G-IL and Pt-citrate were made on indium-tin-oxide (ITO) by layer-by-layer self-assembly.

Pt deposited on exfoliated GO by chemical routes showed a mesoporous character with average pore diameter of 11–12 nm (164). In a study by Seger and Kamat (165) Pt nanoparticles were deposited on GO partially reduced by $NaBH_4$ and applied at the cathode of a PEMFC. A further attempt at GO reduction by hydrazine, followed by heat treatment to remove hydrazine, resulted in poorer PEMFC cathode performance than the partially reduced Pt/GO at 0.6 V, 60 °C. Under these conditions, the current density was only 190 mA cm^{-2}, lower than conventional Pt/C. Thermal exfoliation of GO by rapid heating (up to 1050 °C) gives rise to highly wrinkled graphene sheets (WGO) (166, 167). Here, 20 wt % Pt/WGO showed higher initial ECA ($\sim$110 m^2 $g_{Pt}{}^{-1}$) and ORR activity ($\sim$75 A $g_{Pt}{}^{-1}$) than that of a commercial ETEK 20 wt % Pt/C catalyst, ($\sim$75 m^2 $g_{Pt}{}^{-1}$ and $\sim$65 A $g_{Pt}{}^{-1}$) (168). After 5000 voltage cycles between 0 and 1.0 V in 0.5 M H_2SO_4, Pt/WGO retained 62.4% of initial ECA and 49.8% of ORR activity compared to 40.0% and 33.6% of ECA and ORR activity retained by the ETEK Pt/C.

2.3. Carbon Nanofibers

Carbon nanofibers (CNFs) or graphitic nanofibers (GNFs) were first reported by Hughes and Chambers in 1889 (169). They are attractive as potential catalyst supports because their size (diameter: 3–100 nm, length: 0.1–1000 μm), structure, and surface chemistry is similar to that of CNTs (106, 170) with less complex processing. There are three different types of CNFs: fishbone (herringbone) type with graphene layers inclined at an angle against the growth axis; deck-of-cards (platelet) type with graphene layers perpendicular to the growth axis; and parallel (tubular) type with graphene parallel to the growth axis (127). Though tubular CNFs look like MWNTs at a glance, the latter have a hollow cavity while the other does not (106). The diameter of CNFs is usually larger than that of CNTs and can be varied by the size of the metal particle that catalyzes its growth (106, 170). Despite its similarity with CNTs, it has a low specific surface area, 80 to 200 m^2 g^{-1} (170, 171), which is comparable to that of Vulcan carbon.

As the CNF surface is highly graphitic, it is also very hydrophobic. Similar to CNTs, surface functionalization with HNO_3, or $H_2SO_4 + HNO_3$ increases its hydrophilicity and facilitates the deposition of Pt. Pt nanoparticles deposited using colloidal methods on functionalized fishbone and platelet-type CNFs have a larger average diameter than that on non-functionalized CNFs (172, 173). On the contrary, Oh et al. found that the Pt cluster size decreases with

the degree of oxidation when same method of deposition was applied (174). Pt dispersion and loading also depends on the diameter and morphology of the CNF (173, 175). Also, better dispersion was obtained using polyol processes where ethylene glycol (EG) acts as a mild reducing agent (176); its viscosity hinders Pt surface diffusion during deposition and, thus, increases homogeneity among nanoparticles. However, surface oxidation decreases conductivity and promotes corrosion, reducing the long-term stability of the support (174).

CNFs also allow researchers to engineer tertiary structures into their architecture (170). CNFs with twisted morphology have shown improved performance in PEMFCs compared to bundles of linear CNFs (177, 178). Furthermore, twisted Pt/CNF with a smaller diameter (65 nm) performed better than Pt/CNT (diameter 15 nm) in a PEMFC (178). Zhang et al. obtained arrays of vertically standing CNFs (80 nm diameter, 100 nm height) by pyrolyzing polyacrylonitrile (PAN) fibers in hexagonally packed porous anodic aluminum oxide (AAO) membranes as a template (179). They deposited Pt nanoparticles in-situ during polymerization of acrylonitrile to form PAN. Another approach towards making arrays of vertical standing CNFs (37 nm diameter, 2 μm height) was taken by Caillard et al. (180) using helicon plasma enhanced chemical vapor deposition (helicon-PECVD). In this study, the authors grew CNFs on Ni-sputtered gas diffusion layers (GDLs). Pt was subsequently sputtered on these CNFs. Because of the low surface area (15–20 $m^2\ g^{-1}$) and the physical dimensions of the CNFs, there is a limit to Pt loading that can be obtained without significant agglomeration and the maximum observed power density was 300 mW cm^{-2}. This was 80% of the value of Pt/C with only 1/5 of the Pt loading. After optimizing both Nafion® content, PTFE content, Pt loading, and MEA fabrication method, other groups have shown Pt/CNF electrodes that perform slightly better at higher current densities than Pt/C with identical Pt loading (175, 181, 182), which was likely due to higher electronic conductivity and improved Pt dispersion.

One of the parameters that researchers have focused on for CNF supports is the density of exposed graphitic edge planes on the surface. This is likely due to the significantly higher (10^7 times) conductivity of the edge plane compared with the graphitic basal plane (161). Hence, Pt/fishbone and Pt/platelet-type CNFs are expected be better ORR electrocatalysts for PEMFC applications than Pt/tubular-type CNFs. Biddinger and Ozkan (183) synthesized platelet-type CNFs with a high edge:basal and parallel-type CNFs with low edge:basal plane ratios. They compared activity of unplatinized CNFs for the ORR and found that the platelet type catalyst had higher activity. Similar studies were conducted by Ismagilov et al. (184) on platinized CNFs in a PEMFC, though interpretation of the results was not straightforward. For all experiments, the platinum content was maintained as 30 wt % Pt/CNF. At higher catalyst loadings, catalyst layers with parallel-type CNF (0.0639 $g_{Pt}\ cm^{-2}$) showed better

performance than that of platelet-type CNF (0.0914 mg_{Pt} cm^{-2}), though a catalyst layer with platelet-type CNF with a very low loading (0.0185 mg_{Pt} cm^{-2}) showed the best overall performance. In fact, its performance was comparable to that of a Pt/C electrode with more than twice the loading (0.0380 mg_{Pt} cm^{-2}). Since Pt loading on the catalyst was held constant, the thickness of the prepared catalyst layers varied considerably, which affect water and O_2 mass transport within the catalyst layer, Nafion® ionomer volume, and electronic conductivity. This makes the deconvolution of the author's data in its current form, and evaluation of the effect of the CNTs on ORR activity and durability in the PEMFC cathode, difficult.

2.4. Carbon Aerogels

Carbon aerogels are prepared by carbonization of an organic aerogel, which is usually a resorcinol-formaldehyde (R-F) sol-gel. Typically, R and F are mixed in a particular molar ratio with an acid or alkaline catalyst to form a sol. The sol is then heated, which facilitates its hydrolysis and polycondensation to its gel form. The aqueous gel can be solvent exchanged with a suitable organic or left in the aqueous phase. Finally, the gel is dried using supercritical CO_2, subcritical N_2, or freeze-dried and carbonized in inert atmosphere to produce aerogels, xerogels, or cryogels, respectively (185, 186).

Carbon aerogels were first synthesized by and reported by Pekala (187). They have high surface area, good electronic conductivity, and large mesopore to micropore area. The primary aerogel structure consists of carbon nanospheres similar to carbon black; however, they differ significantly in their secondary structure. In carbon black, the carbon nanospheres (10–30 nm) aggregate through a combination of covalent and Van der Waals forces, whereas in aerogels, the carbon nanospheres slightly overlap with each other in a continuous chain that forms a 3D interconnected network (188). The relative mesopore and macropore content is determined by an inter-nodular structure while micropore content is determined by an intra-nodular structure (189). Since micropores are intra-nodular, the mesopore structure can be tailored independent of the micropores (186). Depending on the synthesis conditions for the organic aerogel (reactant ratio, pH, catalyst, curing process, etc.) and carbonization temperature, the surface area, mesoporosity/microporosity, pore size distribution, and surface texture can be tuned (185, 189). This provides a level of architectural control that is not available using CNTs and CNFs, making carbon aerogel supports extremely attractive.

Various studies of Pt deposited on aerogels/xerogels have shown that their porosity plays a significant role in their performance as a PEMFC cathode catalyst (190–196). Moreover, it is important that the primary pore size falls in the mesoporous region (195) to obtain good performance. Unfortunately, even after

optimizing Pt and Nafion® loadings and cell temperature, performance better than that of commercial Pt/C catalyst could not be obtained in a PEMFC, though ex-situ tests by Marie et al. in a three electrode electrochemical cell showed that platinized carbon aerogels (20 wt % Pt) activated at 300 °C in air for 30 min with pore size distribution centered at 200 nm had higher specific activity but lower mass activity than that of commercial catalyst (10 wt % Pt/C) (190, 191, 194, 197).

2.5. Hierarchical/Macroporous Carbon

Hierarchical carbons with an interconnected mesoporous-macroporous bimodal pore distribution are attractive as a metal support because they offer advantages of both mesoporous (large surface area, uniform metal dispersion) and macroporous (efficient mass transfer) structures. In hollow core mesoporous shell carbon (HCMSC) (198), the macroporous capsule and the mesoporous shell can be independently adjusted giving good control over their porosity (199). In HCMSCs, the mesopores form porous walls between an interior hollow core and submicron external hollow spheres. Hence, continuous channels of mesopores and macropores are formed that provide an unhindered flow of reactants and products.

The benefits of such structures, shown in Figs. 5a and 5b, were shown by Fang et al. in a laboratory scale PEMFC (200, 201). Here, 20 wt % Pt/HCMSC showed better performance than two commercial (ETEK and Johnson-Matthey) Pt/C catalysts of equivalent loading in several areas. First, the Pt/HCMSC catalyst had a larger ECA. Second, the catalyst showed a lower R_{CT} than the commercial catalysts and achieved a higher mass activity (0.14 A mg_{Pt}^{-1}) than Gasteiger et al. (144) (0.11 A mg_{Pt}^{-1}) using Nafion®-112 electrolyte. Similar enhancement in performance compared to commercial catalyst was observed for hierarchical erythrocyte-like hollow core mesoporous shell carbon supports in a PEMFC and ordered hierarchical nanostructured carbon (Figs. 5c and 5d) (202, 203). Contradicting above results, Fiçicilar et al. could not obtain better power density at 0.6 or 0.4 V than either synthesized or commercial Pt/C (Pt/Vulcan XC72 or Pt/C ETEK); however, the power density and current density at 0.4 and 0.6 V were higher than that of Pt/BP2000 and Pt/Regal for a 20 wt % Pt catalyst and 0.4 mg_{Pt} cm^{-2} cathode loading (204).

2.6. Ordered Mesoporous Carbon

Ordered mesoporous carbon (OMC) was first synthesized in 1999 by Ryoo et al. by casting sucrose into a cubic (*Ia3d*) mesoporous silica template, MCM-48, and carbonizing at high temperature (205). Though an OMC with a narrow pore size distribution was prepared, x-ray diffraction (XRD)

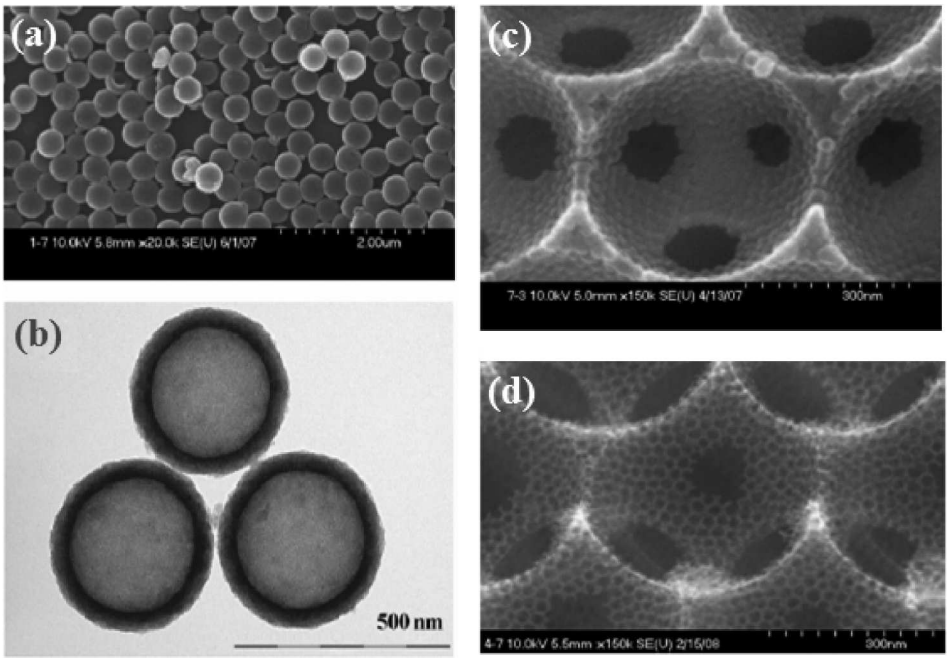

Figure 5: Examples of hierarchical nanostructured carbon: (a) and (b) SEM and TEM images of hollow core mesoporous shell carbon (HCMSC), respectively; (c) and (d) SEM images of ordered hierarchical nanostructured silica (OHNS) and ordered hierarchical nanostructured carbon (OHNC), respectively (200, 203).

revealed that the resulting carbonized material was comprised of a structure that was significantly different than the template. The following year, Jun et al. (206) reported the first OMC with identical hexagonal symmetry (*p6mm*) to its template using SBA-15. The ordered mesoporous structure is a result of the three-dimensional matrix of interconnecting micropores and mesopores in the walls of the template that are a result of solution phase self-assembly of solubilized surfactant with the carbon precursor during synthesis (207, 208). Since then, several other silica templates have been explored to synthesize OMCs. In addition, soft template methods have been developed that can be completed in fewer synthesis steps by directly incorporating carbon precursors into the structure-directing surfactant (207, 209). Soft-template OMCs can be highly stable, up to 1400 °C, in contrast to OMCs made from hard template methods, which are generally stable to around 900 °C (208, 210). One of the advantages of the OMC synthesis is that various precursors can be used to produce carbons with different surface chemistry and pore structure depending on the template or surfactant. This has been successfully exploited to make novel carbon materials for electrochemical applications (211).

Song et al. analyzed OMCs from a CMK-3 template and wormhole-like mesoporous carbon (WMC). Both showed a very narrow pore size distribution centered around 4.3 nm, comparable BET surface area (992 and 1076 $m^2\ g^{-1}$ for CMK-3 and WMC, respectively), similar mesopore volume (1.21 and 1.24 $cm^3\ g^{-1}$ for CMK-3 and WMC, respectively), and nearly identical average Pt size (3.2 and 3.1 nm for Pt/CMK-3 and Pt/WMC, respectively) (212). The Pt/WMC catalyst showed higher electrochemically active surface area and higher activity for ORR. This shows that having a large surface area and uniform pore size alone do not yield a high performance catalyst support with improved mass transfer; accessibility and interconnectivity of these pores also play significant roles. This was supported by Du et al. (213) who reported a 1-D, steady-state numerical model comparing ordered active layers (OAL) oriented perpendicular to the membrane against a conventional active layer (CAL) with randomly distributed pores and agglomerates as that of in Pt/Vulcan. The authors showed that alignment of the OAL in the direction of the mass transfer reduced the electrode concentration polarization due to faster O_2 diffusion through the thin electrolyte wrapping the OAL rather than an increase of O_2 concentration throughout the active layer.

Joo and coworkers (214) synthesized a 33 wt % Pt/OMC catalyst with pipe-like carbon fibers, 5.9 nm inside diameter, 4.2 nm between adjacent fibers, and 2000 $m^2\ g^{-1}$ BET surface area prepared using a SBA-15 template and furfuryl alcohol as the carbon precursor (Fig. 6). They reported a mass activity for Pt/OMC of 0.1 A mg_{Pt}^{-1} in O_2 saturated 0.1 M $HClO_4$ at 10,000 RPM, which was more than 10 times greater than the mass activity of 33 wt % Pt/C under identical experimental conditions. Likewise, Hayashi et al. reported enhanced ORR for a 30 wt % Pt/OMC (7–9 nm pore diameter, 600 $m^2\ g^{-1}$ BET surface area) synthesized through a soft-template method when compared with 50 wt % Pt/C (215). Interestingly, they also reported a mass-transfer limited current higher than the Levich theoretical value, which they assigned to the transport and storage of O_2 in the pores (215, 216). Ding et al. also have demonstrated a 669 $m^2\ g^{-1}$ BET surface area, 3.2 nm pore diameter Pt/OMC with greater ORR performance than commercial Pt/C when used in gas diffusion electrodes (217).

Therefore, OMCs display unique and unusual properties regarding mass-transfer enhancement or attenuation of concentration polarization during the ORR, though the mechanism for this enhancement is currently not well understood. Hence, it has proven difficult to translate the high activity observed in ex-situ, three electrode experiments into high performance PEMFCs. The PEM fuel cell performance of a 20 wt % Pt/OMC (754 $m^2\ g^{-1}$ BET surface area, 3.1 nm pore diameter) could not match the performance of 20 wt % Pt/C (ETEK) in real fuel cell conditions (218–221), which suggests that the internal pores of the OMC were not entirely accessible to the ion-conducting phase during fuel cell testing. Therefore, to exploit the full potential of Pt/OMC

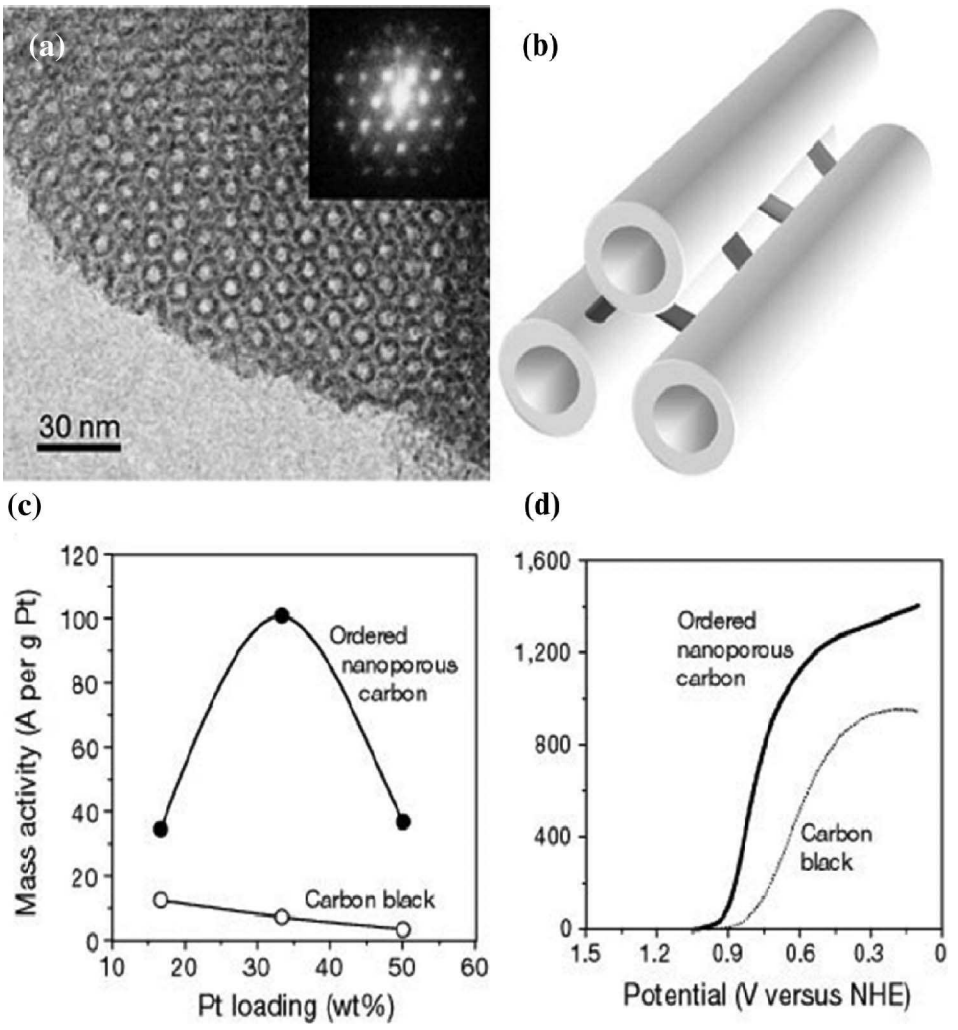

Figure 6: (a) TEM image of ordered nanoporous carbon (ONC) and its Fourier diffraction; (b) Schematic of pipe-like ONC; (c) Mass activities (A/g) of ONC compared to carbon black at different Pt loading; (d) Polarization curves in 0.1 M $HClO_4$ at 10,000 RPM with a scan rate of 50 mV/s of carbons with 33 wt % Pt (214).

electrocatalysts, it is imperative to optimize the pore diameter, the ionomer type and loading, and Pt size and loading (215, 222, 223). One advantage with OMCs is the flexibility of the synthesis procedure, which allows for numerous variations. This should facilitate the synthesis of next generation OMCs with increased diameter, which will allow for the penetration of ionomer into the internal structure, leading to high activity Pt/OMC catalysts for PEMFCs.

To increase the stability of Pt nanoparticles on OMCs, Gupta et al. (224) prepared a highly graphitic OMC from mesophase pitch and compared it to an amorphous OMC made from furfuryl alcohol. After Pt deposition, the OMCs were subjected to ADT. The Pt/graphitic OMC showed little or no alteration while significant changes were observed for Pt/amorphous OMC in terms of mass activity, specific activity, and ECA. Compared to Pt/Vulcan XC72R, even the Pt/amorphous OMC demonstrated enhanced stability, leading to higher activity retention and maintained high ECA. This was also supported by Shanahan et al. (225), who fabricated graphitized OMCs using a soft template method followed by high temperature carbonization at 2600 °C. This material also showed higher stability than Pt/Vulcan. The stability enhancement was mainly assigned to interaction between the Pt d and carbon π orbitals, though no supporting data was presented.

2.7. Surface Functionalized Carbon

As noted in the previous sections, DFT studies have suggested that the electrocatalytic activity of Pt clusters can be enhanced by interaction between carbon π orbitals and the Pt d-band. Unfortunately, the catalytic enhancement effect is difficult to harness, control and reproduce with amorphous carbon blacks that are turbostratic due to random surface irregularities. One method to overcome this is to increase the graphitic character of the support through high temperature pyrolysis; however, porosity is typically compromised in such cases. An alternative method to increase the π–d interaction is to dope the carbon support with heteroatoms, such as nitrogen, sulfur, and boron. These heteroatoms, when incorporated into the carbon matrix, can affect the electronic and physical properties of the carbon materials.

Several researchers have recently reported a myriad of studies for direct ORR on unplatinized supports with a wide range of N functional groups (183, 226–232). To date, the best performance for N-containing carbons for the ORR was obtained in alkaline electrolyte when there is some ordered graphitic structure such as in vertically aligned CNTs. In acidic systems, activities are generally orders of magnitude lower than Pt/C, making raw nitrogen-doped carbons a poor option for the PEMFC cathode catalyst.

On the other hand, a fair amount of evidence currently exists for enhancing the dispersion and ORR activity of Pt clusters supported on several types of N-doped carbon. Well dispersed Pt clusters with a small mean Pt size of (ca. 2.4 nm) have been reported on nitrogen doped carbon supports. Roy et al. (233) reported that Pt/N-containing Vulcan carbon showed higher ORR activity compared to raw Pt/C for direct methanol fuel cells (DMFCs); however, significant sulfur impurities were present in their carbons. Studies regarding the ORR in acidic electrolyte have been done for Pt clusters supported on functionalized highly ordered graphitic structures, such as CNTs (230, 234)

and GO (235). Vijayaraghavan and Stevenson (234) reported an increase in ORR activity of dendrimer encapsulated Pt on nitrogen doped CNTs compared to undoped CNTs. Moreover, the activity increased when the nitrogen doping was increased from 4 to 7.5 atom %. However, the mass-transport-limited current density and mass activity of their most active catalyst fell short of Pt/C. Higgins et al. have shown that Pt on nitrogen-doped, bamboo like CNTs (ED-CNT) synthesized from ethylenediamine (EDA) precursor have enhanced ORR activity than both undoped CNTs and Py-CNTs made from a pyrrole precursor (230). The ED-CNT had higher total nitrogen concentration (4.74 atom %) than that of Py-CNT (2.35 atom %), higher relative amount of pyridine-type nitrogen, more structural defects, smaller and rounder bamboo compartments as opposed to longer and rectangular compartments, increased Pt dispersion, and smaller Pt nanoparticles, which resulted in higher ECA than that of Pt/CNT or Pt/Py-CNT. This ex-situ observation was also supported by testing in a laboratory scale PEMFC. Jafri et al. (235, 236) reported Pt/N-functionalized graphene and Pt/N-functionalized multiwall carbon nanocoils with enhanced ORR activity performance in PEMFCs compared to their unfunctionalized counterparts.

Platinized, N-doped carbon composite and nanosphere catalysts were shown to have superior ORR activity to Pt/C by Li et al. (237) and Su et al., respectively (238). Li et al. prepared nitrogen modified carbon composite (NMCC) from ethylene diamine, carbon black, and $Co(NO_3)_2$. At 0.9V vs. RHE, the mass activity of Pt/NMCC was 0.16 A mg_{Pt}^{-1}, which was 33% greater than Pt/C. In addition, Pt/NMCC was more stable than Pt/C under both potentiostatic hold and electrochemical cycling in a PEMFC. At 100% relative humidity, 0.4 mg_{Pt} cm^{-2} loading, and 0.7V the specific activity of Pt/NMCC was 1.2 A mg_{Pt}^{-1} while that of Pt/C was 0.6 A mg_{Pt}^{-1}. Similar enhancement in ORR activity vs. Pt/C was observed by Su et al. (238) for platinized nitrogen doped porous carbon nanospheres.

Various nitrogen functional groups have been observed experimentally on nitrogen functionalized highly ordered pyrolytic graphite (HOPG): pyridinic, pyrrolic, quaternary, and pyridine-N-oxide (239). Also, vacancy and interstitial N can be present on the support surface (240). Understanding the role of the nitrogen functionality is further complicated by the fact that defects tend to aggregate and electronically interact. However, several recent first principles DFT studies have yielded valuable insight into the complex relationship between N and C atoms for N-functionalized graphene structures (240, 241). First, the interaction of the N and C atoms in the support matrix lead to a partial withdrawing of electrons from the carbon matrix by adjacent nitrogen sites caused by the higher electronegativity of N (3.0 P.U.) compared with C (2.5 P.U.) (240). The resulting charge redistribution gives the carbon atoms an electron-deficient structure with a positively charged center that can be stabilized by accepting an electron from Pt during cluster deposition. Thus, the

carbon atoms adjacent to the functionality act as Pt nucleation sites. Therefore, the electron transfer between Pt and the functionalized support should both increase Pt dispersion and selectivity since anchor sites are built into the structure as well as shift the Pt d-band center (240), affecting catalytic activity.

Experimentally, the Pt nucleation rate on N-HOPG was greater than that on pristine HOPG and Ar irradiated HOPG (Ar-HOPG), yielding well-dispersed Pt clusters. In addition, Pt stability on N-HOPG was very high compared to both raw and Ar-HOPG (239). As shown in Fig. 7, while Pt agglomeration was clear on undoped HOPG after 1000 potential cycles, Pt clusters on both N-HOPG and Ar-HOPG showed good stability. However, after 10,000 potential cycles only Pt clusters on N-HOPG were stable against agglomeration. This shows that while Ar irradiation produces defects and disordering, only nitrogen-containing defects are able to bring enhanced interaction between the Pt atoms and the graphitic substrate. The nitrogen defects also change the electronic structure of Pt and Groves et al. (241) showed that the binding energy between Pt and C atoms was a strong function of the N-site density.

Nitrogen doping also has been shown to induce several structural changes. The structure of bamboo-like CNTs has been attributed to the presence of nitrogen. Such CNTs have greater conductivity than raw CNTs. Also, it has been suggested that nitrogen defects bring about turbostratic disorder in graphene stacking caused by dislocations (242). Such structural disorder is evident in the walls of the N-doped CNFs shown in Fig. 8. This implies that

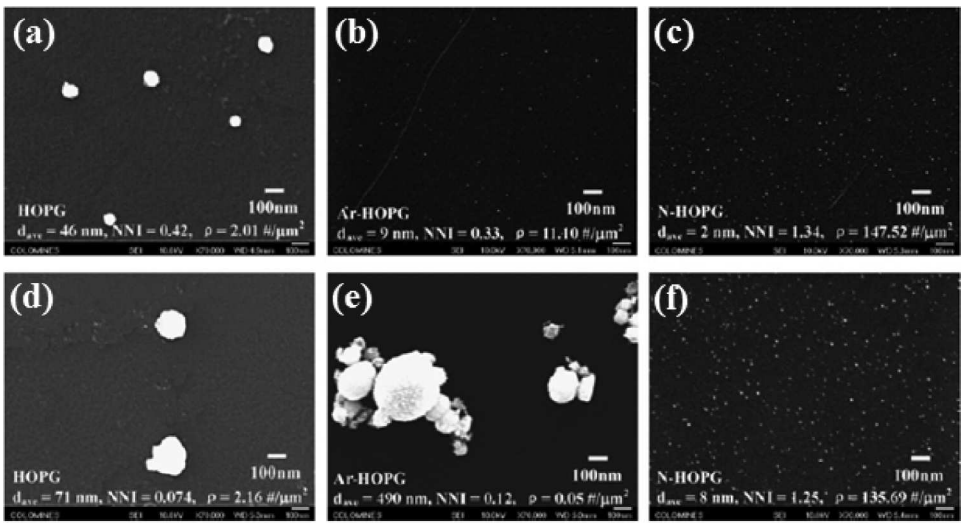

Figure 7: SEM images of Pt clusters after potential cycling (239): (a), (b), and (c) After 1000 cycles on undoped HOPG, Ar-HOPG, and N-HOPG, respectively; (d), (e), and (f) After 10,000 cycles on undoped HOPG, Ar-HOPG, and N-HOPG, respectively.

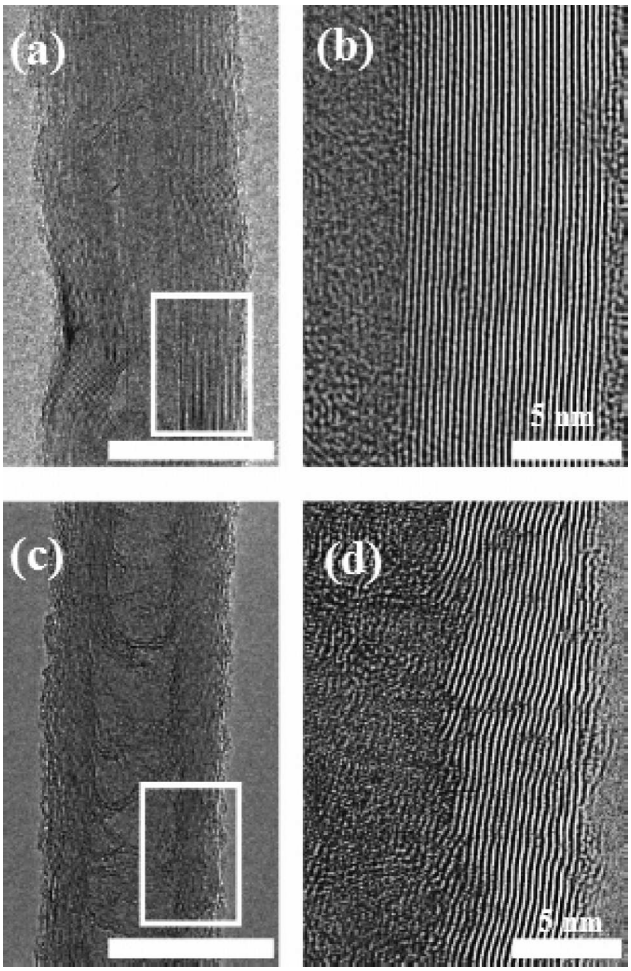

Figure 8: TEM images for the bulk and walls of raw (a, b) and nitrogen doped (c, d) CNFs (242).

nitrogen defects are likely to have a more stable/relaxed geometry than amorphous carbon, meaning that N sites can play different roles on highly graphitic and amorphous surfaces. However, extensive studies into the role of N-induced physical modifications in the enhancement of the ORR have not yet been performed.

A few studies on other surface heteroatoms have been reported, including sulfur on Vulcan carbon (233), sulfur on aerogels (243), sulfur on OMC (244), and boron on carbon black (245). Pt nanoparticles deposited on both S and B heteroatom-functionalized carbon had enhanced stability against Pt growth and agglomeration (244, 245), though very few studies reported the ORR activity. In one study, the ORR activity for Pt/S-functionalized carbon was higher than Pt/C (233); however, more rigorous investigation is needed

to understand the role of surface-doped sulfur, and for that matter boron, on ORR activity and stability. However, it can be hypothesized that the underlying Pt-support interaction for the two will be different from each other and N since the electronegativity for S (2.5 P.U.) is nearly identical to carbon, while B is lower (2.0 P.U.). S functional groups may disrupt the sp^2 hybridization of the support and provide a lower charge density site, though its role in Pt deposition, electron transfer and ORR activity is unclear. One interesting thing to note is that researcherss have not observed that the Pt catalyst activity is negatively affected by the organic sulfur functional groups. This is most likely due to the significant differences between the structure and chemistry of organic sulfur and well-known fuel cell poisons, H_2S and elemental sulfur. B functional groups transfer electrons to carbon atoms, making the B site electron deficient and the most likely Pt bonding site, exactly opposite to the N case.

Functionalized carbons have shown significant promise as Pt supports for the ORR. In addition to enhancing the ORR, synthesis of these materials are also relatively straightforward and do not introduce intrinsic instabilities into the structure. This provides a relatively simple, low cost alternative to alloys and core-shell structures that enhance ORR activity through metal-support interactions, making functionalized carbons attractive ORR electrocatalyst supports (246, 247). However, several questions remain regarding the influence of the type of functional group on Pt bonding and ORR enhancement, the ability of researchers to tailor the direction and magnitude of electron transfer between Pt and the support, and the long-term stability of the functional site with potential cycling and its implication on PEMFC applications. Also, it is currently not possible to make a graphitic surface functionalized support with only one type of functional group.

3. CONDUCTIVE CERAMICS

Though some success has been reported using advanced carbon support materials to enhance the stability and electrocatalytic activity of Pt clusters in PEMFCs, their main drawback remains the thermodynamically favored dissolution of carbon at elevated potentials. It is also clear from the discussion in Section 2 that deposition of Pt onto highly graphitic sp^2 carbon is difficult. To encourage Pt deposition, researchers are forced to introduce surface defect sites into the highly graphitic supports, which compromise their long-term stability. Therefore, several research groups are currently looking to unconventional supports to not only reduce support corrosion, but also improve Pt cluster stability and dispersion and enhance Pt electrocatalytic activity. Some candidate materials include transition metal oxides, carbides and nitrides.

3.1. Oxides

Studies on oxide supports as alternatives to carbon have generally shown improved corrosion resistance and reduced ECA degradation rates (248–254). Oxide supports also can affect the electrocatalytic activity of the supported noble metal due to metal−support interactions. These interactions manifest in several ways including: (i) modification of the electronic states or Fermi level of Pt that pushes the formation of Pt-OH groups to higher potentials (255); (ii) spillover of OH groups onto the oxide support (255); and (iii) reduction of the equilibrium OH adsorption by lateral repulsion between Pt−OH and oxide surface (256).

Titanium Oxides

TiO_2 is an interesting candidate support material due to its high stability in hydrous, acidic environments at potentials relevant to the PEMFC cathode. Though pure TiO_2 is a wide bandgap semiconductor (4.85 eV) with an electronic conductivity of only 10^{-13} S cm^{-1} at 298 K (257), it can still be used as an electrocatalyst support material if defects are introduced into the structure by partial reduction to TiO_{2-x} or a more complete reduction to give the sub-stoichiometric phases with the general formula Ti_xO_{2x-1} (the Magnelli phase, where x is between 4 and 10, is commercially termed Ebonex®) (251, 258, 259). Ti_4O_7, in particular, exhibits high electronic conductivity (~1000 S cm^{-1}) at room temperature (260), which is comparable to graphitized carbon (727 S cm^{-1} (251)). Moreover, labile protons have been observed on titanium oxide, imparting some proton conductivity (261, 262) and titanium oxides have even been used as fuel cell electrolytes (263).

Furthermore, these oxides show better electrochemical stability than Pt/C (264–266). Sub-stoichiometric Ti_xO_{2x-1} has been reported to have high stability as a PEMFC cathode support (251), while also increasing the electrochemically active area compared to Pt/C (249, 267). Single-phase sub-stoichiometric titanium oxide powder was prepared by Ioroi et al. (251) by the reduction of TiO_2 at high temperature under flowing H_2. Tests on Pt-free Ti_4O_7 and Vulcan XC-72 supports showed that the onset corrosion potential was much higher for Ti_4O_7 than for Vulcan XC-72, suggesting that Ti_4O_7 would be significantly more oxidation resistant under true PEMFC operating conditions, though there is a slow oxidation of the reduced phase back to TiO_2 during operation. On the other hand, polarization curves for an operating PEMFC with 5 wt % Pt/Ti_4O_7 and conventional 20 wt % Pt/C indicated that the mass activity of Pt/Ti_4O_7 was lower than that of Pt/C. The lower mass activity was most likely caused by the lower specific ECA for Pt/Ti_4O_7, facilitated by a larger mean Pt cluster size than Pt/C. This is supported by the fact that the specific activities of both catalysts were similar.

Novel titanium oxide nanostructures have also been developed recently as Pt electrocatalyst support materials, including spheroidal nanocrystallites, elongated nanotubes, nanosheets, and nanofibers (261). Because of their high stability, high surface area, and moderate electrical conductivity, titanium dioxide nanotubes (TONTs) have been investigated as potential catalyst supports (250, 253, 268, 269). PtNi/TONT and PtCo/TONT catalysts have been investigated for the ORR (253) with some promising results. Here, elongated TiO_2 nanotube arrays ($\sim$1 μm length, 120 nm diameter) were reproducibly formed on a Ti substrate using an electrochemical anodization process. The PtNi and PtCo catalysts were co-sputtered onto the TONT and were shown to be well dispersed and cover both the interior and exterior of the tubes. PtNi/TONT catalysts annealed at 400 °C under hydrogen atmosphere displayed a significantly higher activity for the ORR than PtNi/C (253). To clarify the effects of the nanotubular TiO_2 structure and pore size, compact TiO_2 films on Ti substrate were prepared and compared to TiO_2 nanotube arrays. A remarkable increase in the ORR activity and a positive shift in the ORR half-wave potential were achieved using $Pt_{70}Co_{30}$/TONT. This phenomenon was attributed to favorable accessibility of the high surface area PtCo on the TONT inner wall (250, 253, 261, 268).

Titanium oxides have also been used as co-supports with carbon to improve Pt stability and catalytic performance while utilizing the carbon phase for its high electronic conductivity (267, 270). Pt/TiO_x/C nanocomposites have been synthesized by depositing hydrated titanium oxide on Pt/C, reducing H_2PtCl_6 on carbon-supported hydrated titanium oxide (TiO_2/C) and one-pot synthesis where Pt nanoparticles and hydrated titanium oxide are simultaneously deposited onto the carbon support. Among these methods, the catalyst synthesized by reducing H_2PtCl_6 onto TiO_2/C exhibited the highest performance toward the ORR and the best methanol tolerance in a DMFC (267). This method has also been used to synthesize Pt/TiO_2/CNT (270) and PtRu/TiO_2/C (271) with similar results.

An alternative method for imparting TiO_2 with high enough electronic conductivity for use in the PEMFC cathode is doping with secondary metals, like niobium (272). For TiO_2, an extrinsic semiconductor, impurities/dopants can be added to either increase the number of free electrons (n-type) or holes (p-type). This is illustrated in Fig. 9A (273) for an n-type semiconductor where a pentavalent donor dopant is added to a semiconductor material (i.e., TiO_2). The pentavalent element has five outer-shell electrons, of which only four are used for bonding; this leaves an excess electron whose energy level is not far below the semiconductor's conduction band. In this case, the Fermi level is slightly raised and the energy required to ionize the donor electron is much lower compared to ionizing an electron from the host atom ($E_D << E_g$, Fig. 9B). Thus, the conductivity of the semiconductor is drastically improved.

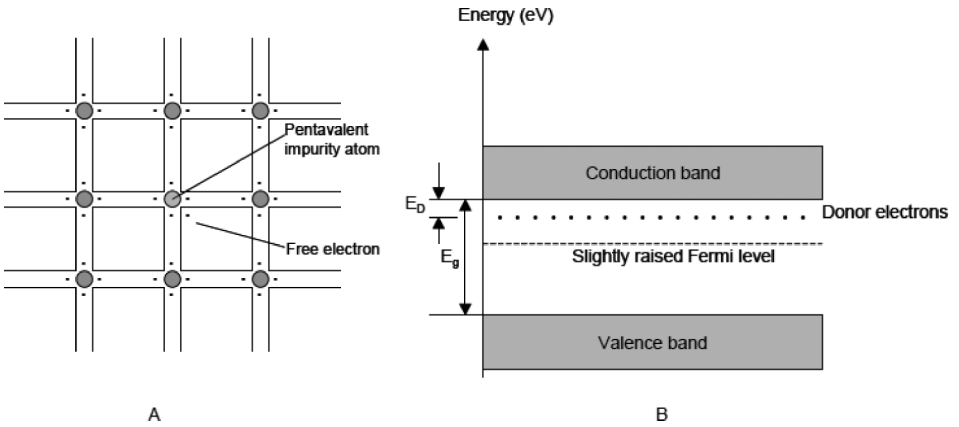

Figure 9: Schematic showing (A) an n-type semiconductor and (B) the resulting energy diagram (273).

It has been shown that mixtures of NbO_2 and TiO_2 sintered at 1000 °C yield an electrically conducting material where Nb is doped into the TiO_2 structure (274, 275). However, the high synthesis temperature leads to a low surface area material with lower electronic conductivity due to a phase transition of TiO_2 from anatase to rutile near 700 °C (276). This led Garcia et al. (277) to develop a low temperature synthesis route for $Nb_{0.1}Ti_{0.9}O_2$ via a surfactant templating method. This method resulted in a BET surface area for $Nb_{0.1}Ti_{0.9}O_2$ of 136 $m^2\ g^{-1}$, which is two orders of magnitude higher than the same material synthesized at a high temperature (278). Park and Seol (279) prepared 40 wt % Pt/Nb–TiO_2 electrocatalysts by hydrothermal synthesis at 120 °C using Ti(IV) isopropoxide and Nb(V) ethoxide as metal precursors. To activate the Nb donor dopant in TiO_2, the nanoparticles were annealed at 400 °C for 2 h under pure H_2. Next, Pt was deposited on the support by chemical reduction with $NaBH_4$. The authors reported a good dispersion of Pt clusters (~3 nm) on the Nb-TiO_2 support (~10 nm). The Pt/Nb–TiO_2 showed a higher activity for oxygen reduction than that of Pt/C prepared by the same method. XANES spectra of Pt L edge on Pt/Nb-TiO_2 suggested significant altering of the Pt electronic structure following its deposition, which may be responsible for the improved ORR activity.

Chen et al. (278) compared the activity and stability of Ti_4O_7 and $Nb_{0.1}Ti_{0.9}O_2$ synthesized by either reducing or doping rutile TiO_2. The synthesis of both Ti_4O_7 and $Nb_{0.1}Ti_{0.9}O_2$ started from the same precursor, ultrafine rutile TiO_2 having a BET surface area of 110 $m^2\ g^{-1}$. Ti_4O_7 was obtained by hydrogen reduction of TiO_2 at 1050 °C, while $Nb_{0.1}Ti_{0.9}O_2$ was prepared by heating an intimately ground mixture of TiO_2 and NbO_2 in a sealed quartz tube under vacuum at 650 °C for 1 day, 950 °C for 2 days, and 1000 °C for 5 days. The resulting supports had comparable, though extremely low,

surface areas (1.5–2 $m^2\ g^{-1}$). The support surfaces were decorated with PtRu nanoparticles by chemical reduction of metal precursors with borohydride and tested in a gas diffusion half-cell for the ORR and oxygen evolution reaction. PtRu supported on $Nb_{0.1}Ti_{0.9}O_2$ showed superior ORR activity and very high electrochemical stability. On the other hand, the Ti_4O_7-supported catalyst showed significant performance degradation due to the partial oxidation of Ti_4O_7 during electrochemical treatment, which creates a high resistance TiO_2 surface layer. This suggests that although conductive oxides can be created either by partial oxidation, doping is the preferred method for enhancing electrical conductivity and stability in oxidizing environments.

Tungsten Oxides

Tungsten oxides have received significant attention recently due to their large number of stable oxidation states, which enables unique properties for a number of chemical and electrochemical applications. The most stable of these states is hexavalent tungsten oxide, WO_3, which has low electronic conductivity due to its large bandgap (280). However, synthesized WO_3 typically shows at least some electronic conductivity due to the formation of nonstoichiometric oxides, which yields conductive oxygen vacancies (281). Thus, there has been significant interest in tungsten oxides as an electrocatalyst support at the PEMFC anode. Several groups (249, 282–288) have investigated Pt/WO_{3-x} electrocatalysts for the methanol oxidation reaction (MOR) as well as the HOR in the presence of impurities like CO.

Kulesza et al. (289) have reported several studies of Pt immobilized in a tungsten oxide matrix, showing that such immobilization leads to an enhancement in the activity of Pt for the MOR in acid solution. It was found that the presence of adsorbed hydroxide species on the tungsten oxide surface facilitated the removal of passivating CO. They also reported hydrogen peroxide decomposition by WO_3 during the co-reduction of oxygen with chalcogenide catalysts (290). Barczuk et al. (291) also observed enhanced MOR for WO_{3-x} immobilized PtRu; however, they also observed poor utilization and mass activity of the catalyst due to large agglomerate formation (150–200 nm). To increase catalyst utilization, Rajesh et al. (292) dispersed Pt/tungsten oxide on high-surface-area carbon nanotubes. The combination exhibited higher activity than Pt alone supported on carbon nanotubes. Ganesan and Lee (284) prepared platinized WO_3 microspheres of 2–4 μm diameter by controlled oxidation of tungsten carbide microspheres. The Pt/WO_3 catalyst showed MOR activity 1.9 times greater than commercial Pt–Ru/C with a 100 mV negative shift in the onset potential and good stability up to 100 cycles in 1 M H_2SO_4. Enhanced MOR activity and good electrochemical stability have also been reported for platinized ordered mesoporous WO_3 (293), WO_3 nanowires (Fig. 10) (294–298), and WO_3 nanorods (299, 300).

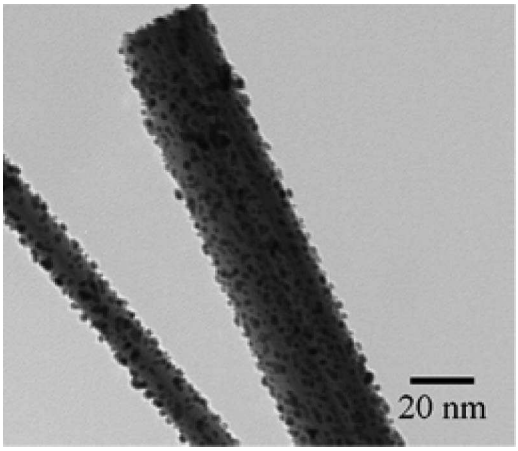

Figure 10: Well dispersed Pt nanoparticles deposited on the$W_{18}O_{49}$ nanowires (295).

On the other hand, there is limited evidence that WO_3 supports enhance the electrocatalytic activity of Pt for the ORR. Chhina et al. (301) showed that WO_3 had a significantly higher stability during accelerated degradation testing in sulfuric acid electrolyte than Vulcan XC-72R, which allowed supported catalysts to have higher stability on the oxide than carbon. Shim et al. (249) prepared Pt-WO_3/C electrocatalysts by oxide deposition onto commercial Pt/C in HCl. They reported a reduction in the Tafel slope for the ORR using PEMFC polarization data; however, it appears that the main enhancement was in the proton conductivity within the catalyst layer, which caused a shift in the Ohmic region of the polarization curve. Pt nanoparticles supported on commercial WO_3 have also been studied ex-situ in a three electrode cell (302). Here, no enhancement in the ORR was observed when Pt was supported on WO_3 compared to Pt/C. Also, the authors reported significant performance decay after 300 cycles due to Pt agglomeration on the oxide surface.

These results suggest that the primary enhancement mechanism between Pt clusters and WO_3 supports arises from the formation of OH groups on the support surface, which facilitates the removal of adsorbed impurities like CO that are either available from the atmosphere or intermediates from partial oxidation of alcohols. However, sufficient evidence to suggest electron transfer between the catalyst and support in this system is significant. This limited interaction between Pt and WO_3 facilitates the agglomeration of particles during deposition and electrochemical treatment, yields low ECA and does not provide a mechanism to enhance the intrinsic activity of the electrocatalyst. Another possible limitation of tungsten oxide supports is its stability in acid media (303), though conflicting reports are present in the literature. Chen and Tseung (304) reported up to 80% W loss after electrochemical cycling.

On the other hand, Shim et al. (249) found that tungsten oxide was stable in 2 M H_2SO_4 at room temperature. Raghuveer and Viswanathan (305) reported that WO_3 stability in acid media can be improved by transition metal ion substitution (such as Ti^{+4}) into the oxide framework. The improvement in the stability could be due to an alteration in the rate of hole capturing processes on surface WO_3 by the Ti^{+4} at the interface, which is responsible for the dissolution of tungsten in acid media.

Tin Oxides

Synergistic effects between the catalyst and support, including the adsorption of OH species on SnO_2 and electronic rearrangement of supported metals, have led several researchers to investigate SnO_2-supported Pt and Pd metals as high activity catalysts for various chemical reactions, such as low temperature oxidation of CO and methane (306–308), selective reduction of NO by hydrocarbons (309), and crotonaldeyde hydrogenation (310). These effects have led a few PEMFC researchers to propose SnO_2 as a support material for fuel cell electrocatalysts, which have been shown to promote the electrooxidation of CO (311) and low molecular-weight alcohols, such as methanol (312) and ethanol (313) on Pt. In addition, Ota and coworkers (314) recently found that SnO_2 influenced the oxidation and reduction behavior of supported Pt, where the formation of Pt-oxide species at elevated potentials was suppressed. This oxide suppression has the potential to improve both the Pt ORR activity by providing a clean surface over a wide potential range ORR (315) and Pt stability since oxide species are a key intermediate in Pt dissolution (77, 78). ORR enhancement for Pt supported on tin oxide nanowires was recently reported (316), though the conclusions were made on stationary CVs in O_2 saturated H_2SO_4 and no PEMFC data was presented, suggesting that further study is needed.

Though these results are promising, raw SnO_2 suffers from two important limitations that may preclude its use as a PEMFC support. First, SnO_2 undergoes redox processes at potentials relevant to the ORR and is at least somewhat unstable. Second, tin dioxide is a wide bandgap semiconductor ($E_g = 3.6$ eV) with electrical resistivity varying from 10 to 10^6 Ω cm, depending on the temperature and the stoichiometry of the oxide (317, 318); this low conductivity yields high electrical resistance within the catalyst layer, which is detrimental to fuel cell performance. Two methods have generally been used to overcome the limitations of SnO_2. First, SnO_2 has been mixed with highly conductive carbonaceous materials (254, 319–323). Recently, Parrondo et al. (323) prepared $Pt/SnO_x/C$ catalysts through a wet chemistry route. The resulting Pt particle size was large (~6 nm), though good performance was achieved with 7 wt % SnO_2 in the cathode, showing a 180 mV improvement at 200 mA cm^{-2} compared with Pt/C. Higher oxide loadings resulted in a decrease in

performance due to mass transport limitations in the cathode. Durability testing also suggested that $Pt/SnO_x/C$ catalysts were more stable than Pt/C under PEMFC conditions. Pang et al. (320) and Hsu et al. (321) have also reported good electrochemical stability for SnO_2–CNT composite electrodes. Du et al. (322) have seen similar results for SnO_2-coated carbon nanotubes while also noting that the $Pt/SnO_2/CNT$ catalyst exhibited comparable ORR activity to Pt/CNT. Also, the authors noted that the Pt supported on SnO_2/CNT was more immune to agglomeration.

Though the catalyst layer conductivity and Pt stability have been improved, this does not overcome the intrinsic instability of the raw tin oxide. Thus, the second enhancement method has been doping SnO_2 to both improve its conductivity and stability (324). In one case, the electrical conductivity increased by several orders of magnitude by doping SnO_2 with antimony (319). Sb (254, 325, 326) and Ru (319, 324) doped SnO_2 have shown that the MOR is further enhanced with the dopant due to an increase in electronic conductivity, improved electrochemical stability of doped-SnO_2 compared with both Vulcan carbon and raw SnO_2 and a decrease in the R_{CT}. According to the authors, electronic interaction between RuO_x and SnO_2 promotes the formation of hydroxyl species on the support surface, which catalyzes the oxidation of poisonous species (i.e., CO) adsorbed on Pt.

Indium-doped tin oxide (ITO) has also received attention over the past few years as an electrocatalyst support. Chang and coworkers (327, 328) reported the electrocatalytic activity of Pt/ITO and Pd/ITO nanoparticles for the ORR, MOR, and ferri/ferrocyanide (FEFI) redox couple. Electrochemical impedance experiments for the FEFI couple on both Pt and Pd showed nearly an order of magnitude decrease in R_{CT} on top-performing compositions compared with bulk metal electrodes, which suggests that the ITO support altered the intrinsic electron transferability of the supported metal. This was mirrored in ORR experiments where the half-wave potential for supported catalysts was shifted slightly to more positive values and significant increases in the kinetic current densities were observed. Also, a recent DOE report by researchers at Pacific Northwest National Lab (329) showed that Pt/ITO/graphene electrocatalysts show significantly improved initial activity than Pt/C, Pt/CNT, Pt/graphene, and Pt/TiO_2, and improved ECA retention. Unfortunately, the ITO was post-deposited onto Pt/graphene and true evaluation of Pt/ITO was not possible. This post treatment also led to the Pt mass activity of Pt/ITO to be low due to Pt encapsulation, though this did result in the greatest ECA retention during testing.

Tantalum Oxyphosphate

Garsany and coworkers (330) recently reported Pt nanoparticles supported on tantalum oxyphosphate (TOPh). In this study, a nanosized TOPh film was

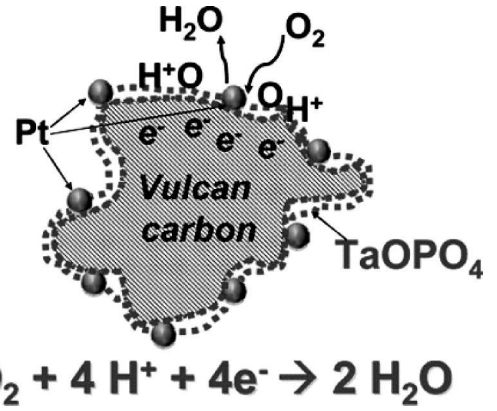

Figure 11: Schematic for Pt/TOPh/C electrocatalysts (330) that have shown good electrochemical performance for the ORR.

coated onto Vulcan XC-72 and then platinized. This is illustrated in Fig. 11. Thin TOPh coatings were applied since TOPh has low electronic conductivity. It was suggested by the authors that the Vulcan carbon core would provide much of the particle-to-particle electronic conductivity while the surface TOPh layer would manipulate the activity and stability of the Pt particles through metal-support interactions.

Linear sweep voltammograms for the Pt/TOPh/C electrode in O_2-saturated perchloric acid, Fig. 12a, showed that the Pt ORR activity was enhanced significantly compared to Pt/C, which is indicated by the significant increase in the half-wave potential. The authors reported a mass activity for the Pt/TOPh/C of 0.46 A mg^{-1} Pt, which was more than twice that of Pt/C with increased ECA (Fig.12b). This was attributed to electronic interactions between the Pt catalyst and phosphorus atoms on the support surface, which not only enhanced the ORR, but also improved the Pt stability by introducing Pt anchor sites. The authors speculated that this electron transfer between the catalyst and the TOPh phase shifted the surface coverage of OH on Pt to more positive potentials, allowing for a greater density of ORR active sites at high potentials compared with conventional catalysts. One possible limitation for the TOPh/C support is the carbon core, which will have the same thermodynamic limitations as conventional supports if poor TOPh coating is achieved. These are promising results, warranting future study into this class of materials.

3.2. Carbides

Transition metal carbides are an interesting class of materials as electrocatalyst supports since they are typically chemically inert to highly acidic and alkaline media, are mechanically durable, have good electronic

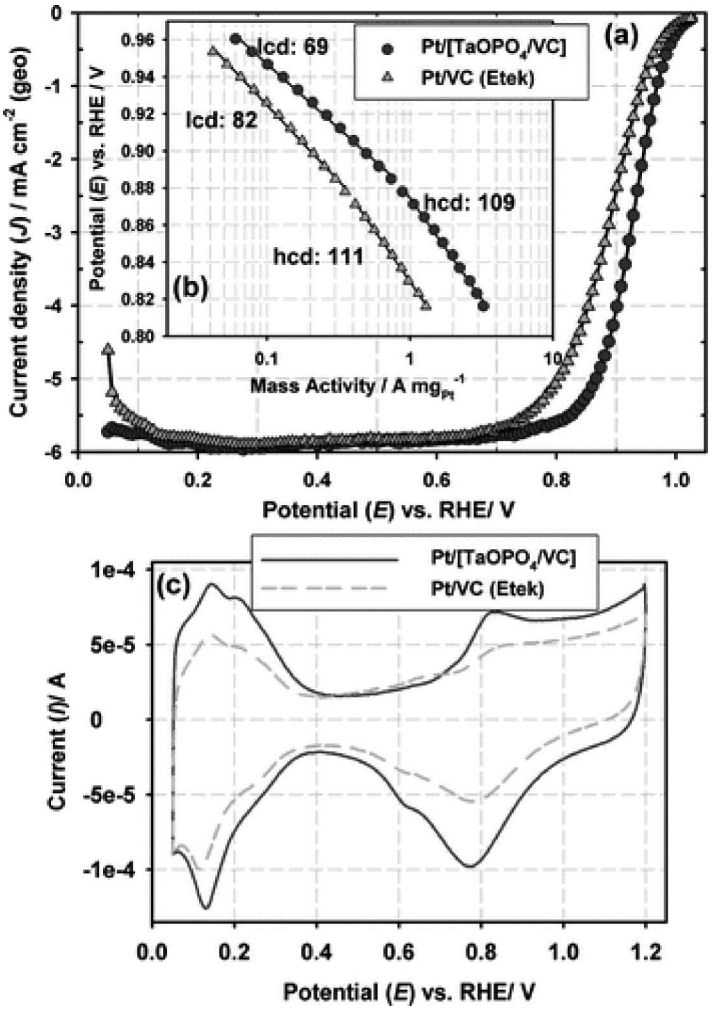

Figure 12: (a) Ex-situ ORR polarization Pt/C (triangles) and Pt/TOPh/C electrocatalysts (circles) in O_2-saturated perchloric acid. (b) Tafel plots for both catalysts. (c) Cyclic voltammograms for Pt/C and Pt/TOPh/C in N_2-saturated 0.1 M $HClO_4$ (330).

conductivity and can form covalent-type bonds with deposited metals (331). Thus, carbides may be able to yield electrocatalysts with high ORR activity and good electrochemical stability.

Tungsten Carbide

Of all the carbides, tungsten carbide has received the most attention in recent years for catalytic applications. This is most likely due to the fact that near the Fermi level its electronic density of states closely resembles that of Pt (332) and WC has shown some Pt-like catalytic properties (333). This has

led several researchers to investigate WC and W_2C as both electrocatalysts (334–336) and supports (337–339). Tungsten carbides have shown stability in acid solutions, high catalyst selectivity (340), resistance to typical PEMFC impurities like CO and H_2S (341), and good electronic conductivity (342). This has led some to suggest that they are the most promising of the carbides for electrochemical applications (343) and a significant effort has been put forth to investigate them as electrocatalyst supports for Pt and the ORR.

Zhang et al. (343) prepared Pt/W_xC and Pt/C and investigated them as cathode catalysts for a PEMFC. The ECA of the two catalysts was initially close and it was found that the Pt/W_xC catalysts were able to retain a higher percentage of their ECA after cycling. Though their initial performance was similar, the lower ECA degradation led to laboratory-scale PEMFCs using Pt/W_xC to have increased performance after long-life testing compared to Pt/C. Ganesan and Lee (344) investigated W_2C microspheres as of Pt supports. Using cyclic voltammetry in acidic solutions, the authors determined that the ECA of Pt supported on W_2C was several times higher than Pt supported on both carbon microspheres and commercial carbon at identical loading, which suggested that the Pt particles were better dispersed on the carbide. However, Zellner and Chen (345) showed that the W_2C phase is electrochemically unstable at potentials greater than 0.4 V vs. NHE, suggesting that they are unsuitable as ORR supports.

In two studies (342, 346), Chhina and coworkers investigated the stability of Pt supported on commercial WC to in-house and commercial Pt/C. They found that the Pt/WC was more stable than both Pt/C samples, where the ORR activity of Pt/WC was nearly constant during accelerated degradation testing, while Pt/C performance dropped precipitously. This high stability was attributed to the formation of a surface oxide layer during the first scan, which acted like a passivating layer, protecting the inner WC core from corrosion. Liu and Mustain (302) also investigated Pt/WC electrocatalysts for the ORR. In this study, the authors observed a significant increase in the ORR half-wave potential compared with WC during polarization tests on a thin-film RDE and excellent dispersion of 3nm Pt clusters on the surface. However, after 300 cycles between 0.2 and 1.0 V vs. NHE, the activity enhancement was lost. In post-mortem analysis, it was observed that surface WC was oxidized to WO_x at potentials >0.8 V vs. NHE. This oxide formation led to two different Pt surface species. The first were still strongly bonded to the support surface and remained well dispersed with an average size of 3 nm (Fig. 13a). Particles of the second type were detached during the surface reorganization that accompanied oxide formation during potential cycling. Since these clusters had limited interaction with the newly formed tungsten oxide surface, which was discussed in Section 3.1, they migrated on the support surface and agglomerated into 50–200 nm Pt superclusters (Fig. 13b). These superclusters dominated the ORR activity in the catalyst layer. This study suggests

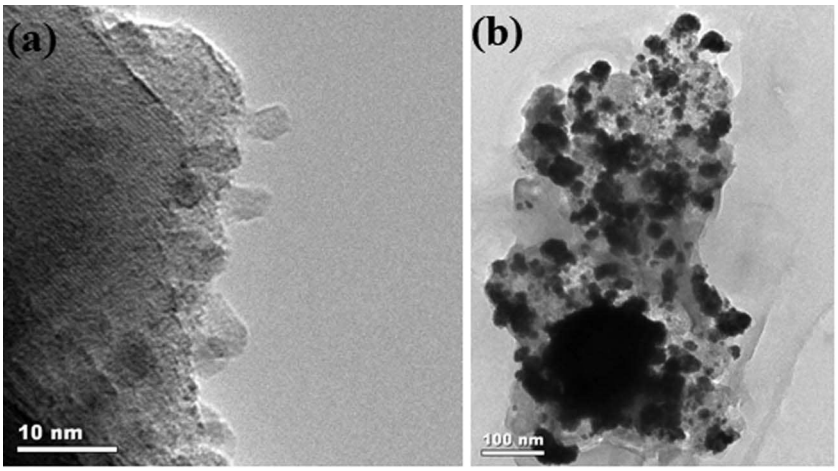

Figure 13: Platinum clusters deposited on WC supports before (a) and (b) after electrochemical treatment (302) showing the poor stability of the Pt particles following the formation of surface oxides.

that the most important factor in realizing the activity enhancement of Pt/WC compared with Pt/C lies in finding methods to push the WC oxidation to WO_x to higher potentials.

Another potential drawback to the widespread implementation of WC supports is their low surface area, which is typically between 1 and 10 $m^2\ g^{-1}$ from high temperature routes (342, 347–349). To address this, Wang et al. (350) used a hydrothermal method to synthesize high surface area, 256 $m^2\ g^{-1}$, WC tungsten carbide microspheres. Liu and Mustain (302) used a molten salt route and obtained WC particles with a surface area of 143 $m^2\ g^{-1}$. Finally, Liang and coworkers (351) prepared an extremely high surface area WC by deposition on CNTs using microwave irradiation of solvated precursors. Not only did they see significantly enhanced ORR activity, they also found no noticeable WC oxidation to WO_x during electrochemical treatment, suggesting that there may be a size or surface thermodynamic effect to the electrochemical oxidation that can be overcome at the nanoscale.

Molybdenum Carbide

Molybdenum carbides (352, 353) have also been shown to be highly active catalysts in several chemical reactions including Fischer–Tropsch conversion (354) and ammonia synthesis (355) as well as posses high stability in harsh environments. Theoretical studies suggest (356, 357) that the high activity is a result of electron donation from Mo to the carbon atoms, which tailors its binding energy toward adsorbates. These properties, combined with good electronic

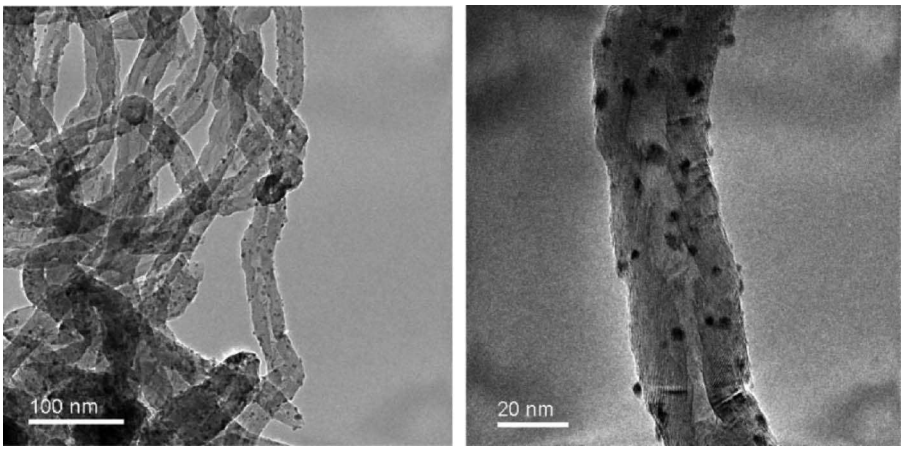

Figure 14: TEM images unplatinized (left) and plaintized (right) Mo_2C/CNT catalysts that show homogenous support structure and well, dispersed supported Pt nanoparticles (358).

conductivity, make Mo_2C a promising candidate support for Pt nanoparticles in PEMFCs.

Pang et al. (358) synthesized nanostructured Mo_2C/CNTs composites by a microwave assisted thermolytic route, which was followed by platination through a polyol processs. The Pt loading was 20 wt % Pt/Mo_2C/CNT. Pt/CNTs samples with identical Pt loading were also prepared. TEM images of the Pt/Mo_2C/CNTs catalysts show well dispersed 5 nm particles (Fig. 14). Electrochemical measurements also indicated that the ECA for the Pt/Mo_2C/CNT catalyst was higher than Pt/CNT and shifted the onset for the ORR positive (Fig. 15). Though this was a promising result, the authors did not report any long-term stability testing and did not investigate the effects of potential cycling on the surface composition of the support, which was one of the limiting factors with WC supports.

3.3. Nitrides

Transition metal nitrides have similar structure and physicochemical properties to their carbide counterparts. Akin to carbides, they have high melting points, good mechanical strength, and are both corrosion and sintering resistant, which makes them promising for catalyst applications. There are a couple of differences, however, between carbides and nitrides including the stoichiometry and coordination of the lattice, which is dictated by the stable oxidation state for N (−3) compared to C (−4) and the magnitude of electron transfer between the adatom and metal since N has a significantly lower electronegativity than C. Therefore, the density of unfilled states is broadened compared to the pure metal (359); this d-band deficiency gives

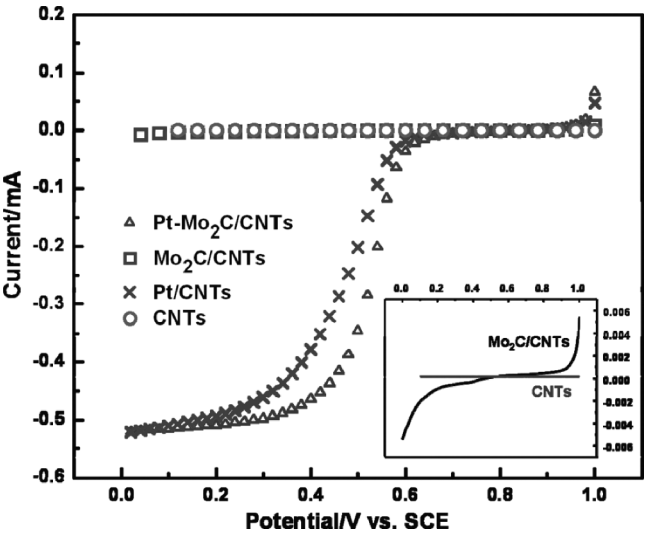

Figure 15: ORR polarization curves for $Pt/Mo_2C/CNT$ (triangles) and Pt/CNT (crosses) catalysts. Both show significant improvements in ORR performance over their raw support and the addition of molybdenum carbide shift the half-wave potential for the ORR positive significantly (358).

nitrides the ability to accept electrons from both adsorbates and catalytic Pt clusters.

Titanium Nitride

Titanium nitride (TiN) is typically used as a conducting, corrosion-resistant coating for titanium alloys, steel, and aluminium (360, 361). It also has very low creep when introduced to multicomponent systems (263, 362) and is biocompatible (363). Pt/TiN electrocatalysts were recently reported by Musthafa and Sampath (364) for methanol oxidation in a DMFC. Physical characterization indicated that Pt was well dispersed on the TiN surface. Electrochemical characterization in methanol-solvated sulfuric acid showed that the anodic methanol oxidation peak potential was close to that of a commercial Pt/C electrode (365), though the peak current was higher and performance was significantly more stable due to the formation of less poisoning intermediates present on the surface. Avasarala et al. (366) synthesized Pt/TiN using commercial TiN nanoparticles. Here, the TiN was ultrasonically dispersed in ethylene glycol. Next, H_2PtCl_6 was slowly added to the dispersion, allowing the Pt ions enough time to reduce. Well dispersed Pt particles were obtained with high ECA and high ORR activity. This is shown in Table 1. One limitation of the ORR activity data was that it was taken on stationary electrodes at unconventional potentials, which makes it difficult to compare with other electrocatalysts. The authors hypothesized that the intrinsic activity of

Table 1: ECA, specific activity, and mass activity for the ORR on Pt/Tin and Pt/C electrocatalysts at several potentials (366).

ECSA (m^2/g_{Pt})	**20 wt% Pt/C 68.7**	**20 wt% Pt/TiN 75.6**
Mass Activity (mA $mg^{-1}{}_{Pt}$), i_m		
0.9 V	6.2	16.4
0.8 V	90.6	294.2
0.7 V	586.2	1221.4
Specific Activity ($\mu A\ cm^{-2}{}_{Pt}$), i_s		
0.9 V	9.1	21.7
0.8 V	131.8	389.2
0.7 V	853.3	1615.6

[a]Catalysts were supported on glassy–carbon disk electrodes (for Pt–loading of $20\mu g_{Pt}/Cm^2$) and tested in 0.1 $MHClO_4$ at 60°C.

the Pt clusters was enhanced by both increased dispersion and electron transfer between Pt and TiN, though no experiments were done to further elucidate the enhancement mechanism.

Tungsten Nitride

Raw carbon-supported tungsten nitride, W_2N/C, was investigated for the ORR in a PEMFC (336). W_2N/C (18 wt % W) showed some activity for the ORR, yielding a PEMFC with a peak power density of approximately 40 mW cm^{-2} at 80 °C. This activity is not too surprising since tungsten oxide, which likely covers the nitride surface, has shown an ability to decompose hydrogen peroxide in acid media (290). From this data, it is difficult to forsee what effect the W_2N would have on the activity and stability of supported Pt clusters. One promising piece of data from the Zhong et al. study (336) is that the W_2N PEMFC was able to run for 80 h without any sign of catalyst degradation or deactivation.

Molybdenum Nitride

MoN/C catalysts have also been investigated for the ORR in sulfuric acid (367). In this study, not only did the catalyst exhibit some ORR activity, it also showed excellent tolerance to methanol, making it a potential catalyst or support for DMFCs. In addition, 18 wt % Mo_2N/C catalysts were tested in a PEMFC (368) at 80 °C. The peak power density for the cell was 65 mW cm^{-2} and no catalyst deactivation was observed during constant current operation for 60 h. Similar to W_2N, these results are encouraging and point to at least some resistance to corrosion; however, significant additional study is needed to make any strong conclusions regarding MoN as a catalyst or support for PEMFCs.

4. Pt MONOLAYERS ON METALS

Platinum monolayers deposited on top of metal underlayers have recently become a popular method to enhance the electrocatalytic properties of Pt. It has been suggested that the deposition of ultra-thin Pt layers onto metallic surfaces has the ability to improve Pt activity and stability while concomitantly decreasing the Pt loading (369). The synergistic effects between thin Pt overlayers and metal supports have been studied on several substrates including single crystals, pure metals and alloys, which are discussed below.

Nearly a decade ago, the Adzic group at Brookhaven National Lab found that 1.5 monolayers of Pt on single crystal Ru greatly enhanced the ORR activity compared to both Pt and Ru metal. In fact, the deposition of this very small amount of Pt on the surface shifted the half wave potential for the ORR positive approximately 350 mV relative to naked Ru single crystals (370). This presented a new, exciting oppurtunity to greatly reduce Pt loadings while obtaining a high activity catalyst. A similar enhancement was also obtained on Ru nanocrystals with only 0.5 deposited monolayers. Initially, monolayer deposition was carried out by spontaneous deposition of Pt on Ru, which resulted in small islands of Pt atoms surrounded by Ru atoms. To improve the Pt dispersion, a new method was developed by the same group where a metal adlayer (usually Cu) was deposited by underpotential deposition (UPD) and replaced spontaneously by Pt cations, which allowed for more homogeneous Pt submonolayers to be deposited on the Au (111) surface (371). Since then, this method has been widely used to deposit monolayers of Pt on various metal surfaces. This group has also used this method to deposit sub-monolayers and monolayers of Pt on several transition metal surfaces including Pd, Ru, Ir, and Rh (47, 49, 372–375). The size and coverage of Pt monolayers can be controlled by coating the support with self-assembled monolayers of thiols, such as 1-octanethiol/3-mercaptopropionic acid (376).

In collaboration, the Adzic and Mavrikakis groups (49) also found an excellent correlation between the theoretical d-band center and experimentally derived ORR activity for Pt monolayers supported on sub-surface Ru (0001), Ir (111), Rh (111), Au (111), Ag (111), and Pd (111) in both alkaline and acidic media. The authors were able to correlate the experimental ORR activity (kinetic current at 0.8 V) with the binding energy of O atoms on the surface, O_2 bond dissociation energy ($O_2 \rightarrow O + O$) and OH formation energy ($O + H \rightarrow OH$), which were related to each other and the d-band center position (Fig. 16). The maximum ORR activity was found by the authors for Pt_{ML}/Pd (111). Experiments, combined with DFT studies, attributed the enhanced activity to the ease of OH hydrogenation. In addition, the formation of PtOH was delayed to higher potentials, thereby reducing OH coverage compared to Pt/C. $Pt_{ML}/Pd/C$ also showed 120 and 25 mV positive shifts in the

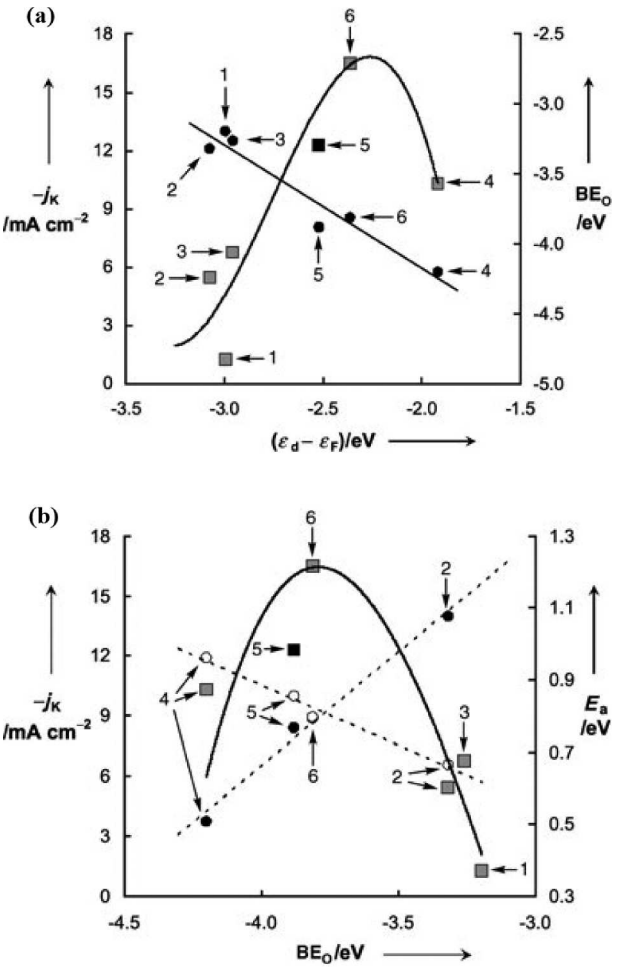

Figure 16: (a) Relationship between position of the d-band center relative to the Fermi level and both the kinetic current (filled squares) and oxygen binding energies (filled circles) for Pt monolayers supported on: (1) Ru (0001), (2) Ir (111), (3) Rh (111), (4) Au (111), (5) Pt (111), and (6) Pd (111). (b) Effect of the binding site of oxygen on the ORR kinetic current (filled squares), activation energy for O_2 dissociation (open circles) and activation energy for OH formation for Pt monolayers deposited on: (1) Ru (0001), (2) Ir (111), (3) Rh (111), (4) Au (111), (5) Pt (111), and (6) Pd (111) (49).

half-wave potential compared to Pd/C and Pt/C, respectively (47, 375), with improved mass activity compared to Pt/C.

Perhaps the most notable attribute of the d-band center model is that it can be verified experimentally, which was shown by Mun et al., from difference spectra obtained by subtracting a scaled valence band (VB) spectrum of clean underlying surface from a VB spectrum with surface coverage (377). On Pt_3M (M = Fe, Co, Ni, Ti) alloys with pure Pt on the surface, a good correlation between experimental and theoretical d-band center with regard to

ORR activity was shown by Stamenkovic et al. (56). In this work, the authors obtained a pure Pt surface (Pt skin) by surface segregation at high heat under ultrahigh-vacuum (UHV). However, this resulted in depletion of Pt in the first 2–3 atomic sub layers. According to their study, the d-band center controls the active site availability for O_2 adsorption and the heat of adsorption of O_2 and reactive intermediates on the surface covered already by OH_{ad} (378). These two parameters are generally autonomous. The highest ever reported ORR activity with turnover frequency (TOF) of 2800 s^{-1} compared to 25 s^{-1} of Pt/C, was obtained on a Pt_3Ni (111) catalyst with a pure Pt skin surface followed by a Ni-rich layer followed by Pt-rich layer (9, 379). The very high activity was assigned to unusually low surface coverage by OH_{ad}, approximately 50% less than that of Pt (111).

Further increases in ORR activity and reduction of Pt loading can be achieved by doping Pt monolayers with metals that oxidize at a lower potential relative to Pt. Very high activity was obtained when Os or Re was mixed with Pt monolayers, increasing Pt mass activity 20 times and total mass activity 4–4.5 times greater (for PtRe) than Pt/C (375). The amplification of ORR activity was attributed to reduced OH coverage on Pt facilitated by O atoms adsorbed on Os/Re, which have a high repulsive interaction with Pt-OH. Of course, the surface coverage of the mixed metal must be optimized to balance the activity enhancement with the number of active sites as very high coverage means that the monolayer is predominantly composed of the doped metal atoms that have low ORR activity.

Though each of the above cases presents a promising enhancement in the intrinsic activity of Pt, high ORR activity was only obtained with samples where Pt was deposited onto other noble metals, some of which are more expensive than Pt itself. This high cost, orders of magnitude greater than any of the supports discussed in Sections 2 and 3, will most likely make these catalysts difficult to transition to commercial or large-scale PEMFCs. Thus, a new type of core-shell electrocatalyst with a non-noble metal core and Pt shell was synthesized by Adzic et al. (380, 381) by surface segregation of noble metals at high temperature (380) and surface oxidation and deposition of the outermost layers of nonnoble metal atoms by redox-transmetalation. The advantage of the latter method was that it allowed the authors to synthesize very small nanoparticles (3–4 nm), while the former method leads to particles 10 nm or greater. The activity of the as-synthesized catalyst particles (Pt_{ML}/AuNi/C, Pt_{ML}/PdCo/C, Pt/PtCo/C) were greater than commercial Pt/C. The greater catalytic activity was attributed to a shift in the d-band center, which reduced PtOH coverage at potentials relevant to the ORR. Several variations of the above chemistry were created by altering the processing methods based on Cu UPD and galvanic displacement by different noble metals. This includes Pt monolayers deposited on intermetallic/alloy cores (382–386), Pt monolayers deposited on a noble metal shell on intermetallic/alloy cores (387), and Pt monolayers on alloy sublayers

(388). The galvanic displacement method and DFT studies are powerful tools that have the potential to be used to rationally prepare superior performing electrocatalysts both in activity and stability for the ORR.

Several other groups have recently reported Pt core-shell catalysts for the ORR in acidic media (389–401). Most of these electrocatalysts contain multiple Pt monolayers. As the number of Pt monolayer increases, the surface area of the particle changes due to an increase in diameter. On Pt/Pd core-shell catalysts, Wang et al. showed that as the number of Pt layers increased from 1 to 3, the Pt-specific activity remained the same while the Pt mass activity decreased (402). Also, as the Pt monolayer grows, the resulting structure distributes the lattice strain and the outer atoms have a weaker interaction with the core, suggesting that the d-band enhancement will have size dependence. On heteroepitaxial monolayers, Pt on Ru (001), using CO as a probe molecule, Schlapka et al. found that the electronic effect no longer matters for structures with more than 3 Pt monlayers whereas lattice strain still affects the d-band center beyond 4 Pt monolayers (403). On Pt/Au core-shell catalyst, an increase in ORR activity has been observed with increasing Pt layers (389) or with decreasing Au/Pt atomic ratio (396). On a 30 nm Pt/Au catalyst with 3 atomic layers of Pt, Hartl et al. (389) achieved specific activity similar to that of polycrystalline Pt particles, while Luo et al. (391) reported activity of 8 nm Pt/Au with a 1 nm Pt Shell (ca. 3.6 monolayer) lower than that of Pt/C. These differing observations may be due to the particle size difference; smaller particles have greater interfacial lattice strain, requiring more Pt monolayers to release the strain compared to larger size particles. Hence, it is necessary to optimize particle size and Pt monolayer thickness to obtain core-shell type catalysts with maximum activity enhancement.

Different intermetallic/alloy cores have been used including Pt/PtCu (390), Pt/PdPt (392), Pt/PdFe (400), and Pt/PdSn (395). They all have reported higher ORR activity than that of commercial Pt/C. Similarly, Pt shells on nonnoble metal cores, such as Cu (399) and Co (393), have been shown to have higher activity than commercial Pt/C. Beside galvanic displacement of UPD Cu, Pt monolayers have been deposited by other methods such as electroless deposition where Pt salt is reduced on the core through some reducing agent, e.g., ethylene glycol, $NaBH_4$, or H_2, and high temperature segregation. Other novel methods reported are microwave synthesis (394) and pulsed electrodeposition (397).

Despite the tremendous research in this field over the past decade, most studies have been done ex-situ where the catalyst was deposited on a glassy carbon or other inert electrode and tested in a three electrode cell. Very little PEMFC data on core-shell catalysts is currently available in the literature. In one study, Malheiro et al. reported that there was no apparent gain in performance between Pt/PtFe/C and PtFe/C despite ex-situ tests that showed

higher activity for the former (401). On the other hand, Mani et al. showed Pt/PtCu/C to have better performance in a PEMFC than commercial Pt/C catalyst in terms of both specific activity and Pt specific mass activity even for comparable ECA (390). Due to the large number of variables involved in making membrane electrode assemblies for PEMFCs and the completely different ionic environment between a fuel cell and ex-situ measurements, it is often difficult to use ex-situ observations to extrapolate fuel cell performance. Hence, more study is needed in PEMFCs to show the viability of these catalysts for commercial purposes.

Though the activities of Pt monolayers on these core-shell structures have been reported widely, there are only a few studies showing the stability of such electrocatalysts. Zhang et al. reported excellent stability of Au/Pt/C catalyst where 30–40% of Pt surface was covered by Au clusters deposited by displacement of Cu UPD atoms on Pt surface (404). Even after 30,000 potential cycles between 0.6 and 1.1 V, the catalyst showed no change in specific activity and ECA. Through study of the XANES spectra, the authors have ascribed the stability to the high oxidation potential of Pt in the presence of Au clusters. Similarly, Adzic et al. reported excellent stabilities for Pt_{ML}/Pd (375, 380, 405), $Pt/AuNi_{0.5}Fe$ (386), $Pt/Pd_{90}Au_{10}$ (388), Pt/Pd_2Co (384), and Pt/PdAu (405), which was attributed to a shift in Pt oxidation to higher potentials. This shift is caused by the oxidation potential of the underlying subsurface atoms, which is lower than that of the Pt atoms, and the geometric and electronic effect which might cause weak adsorption of oxygen species. In an in-situ test, a significant Pd band and some Pt were observed in the Nafion membrane in a PEMFC using $Pt_{ML}/Pd/C$ catalysts after 100,000 potential cycles, which is shown in Fig. 17 (405). It was proposed that at higher potentials, Pd dissolves preferentially over Pt. Surprisingly, the shell structure of the catalyst remained intact, resulting in a hollowing of the core-shell particle and a slight decrease in the average particle diameter. This induces contraction on the outer shell that is likely to decrease ORR activity, but increase stability. The Pd core stability was increased by alloying the Pd core with Au. The loss in mass activity after 200,000 potential cycles was 30%, which easily exceeds DOE requirements. Pt/Pd_2Co catalysts showed 50% ECA loss after 6500 potential cycles during ex-situ testing. In contrast to fuel cell stability testing, the Pt monolayer increased in thickness indicating a different mechanism was at work with the addition of Co compared to Au. On Pt/Co core-shell catalysts (393), Pt appears to limit Co oxidation and dissolution in acidic solution. However, the loss of Co into acid depends upon complete coverage of Co core by Pt and the thickness of the shell. Hence, further experimental work is required to study the long-term stability of core-shell nanoparticles, particularly lower cost options containing non-noble metal core structures.

Ramírez-Caballero et al. used DFT calculations to study the stability of Pt monolayers on different transition metals through evaluation of surface

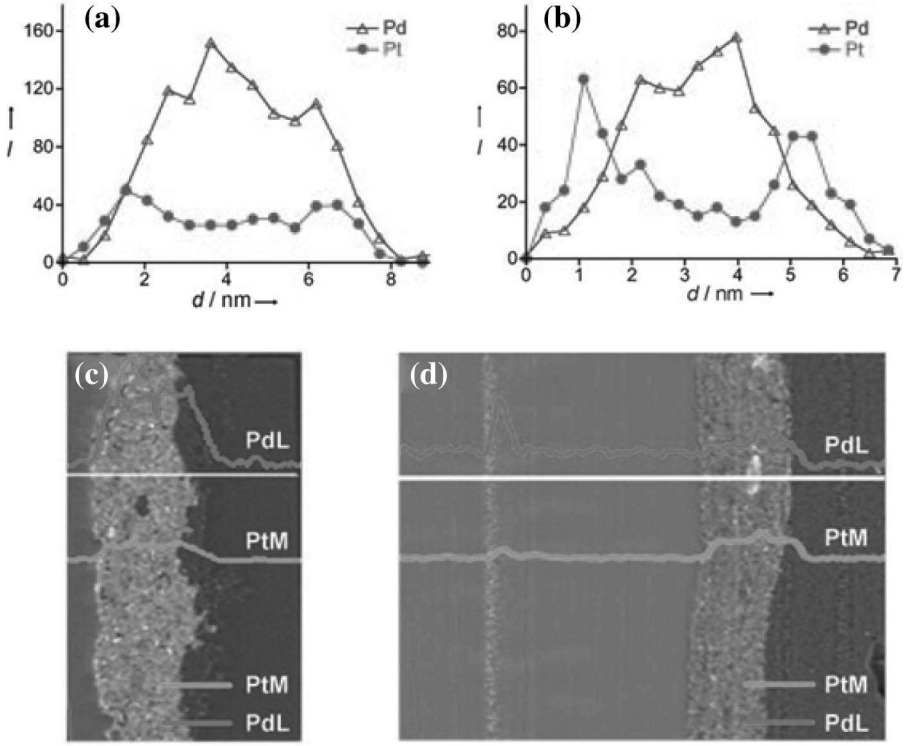

Figure 17: Pt and Pd distribution obtained by EDS line-scan analysis of Pt_{ML}/Pd/C before (a) and after (b) 100,000 cycles. Also included are cross-section SEM images the membrane electrode assembly before (c) and after (d) the degradation test showing the concentration profile of Pt and Pd (405).

segregation energies (406). This study suggested that the surface segregation energy can be altered by adsorbed surface species as well as the purity of the Pt layer on the surface. In this study, 5d (Ir, Au) and 4d (Rh, Pd, Ag) transition metals were found to be very stable while 3d (Co, Ni, Cu) transition metal cores were found to be unstable. Also, core alloying or the addition of an adlayer between the primary core and shell can further increase stability. This secondary core can be added to protect a primary core that is unstable to acid or surface-segregation. Hirunsit and Balbuena studied the effect of adding Pd interlayer between Pt shell and IrCo/Ir_3Co core (407). In another strategy, a carbide-like intermediate layer can be introduced between the core (Ir) and the outermost Pt layer (408). It was suggested that the C atoms will help to diffuse the lattice mismatch between the core and shell and hold the 3d metal atoms in place. On such surfaces, the authors found that the Pt surface oxidation potential should increase, enhancing ORR activity. These studies are yet to be verified experimentally, though they do propose an interesting design to

increase the stability of non-noble metal core and also illustrate the potential for theoretical tools to help researchers design next-generation catalysts.

5. CRYSTALLINE ORGANIC WHISKERS

Over the past several years, 3M has been developing a nanostructured thin film (NSTF) support for PEMFCs. The NSTF supports are crystalline organic whiskers that are synthesized by vacuum deposition of red pigment N,N-di(3,5-xylyl)perylene-3,4:9,10bis(dicarboximide) or perylene red or PR149 at ambient temperature onto microstructured catalyst transfer substrates (MCTS). The MCTS are used to increase surface roughness. Deposition is followed by vacuum annealing between 250 and 270 °C that trasforms the contiguous thin film into crystalline nanowhiskers, which are typically around 1000 nm long, 50 nm wide, and have a surface number density of 3–4 billion per cm^2 (409–411). The organic crystals grow by a screw dislocation mechanism and have a bodycentered cubic (bcc) lattice with a 1.45-nm lattice constant (409, 410).

Platinization of the support is accomplished by sputter coating Pt metal onto the whiskers. The sputtered Pt forms nanosized crystallites along the length of the whisker, which the authors called whiskerretes (412). These whiskerretes can increase the surface roughness by a factor of 6. The surface density and the growth mechanism of the whiskerretes was directed by SMSI. The whiskerrete is dominated by (111) facets with some (100) terrace sites, minimizing the surface free energy. They grow 70° from the whisker axis regardless of the sputtering direction into an elongated pyramid-based pillar with cross-section of ca. 6 nm when fully developed. Also, at the base, its (111) face was somewhat epitaxially similar to the (111) face of the whisker at the side, which has been used as evidence for SMSI between the NSTF and Pt.

The NSTF support is thermally, chemically, and electrochemically inert. Thus, they are believed not to have direct influence on ORR activity. The enhancement in specific activity, 5 times or more than that of Pt/Vulcan, (411) and durability in real PEM fuel cell conditions seems to arise from the way the whisker support influences growth and density of the sputtered metal catalyst as mentioned above. Interestingly, MEA based on NSTF catalysts are 20–30 times thinner and are devoid of any nafion ionomer. The enhancement in specific activity is thought to be mainly due to thin film nature of the catalyst as ex-situ experimental results are consistent with bulk polycrystalline Pt surfaces.

Under different PEM fuel cell conditions, The Pt sputtered NSTF catalyst has shown excellent stability compared to Pt/Vulcan (413). In tests with a 50 cm^2 PEM fuel cell, under repeated potential cycling from 0.6 to 1.2 V at 75 °C, only 32% of the active surface area was lost after 7226 cycles while 95% reduction is active surface was obtained for Pt/Vulcan after 1880 cycles. The

authors have attributed this exceptional stability to the virtue of Pt being a thin film as opposed to individual nanoparticles. First, since the Pt particles are purposely agglomerated to form a continuous film, they are quite large, which eliminates the driving force for common Pt degredation mechanism like crystal migration and Oswald ripening (67). Second, the Pt cystals form a contiguous, encapsulating film on the NSTF whiskers, which minimizes support degredation.

However, a recent article by Kongkanand and Sinha (414) shows that during wet-up transient conditions, very thin (0.3 μm) Pt/NSTF catalyst layers do not perform as well as conventional thick (10 μm) Pt/Vulcan electrodes. During transient operation, the current density is suddenly increased and the rate of water production and electrosmotic drag increases quickly. Concurrently, water removal from the cathode, which depends on water diffusion from the electrode, and water uptake by the membrane and unloading to the anode does not occur fast enough. This results in flooding of the cathode. However, thick electrode layers have a high water storage capacity, which allows sufficient time for water removal. Membrane thickness also plays a significant role here as thinner membranes allow for faster water transport from cathode to anode due to enhanced rate of water vapor diffusion in hydrogen. This difficulty in water management during current-up transient conditions can be attenauted with better design of the pore structure and increasing electrode layer thickness while decreasing membrane thickness.

6. SUMMARY AND PROMISING FUTURE DIRECTIONS

Over the past 20 years, a significant international effort, funded by sovereign nations, private industry, non-profit organizations and individual philanthropists has been put forward to understand and improve the performance and stability of PEMFCs. This work has focused on all aspects of the stack and system including the anode and cathode catalysts, proton exchange membrane, gas diffusion layers, bipolar plates and flowfields, water management, balance-of-plant, etc. This investment, and the dedication and diligence of scientists and engineers, has facilitated significant improvements in the PEMFC during this time, which has the technology on the cusp of commercialization. Though it is an impossible task to give due credit to each of the research groups and individuals who have contributed to the development of PEMFCs, this review has tried to summarize innovations related to the electrocatalyst support and its affect on the intrinsic behavior of Pt catalysts at the PEMFC cathode.

Several approaches have been demonstrated that can: (i) improve the stability of the support material itself; (ii) reduce Pt cluster agglomeration during cell operation; (iii) increase Pt utilization; and (iv) enhance the electrocatalytic activity of supported Pt clusters. Though accomplishing one of these may

incrementally advance the technology, it is clear that truly transformative next generation support materials will accomplish all four simultaneously while avoiding inherent instabilities in the electrocatalyst like Pourbaix dissolution, increasing the number of edge and defect sites in the support or metal, systematic surface oxidation, crystallographic rearrangement and phase transition. Such a support will likely have a strong interaction with the Pt clusters, which will allow for electron transfer between Pt and the support that will both shift the d-band center of Pt considerably and provide a covalent anchor site for deposition.

Taking these strict criteria into account, the authors find it unlikely that carbon-only support materials will lead to extremely high activity, high stability PEMFC cathode electrocatalysts. There is simply insufficient interaction between Pt and highly graphitic surfaces, which forces researchers to very non-selectively corrode the support to provide a weak binding site for Pt. Also, the dissolution of graphitic carbon is thermodynamically favored under ORR relevant conditions and kinetically facile during certain startup/shutdown periods. One interesting option to overcome both of these is surface functionalized carbon. These materials have the promise to allow for a highly graphitic structure while systematically inserting functional groups to the surface to attract, bind and interact with Pt. That being said, no research group has demonstrated the ability to deposit a singular functional group with a given adatom, making it difficult to say if the future will bring sufficient control over the type of group that can be deposited or if the interaction between Pt and the support can be specifically designed. Also, nitrogen functional groups do not appear to have the optimum interaction with the graphite structure or Pt; thus, other groups must be identified and investigated. Finally, the long-term redox stability of N and other adatom functional groups are completely unknown.

Conductive ceramic support materials have shown an ability to enhance the electrocatalytic activity of supported Pt clusters. Some have even shown resistance to dissolution and other types of corrosion. This makes them promising candidates for Pt supports. However, each of the materials discussed in this review suffered from either phase transition or systematic surface oxidation that led to materials with low electronic conductivity, agglomeration/detachment of the Pt catalyst from the surface, and/or loss in the electrocatalytic activity for supported Pt. Though it is clear that an insufficient amount of information exists to make a definitive statement about the long-term feasibility of this class of materials, they do show significant promise. For example, modified WC that shifts the carbide oxidation to higher potentials could yield supported Pt with higher activity than any Pt/carbon electrocatalyst that was reported here due to an enhanced ability of these supports to electronically interact with Pt. Also, doped tin-oxides appear to show more promise than the Magnelli-phase titanates since the latter is prone to surface oxidation to titania, which has negative consequences on ORR activity.

There is also very little information available in the literature related to the ORR on platinized nitrides.

There is no doubt that the top ex-situ performance catalysts to date are the Pt core-shell structures. However, it is unclear what their commercial readiness really is. Limited data is available in the literature for these catalysts in PEMFCs to ascertain their in-situ ECA, activity or stability. It is also hard to see the state-of-the-art processing methods scaling up to an industrial scale. Finally, the material cost here is high. The least costly material used in these studies was Co, which is avoided in Li-ion batteries due to its prohibitively high cost, and showed poor stability during ex-situ testing. More stable versions have contained either Pd or Au cores, which are both prohibitively expensive and will likely increase catalyst cost significantly, even if the Pt mass activity is improved to meet current DOE targets.

Perhaps the most commercial-ready cathode alternative from a performance perspective is the 3M Pt/NSTF whisker catalyst. In both in-situ and ex-situ experiments, the catalysts have good mass and volumetric activity. Also, the extended metal structure gives the catalyst enhanced durability compared to its contemporaries. However, further work remains on this material to address its performance during transient periods and further reducing the Pt loading while not sacrificing the properties that make it attractive. Finally, considering the synthesis procedure, the largest commercialization barrier with these materials may come in large-scale manufacturing; this must be accomplished for these materials to be widely implemented.

Another key to the development of advanced cathode catalysts is the continued integration of first principles calculations with experiments. In recent years, computational power has significantly increased and DFT is quickly becoming the computational equivalent of high-throughput experiments. Combining these two has had a significant effect on heterogeneous catalysts for several processes and has even been applied to the ORR. Though several combined studies are currently extremely fruitful and underway, the strong collaboration between Mavrikakis and Adzic sticks out in the context of this work where they have used both experimental and theoretical results to propose second, third, fourth, etc. generation materials. Also interesting is the theoretical work on multilayered core-shell structures by the Balbuena group; a strong collaboration with an experimental group may yield significant results. Such collaborations between different groups in the private and public sector may speed up the identification of next-generation materials capable of enhancing catalyst performance in all four phases discussed above.

The final point of consideration in the design of the support and the catalyst layer as a whole is microstructure, which will dictate the mass transport of both reactants and products to/from the catalyst surface, gas distribution in the electrode, ion transport, etc. It is likely that these microstructural effects have been the root cause for the differences between in-situ and ex-situ

experiments on many of the ORR catalysts reported here. For example, in nanostructured carbon supports, meso and micro pores that have been engineered into the support are commonly smaller than the axial width of the Nafion® ionomer, which leaves all of the Pt catalyst deposited in these pores unutilized in a PEMFC, where they would be fully accessible in a flooded three electrode experiment. Also, controlling the orientation of engineered structures has the potential to reduce the thickness of the electrode, which may overcome many of these issues. Thus, new structures and industrial processing techniques are needed to extend the activity and durability enhancements observed on existing and next generation electrocatalysts for the PEMFC.

ACKNOWLEDGMENTS

The authors would like to thank the U.S. Department of Energy, Office of Basic Energy Sciences who supported the preparation of this manuscript under Grant No. DE-FG02-10ER16200.

REFERENCES

[1] EG&G Technical Services, Inc. *Fuel Cell Handbook*, 7th ed.; US Department of Energy, National Energy Technology Laboratory: Morgantown, WV, 2004.

[2] Qi, Z.; Kaufman, A. Improvement of Water Management by a Microporous Sublayer for PEM Fuel Cells. *J. Power Sources* **2002**, *109*, 38–46.

[3] Satija, R.; Jacobson, D.L.; Arif, M.; Werner, S.A. In situ Neutron Imaging Technique for Evaluation of Water Management Systems in Operating PEM Fuel Cells. *J. Power Sources* **2004**, *129*, 238–245.

[4] Berg, P.; Promislow, K.; Pierre, J.S.; Stumper, J.; Wetton, B. Water Management in PEM Fuel Cells. *J. Electrochem. Soc.* **2004**, *151*, A341–A353.

[5] Kreuer, K.D. On the Development of Proton Conducting Polymer Membranes for Hydrogen and Methanol Fuel Cells. *J. Membr. Sci.* **2001**, *185*, 29–39.

[6] Van Nguyen, T.; Knobbe, M.W. A liquid Water Management Strategy for PEM Fuel Cell Stacks. *J. Power Sources* **2003**, *114*, 70–79.

[7] Natarajan, D.; Van Nguyen, T. Three-Dimensional Effects of Liquid Water Flooding in the Cathode of a PEM Fuel Cell. *J. Power Sources* **2003**, *115*, 66–80.

[8] Ji, M.; Wei, Z. A Review of Water Management in Polymer Electrolyte Membrane Fuel Cells. *Energies* **2009**, *2*, 1057–1106.

[9] Gasteiger, H.A.; Markovic, N.M. Just a Dream—Or Future Reality? *Science* **2009**, *324*, 48–49.

[10] Gasteiger, H.A.; Kocha, S.S.; Sompalli, B.; Wagner, F.T. Activity Benchmarks and Requirements for Pt, Pt-Alloy, and Non-Pt Oxygen Reduction Catalysts for PEMFCs. *Appl. Catal. B: Environ.* **2005**, *56*, 9–35.

[11] United States Department of Energy, Office of Energy Efficiency and Renewable Energy. http://www1.eere.energy.gov/hydrogenandfuelcells/fuelcells/ (last accessed February 3, 2011).

[12] Appleby, A.J. Electrocatalysis and Fuel Cells. *Catal. Rev.* **1970**, *42*, 221–244.

[13] Jalan, V.; Taylor, E.J. Importance of Interatomic Spacing in Catalytic Reduction of Oxygen in Phosphoric Acid. *J. Electrochem. Soc.* **1983**, *130*, 2299–2302.

[14] Glass, J.T.; Cahen, J.G.L.; Stoner, G.E.; Taylor, E.J. The Effect of Metallurgical Variables on the Electrocatalytic Properties of PtCr Alloys. *J. Electrochem. Soc.* **1987**, *134*, 58–65.

[15] Paffett, M.T.; Beery, J.G.; Gottesfeld, S. Oxygen Reduction at Pt0.65Cr0.35, Pt0.2Cr0.8 and Roughened Platinum. *J. Electrochem. Soc.* **1988**, *135*, 1431–1436.

[16] Beard, B.C.; Philip N.; Ross, J. The Structure and Activity of Pt-Co Alloys as Oxygen Reduction Electrocatalysts. *J. Electrochem. Soc.* **1990**, *137*, 3368–3374.

[17] Mukerjee, S.; Srinivasan, S. Enhanced Electrocatalysis of Oxygen Reduction on Platinum Alloys in Proton Exchange Membrane Fuel Cells. *J. Electroanal. Chem.* **1993**, *357*, 201–224.

[18] Toda, T.; Igarashi, H.; Watanabe, M. Enhancement of the Electrocatalytic O_2 Reduction on Pt-Fe Alloys. *J. Electroanal. Chem.* **1999**, *460*, 258–262.

[19] Mukerjee, S.; Srinivasan, S.; Soriaga, M.P.; McBreen, J. Role of Structural and Electronic Properties of Pt and Pt Alloys on Electrocatalysis of Oxygen Reduction. *J. Electrochem. Soc.* **1995**, *142*, 1409–1422.

[20] Toda, T.; Igarashi, H.; Uchida, H.; Watanabe, M. Enhancement of the Electroreduction of Oxygen on Pt Alloys with Fe, Ni, and Co. *J. Electrochem. Soc.* **1999**, *146*, 3750–3756.

[21] Gasteiger, H.A.; Panels, J.E.; Yan, S.G. Dependence of PEM Fuel Cell Performance on Catalyst Loading. *J. Power Sources* **2004**, *127*, 162–171.

[22] Wee, J.-H.; Lee, K.-Y.; Kim, S.H. Fabrication Methods for Low-Pt-Loading Electrocatalysts in Proton Exchange Membrane Fuel Cell Systems. *J. Power Sources* **2007**, *165*, 667–677.

[23] Markovic, N.M.; Ross, P.N. Surface Science Studies of Model Fuel Cell Electrocatalysts. *Surf. Sci. Rep.* **2002**, *45*, 117–229.

[24] Stamenkovic, V.; Schmidt, T.J.; Ross, P.N.; Markovic, N.M. Surface Composition Effects in Electrocatalysis: Kinetics of Oxygen Reduction on Well-Defined Pt_3Ni and Pt_3Co Alloy Surfaces. *J. Phys. Chem. B* **2002**, *106*, 11970–11979.

[25] Mustain, W.E.; Prakash, J. Kinetics and Mechanism for the Oxygen Reduction Reaction on Polycrystalline Cobalt-Palladium Electrocatalysts in Acid Media. *J. Power Sources* **2007**, *170*, 28–37.

[26] Mustain, W.E.; Kepler, K.; Prakash, J. CoPdx Oxygen Reduction Electrocatalysts for Polymer Electrolyte Membrane and Direct Methanol Fuel Cells. *Electrochim. Acta* **2007**, *52*, 2102–2108.

[27] Fernández, J.L.; Walsh, D.A.; Bard, A.J. Thermodynamic Guidelines for the Design of Bimetallic Catalysts for Oxygen Electroreduction and Rapid Screening by Scanning Electrochemical Microscopy. M-Co (M: Pd, Ag, Au). *J. Am. Chem. Soc.* **2004**, *127*, 357–365.

[28] Shao, M.; Liu, P.; Zhang, J.; Adzic, R. Origin of Enhanced Activity in Palladium Alloy Electrocatalysts for Oxygen Reduction Reaction. *J. Phys. Chem. B* **2007**, *111*, 6772–6775.

[29] Liu, H.; Xia, D.; Zhang, J. *Platinum-Based Alloy Catalysts for PEM Fuel Cells*. In Zhang J., Ed.; Springer: London, 2008.

[30] Nørskov, J.K.; Rossmeisl, J.; Logadottir, A.; Lindqvist, L.; Kitchin, J.R.; Bligaard, T.; Jónsson, H. Origin of the Overpotential for Oxygen Reduction at a Fuel-Cell Cathode. *J. Phys. Chem. B* **2004**, *108*, 17886–17892.

[31] Cuong, N.T.; Fujiwara, A.; Mitani, T.; Chi, D.H. Effects of Carbon Supports on Pt Nano-Cluster Catalyst. *Comput. Mater. Sci.* **2008**, *44*, 163–166.

[32] Li, Q.; Qin, W.-Q.; Sun, W.; Qiu, G.-Z. Calculation of Electron Structure by Density Function Theory and Electrochemical Process of Surface (100) of FeS_2. *J. Central South Univ. Technol.* **2007**, *14*, 618–622.

[33] Deshlahra, P.; Wolf, E.E.; Schneider, W.F. A Periodic Density Functional Theory Analysis of CO Chemisorption on Pt(111) in the Presence of Uniform Electric Fields. *J. Phys. Chem. A* **2009**, *113*, 4125–4133.

[34] Hwang, G.S.; Shin, C.B. Dissociative Adsorption of H_2 on the H/Si(100) Surface: The Effect of Intradimer Pi-Bonding Disruption. *J. Electrochem. Soc.* **2001**, *148*, G692–G694.

[35] Roques, J.; Anderson, A.B. Electrode Potential-Dependent Stages in OHads Formation on the Pt3Cr Alloy (111) Surface. *J. Electrochem. Soc.* **2004**, *151*, E340–E347.

[36] Panchenko, A.; Koper, M.T.M.; Shubina, T.E.; Mitchell, S.J.; Roduner, E. Ab Initio Calculations of Intermediates of Oxygen Reduction on Low-Index Platinum Surfaces. *J. Electrochem. Soc.* **2004**, *151*, A2016–A2027.

[37] Vassilev, P.; Koper, M.T.M. Electrochemical Reduction of Oxygen on Gold Surfaces: A Density Functional Theory Study of Intermediates and Reaction Paths. *J. Phys. Chem. C* **2007**, *111*, 2607–2613.

[38] Janik, M.J.; Taylor, C.D.; Neurock, M. First-Principles Analysis of the Initial Electroreduction Steps of Oxygen over Pt(111). *J. Electrochem. Soc.* **2009**, *156*, B126–B135.

[39] Roques, J.; Anderson, A.B. Theory for the Potential Shift for OHads Formation on the Pt Skin on Pt3Cr(111) in Acid. *J. Electrochem. Soc.* **2004**, *151*, E85–E91.

[40] Calvo, S.R.; Balbuena, P.B. Theoretical Analysis of Reactivity on Pt(1 1 1) and Pt-Pd(1 1 1) Alloys. *Surf. Sci.* **2007**, *601*, 4786–4792.

[41] Ma, Y.; Balbuena, P.B. OOH Dissociation on Pt Clusters. *Chem. Phys. Lett.* **2007**, *447*, 289–294.

[42] Li, T.; Balbuena, P.B. Oxygen Reduction on a Platinum Cluster. *Chem. Phys. Lett.* **2003**, *367*, 439–447.

[43] Greeley, J.; Nørshovs, J.K. A General Scheme for the Estimation of Oxygen Binding e\Energies on Binary Transition Metal Surface Alloys. *Surf. Sci.* **2005**, *592*, 104–111.

[44] Zhang, J.; Vukmirovic, M.B.; Sasaki, K.; Nilekar, A.U.; Mavrikakis, M.; Adzic, R.R. Mixed-Metal Pt Monolayer Electrocatalysts for Enhanced Oxygen Reduction Kinetics. *J. Am. Chem. Soc.* **2005**, *127*, 12480–12481.

[45] Jacob, T.; Goddard, W.A. Water Formation on Pt and Pt-based Alloys: A Theoretical Description of a Catalytic Reaction. *Chem. Phys. Chem.* **2006**, *7*, 992–1005.

[46] Jacob, T.; Muller, R.P.; Goddard, W.A. Chemisorption of Atomic Oxygen on Pt(111) from DFT Studies of Pt-Clusters. *J. Phys. Chem. B* **2003**, *107*, 9465–9476.

[47] Zhang, J.; Mo, Y.; Vukmirovic, M.B.; Klie, R.; Sasaki, K.; Adzic, R.R. Platinum Monolayer Electrocatalysts for O_2 Reduction: Pt Monolayer on Pd(111) and on Carbon-Supported Pd Nanoparticles. *J. Phys. Chem. B* **2004**, *108*, 10955–10964.

[48] Shao, M.H.; Huang, T.; Liu, P.; Zhang, J.; Sasaki, K.; Vukmirovic, M.B.; Adzic, R.R. Palladium Monolayer and Palladium Alloy Electrocatalysts for Oxygen Reduction. *Langmuir* **2006**, *22*, 10409–10415.

[49] Zhang, J.; Vukmirovic, M.B.; Xu, Y.; Mavrikakis, M.; Adzic, R.R. Controlling the Catalytic Activity of Platinum-Monolayer Electrocatalysts for Oxygen Reduction with Different Substrates. *Angewandte Chemie Intl. Ed.* **2005**, *44*, 2132–2135.

[50] Ishikawa, Y.; Mateo, J.J.; Tryk, D.A.; Cabrera, C.R. Direct Molecular Dynamics and Density-Functional Theoretical Study of the Electrochemical Hydrogen Oxidation Reaction and Underpotential Deposition of H on Pt(1 1 1). *J. Electroanal. Chem.* **2007**, *607*, 37–46.

[51] Hammer, B.; Nørskov, J.K. Electronic Factors Determining the Reactivity of Metal Surfaces. *Surf. Sci.* **1995**, *343*, 211–220.

[52] Kitchin, J.R.; Norskov, J.K.; Barteau, M.A.; Chen, J.G. Modification of the Surface Electronic and Chemical Properties of Pt(111) by Subsurface 3d Transition Metals. *J. Chem. Phys*. **2004**, *120*, 10240–10246.

[53] Hammer, B.; Nørskov, J.K. Theoretical Surface Science and Catalysis—Calculations and Concepts. *Adv. Catal.* **2000**, *45*, 71–129.

[54] Greeley, J.; Norskov, J.K.; Mavrikakis, M. Electronic Structure and Catalysis on Metal Surfaces. *Annu. Rev. Phys. Chem.* **2002**, *53*, 319–348.

[55] Mavrikakis, M.; Hammer, B.; Ørskov, J.K. Effect of Strain on the Reactivity of Metal Surfaces. *Phys. Rev. Lett.* **1998**, *81*, 2819.

[56] Stamenkovic, V.; Mun, B.S.; Mayrhofer, K.J.J.; Ross, P.N.; Markovic, N.M.; Rossmeisl, J.; Greeley, J.; Nørskov, J.K. Changing the Activity of Electrocatalysts for Oxygen Reduction by Tuning the Surface Electronic Structure. *Angew. Chem.* **2006**, *118*, 2963–2967.

[57] Okamoto, Y.; Sugino, O. Hyper-Volcano Surface for Oxygen Reduction Reactions over Noble Metals. *J. Phys. Chem. C* **2010**, *114*, 4473–4478.

[58] Yu, P.; Pemberton, M.; Plasse, P. PtCo/C Cathode Catalyst for Improved Durability in PEMFCs. *J. Power Sources* **2005**, *144*, 11–20.

[59] Jaouen, F.D.R.; Herranz, J.; Lefèvre, M.; Dodelet, J.-P.; Kramm, U.I.; Herrmann, I.; Bogdanoff, P.; Maruyama, J.; Nagaoka, T.; Garsuch, A.; Dahn, J.R.; Olson, T.; Pylypenko, S.; Atanassov, P.; Ustinov, E.A. Cross-Laboratory Experimental Study of Non-Noble-Metal Electrocatalysts for the Oxygen Reduction Reaction. *ACS Appl. Mater. Interfaces* **2009**, *1*, 1623–1639.

[60] Bezerra, C.W.B.; Zhang, L.; Lee, K.; Liu, H.; Marques, A.L.B.; Marques, E.P.; Wang, H.; Zhang, J. A Review of Fe-N/C and Co-N/C Catalysts for the Oxygen Reduction Reaction. *Electrochim. Acta* **2008**, *53*, 4937–4951.

[61] Wang, B. Recent Development of Non-Platinum Catalysts for Oxygen Reduction Reaction. *J. Power Sources* **2005**, *152*, 1–15.

[62] Bezerra, C.W.B.; Zhang, L.; Liu, H.; Lee, K.; Marques, A.L.B.; Marques, E.P.; Wang, H.; Zhang, J. A Review of Heat-Treatment Effects on Activity and Stability of PEM Fuel Cell Catalysts for Oxygen Reduction Reaction. *J. Power Sources* **2007**, *173*, 891–908.

[63] Lee, J.-W.; Popov, B. Ruthenium-Based Electrocatalysts for Oxygen Reduction Reaction—A Review. *J. Solid State Electrochem.* **2007**, *11*, 1355–1364.

[64] Jaouen, F.; Marcotte, S.; Dodelet, J.-P.; Lindbergh, G. Oxygen Reduction Catalysts for Polymer Electrolyte Fuel Cells from the Pyrolysis of Iron Acetate Adsorbed on Various Carbon Supports. *J. Phys. Chem. B* **2003**, *107*, 1376–1386.

[65] Lefèvre, M.; Proietti, E.; Jaouen, F.; Dodelet, J.-P. Iron-Based Catalysts with Improved Oxygen Reduction Activity in Polymer Electrolyte Fuel Cells. *Science* **2009**, *324*, 71–74.

[66] Jaouen, F.; Proietti, E.; Lefevre, M.; Chenitz, R.; Dodelet, J.-P.; Wu, G.; Chung, H.T.; Johnston, C.M.; Zelenay, P. Recent Advances in Non-Precious Metal Catalysis for Oxygen-Reduction Reaction in Polymer Electrolyte Fuel Cells. *Energy & Environ. Sci.* **2011**, *4*, 114–130.

[67] Shao-Horn, Y.; Sheng, W.; Chen, S.; Ferreira, P.; Holby, E.; Morgan, D. Instability of Supported Platinum Nanoparticles in Low-Temperature Fuel Cells. *Top. Catal.* **2007**, *46*, 285–305.

[68] Wilson, M.S.; Garzon, F.H.; Sickafus, K.E.; Gottesfeld, S. Surface Area Loss of Supported Platinum in Polymer Electrolyte Fuel Cells. *J. Electrochem. Soc.* **1993**, *140*, 2872–2877.

[69] Tada, T. High Dispersion Catalysts Including Novel Carbon Supports for PCM Fuel Cells. In *Handbook of Fuel Cells: Fundamentals, Technology, and Applications*, Vol. 3; Vielstich, W., Lamm, A., Gasteiger, H.A., Eds., Wiley: New York, 2003.

[70] Eberl, D.D.; Drits, V.A.; Srodon, J. Deducing Growth Mechanisms for Minerals from the Shapes of Crystal Size Distributions. *Am. J. Sci.* **1998**, *298*, 499–533.

[71] Ferreira, P.J.; O', G.J.L.; Shao-Horn, Y.; Morgan, D.; Makharia, R.; Kocha, S.; Gasteiger, H.A. Instability of Pt/C Electrocatalysts in Proton Exchange Membrane Fuel Cells. *J. Electrochem. Soc.* **2005**, *152*, A2256–A2271.

[72] Blurton, K.F.; Kunz, H.R.; Rutt, D.R. Surface Area Loss of Platinum Supported on Graphite. *Electrochim. Acta* **1978**, *23*, 183–190.

[73] Gruver, G.A.; Pascoe, R.F.; Kunz, H.R. Surface Area Loss of Platinum Supported on Carbon in Phosphoric Acid Electrolyte. *J. Electrochem. Soc.* **1980**, *127*, 1219–1224.

[74] Borup, R.; Meyers, J.; Pivovar, B.; Kim, Y.S.; Mukundan, R.; Garland, N.; Myers, D.; Wilson, M.; Garzon, F.; Wood, D.; Zelenay, P.; More, K.; Stroh, K.; Zawodzinski, T.; Boncella, J.; McGrath, J.E.; Inaba, M.; Miyatake, K.; Hori, M.; Ota, K.; Ogumi, Z.; Miyata, S.; Nishikata, A.; Siroma, Z.; Uchimoto, Y.; Yasuda, K.; Kimijima, K.-I.; Iwashita, N. Scientific Aspects of Polymer Electrolyte Fuel Cell Durability and Degradation. *Chem. Rev. (Washington, DC, U.S.)* **2007**, *107*, 3904–3951.

[75] Aragane, J.; Urushibata, H.; Murahashi, T. Effect of Operational Potential on Performance Decay Rate in a Phosphoric Acid Fuel Cell. *J. Appl. Electrochem.* **1996**, *26*, 147–152.

[76] Yasuda, K.; Taniguchi, A.; Akita, T.; Ioroi, T.; Siroma, Z. Characteristics of a Platinum Black Catalyst Layer with Regard to Platinum Dissolution Phenomena in a Membrane Electrode Assembly. *J. Electrochem. Soc.* **2006**, *153*, A1599–A1603.

[77] Darling, R.M.; Meyers, J.P. Kinetic Model of Platinum Dissolution in PEMFCs. *J. Electrochem. Soc.* **2003**, *150*, A1523–A1527.

[78] Darling, R.M.; Meyers, J.P. Mathematical Model of Platinum Movement in PEM Fuel Cells. *J. Electrochem. Soc.* **2005**, *152*, A242–A247.

[79] Benke, G.; Gnot, W. The Electrochemical Dissolution of Platinum. *Hydrometallurgy* **2002**, *64*, 205–218.

[80] Johnson, D.C.; Napp, D.T.; Bruckenstein, S. A Ring-Disk Electrode Study of the Current/Potential Behaviour of Platinum in 1.0 M Sulphuric and 0.1 M Perchloric Acids. *Electrochim. Acta* **1970**, *15*, 1493–1509.

[81] Kinoshita, K.; Lundquist, J.T.; Stonehart, P. Potential Cycling Effects on Platinum Electrocatalyst Surfaces. *J. Electroanal. Chem. Interfac. Electrochem.* **1973**, *48*, 157–166.

[82] Rand, D.A.J.; Woods, R. A study of the Dissolution of Platinum, Palladium, Rhodium and Gold Electrodes in 1 M Sulphuric Acid by Cyclic Voltammetry. *J. Electroanal. Chem. Interfac Electrochem* **1972**, *35*, 209–218.

[83] Arvia, A.J.; Canullo, J.C.; Custidiano, E.; Perdriel, C.L.; Triaca, W.E. Electrochemical Faceting of Metal Electrodes. *Electrochim. Acta* **1986**, *31*, 1359–1368.

[84] Canullo, J.C.; Triaca, W.E.; Arvia, A.J. Electrochemical Faceting of Single Crystal Platinum Electrodes. *J. Electroanal. Chem.* **1986**, *200*, 397–400.

[85] Egli, W.A.; Visintin, A.; Triaca, W.E.; Arvia, A.J. The Development of Facetting and Roughening at Platinum Polyfacetted Single-Crystal Electrodes in a Chloroplatinic Acid Solution. *Appl. Surf. Sci.* **1993**, *68*, 583–593.

[86] Passalacqua, E.; Antonucci, P.L.; Vivaldi, M.; Patti, A.; Antonucci, V.; Giordano, N.; Kinoshita, K. The Influence of Pt on the Electrooxidation Behaviour of Carbon in Phosphoric Acid. *Electrochim. Acta* **1992**, *37*, 2725–2730.

[87] Kinoshita, K. *Carbon Electrochemical and Physicochemical Properties*. John Wiley & Sons: New York, 1988.

[88] Roen, L.M.; Paik, C.H.; Jarvi, T.D. Electrocatalytic Corrosion of Carbon Support in PEMFC Cathodes. *Electrochem. Solid-State Lett.* **2004**, *7*, A19–A22.

[89] Kangasniemi, K.H.; Condit, D.A.; Jarvi, T.D. Characterization of Vulcan Electrochemically Oxidized under Simulated PEM Fuel Cell Conditions. *J. Electrochem. Soc.* **2004**, *151*, E125–E132.

[90] Mathias, M.F.; Makharia, R.; Gasteiger, H.A.; Conley, J.J.; Fuller, T.J.; Gittleman, C.J.; Kocha, S.S.; Miller, D.P.; Mittelsteadt, C.K.; Xie, T.; Van, S.G.; Yu, P.T. Two Fuel Cell Cars in Every Garage? *Electrochem. Soc. Interface* **2005**, *14*, 24–35.

[91] Oszcipok, M.; Zedda, M.; Riemann, D.; Geckeler, D. Low Temperature Operation and Influence Parameters on the Cold Start Ability of Portable PEMFCs. *J. Power Sources* **2006**, *154*, 404–411.

[92] Fuller, T.F.; Newman, J. Water and Thermal Management in Solid-Polymer-Electrolyte Fuel Cells. *J. Electrochem. Soc.* **1993**,*140*,1218–1225.

[93] Tang, H.; Qi, Z.; Ramani, M.; Elter, J.F. PEM Fuel Cell Cathode Carbon Corrosion due to the Formation of Air/Fuel Boundary at the Anode. *J. Power Sources* **2006**, *158*, 1306–1312.

[94] Tauster, S.J.; Fung, S.C.; Garten, R.L. Strong Metal-Support Interactions. Group 8 Noble Metals Supported on Titanium Dioxide. *J. Am. Chem. Soc.* **1978**,*100*,170–175.

[95] Fu, Q.; Wagner, T. Interaction of Nanostructured Metal Overlayers with Oxide Surfaces. *Surf. Sci. Rep.* **2007**,*62*,431–498.

[96] Horsley, J.A. A Molecular Orbital Study of Strong Metal-Support Interaction Between Platinum and Titanium Dioxide. *J. Am. Chem. Soc*. **1979**, *101*, 2870.

[97] Vajda, S.; Pellin, M.J.; Greeley, J.P.; Marshall, C.L.; Curtiss, L.A.; Ballentine, G.A.; Elam, J.W.; Catillon-Mucherie, S.; Redfern, P.C.; Mehmood, F.; Zapol, P. Subnanometre Platinum Clusters as Highly Active and Selective Catalysts for the Oxidative Dehydrogenation of Propan. *Nat. Mater.* **2009**, *8*, 213–216.

[98] Yoshida, H.; Yazawa, Y.; Hattori, T. Effects of Support and Additive on Oxidation State and Activity of Pt Catalyst in Propane Combustion. *Catal. Today* **2003**, *87*, 19–28.

[99] Lemonidou, A.A.; Nalbandian, L.; Vasalos, I.A. Oxidative Dehydrogenation of Propane over Vanadium Oxide Based Catalysts: Effect of Support and Alkali Promoter. *Catal. Today* **2000**, *61*, 333–341.

[100] Farrauto, R.J.; Lampert, J.K.; Hobson, M.C.; Waterman, E.M. Thermal Decomposition and Reformation of PdO Catalysts Support Effects. *Appl. Catal. B: Environ.* **1995**, *6*, 263–270.

[101] Ratnasamy, C.; Wagner, J.P. Water Gas Shift Catalysis. *Catalysis Reviews: Science and Engineering* **2009**, *51*, 325–440.

[102] Comotti, M.; Li, W.-C.; Spliethoff, B.; Schüth, F. Support Effect in High Activity Gold Catalysts for CO Oxidation. *J. Am. Chem. Soc.* **2005**, *128*, 917–924.

[103] Arrii, S.; Morfin, F.; Renouprez, A.J.; Rousset, J.L. Oxidation of CO on Gold Supported Catalysts Prepared by Laser Vaporization: Direct Evidence of Support Contribution. *J. Am. Chem. Soc.* **2004**, *126*, 1199–1205.

[104] Baughman, R.H.; Zakhidov, A.A.; de Heer, W.A. Carbon Nanotubes—The Route Toward Applications. *Science* **2002**, *297*, 787–792.

[105] Peigney, A.; Laurent, C.; Flahaut, E.; Bacsa, R.R.; Rousset, A. Specific Surface Area of Carbon Nanotubes and Bundles of Carbon Nanotubes. *Carbon* **2001**, *39*, 507–514.

[106] Serp, P.; Corrias, M.; Kalck, P. Carbon Nanotubes and Nanofibers in Catalysis. *Appl. Catal. A: Gen.* **2003**, *253*, 337–358.

[107] Britto, P.J.; Santhanam, K.S.V.; Rubio, A.; Alonso, J.A.; Ajayan, P.M. Improved Charge Transfer at Carbon Nanotube Electrodes. *Adv. Mater.* **1999**, *11*, 154–157.

[108] Li, W.; Liang, C.; Qiu, J.; Zhou, W.; Han, H.; Wei, Z.; Sun, G.; Xin, Q. Carbon Nanotubes as Support for Cathode Catalyst of a Direct Methanol Fuel Cell. *Carbon* **2002**, *40*, 791–794.

[109] Li, W.; Liang, C.; Zhou, W.; Qiu, J.; Zhou; Sun, G.; Xin, Q. Preparation and Characterization of Multiwalled Carbon Nanotube-Supported Platinum for Cathode Catalysts of Direct Methanol Fuel Cells. *J. Phys. Chem. B* **2003**, *107*, 6292–6299.

[110] Matsumoto, T.; Komatsu, T.; Arai, K.; Yamazaki, T.; Kijima, M.; Shimizu, H.; Takasawa, Y.; Nakamura, J. Reduction of Pt Usage in Fuel Cell Electrocatalysts with Carbon Nanotube Electrodes. *Chem. Commun*. (Cambridge, U.K.) **2004**, 840–841.

[111] Wang, X.; Waje, M.; Yan, Y. CNT-Based Electrodes with High Efficiency for PEMFCs. *Electrochem. Solid-State Lett.* **2005**, *8*, A42–A44.

[112] Girishkumar, G.; Rettker, M.; Underhile, R.; Binz, D.; Vinodgopal, K.; McGinn, P.; Kamat, P. Single-Wall Carbon Nanotube-Based Proton Exchange Membrane Assembly for Hydrogen Fuel Cells. *Langmuir* **2005**, *21*, 8487–8494.

[113] Tang, J.M.; Jensen, K.; Waje, M.; Li, W.; Larsen, P.; Pauley, K.; Chen, Z.; Ramesh, P.; Itkis, M.E.; Yan, Y.; Haddon, R.C. High Performance Hydrogen Fuel Cells

with Ultralow Pt Loading Carbon Nanotube Thin Film Catalysts. *J. Phys. Chem. C* **2007**, *111*, 17901–17904.

[114] Yu, R.; Chen, L.; Liu, Q.; Lin, J.; Tan, K.-L.; Ng, S.C.; Chan, H.S.O.; Xu, G.-Q.; Hor, T.S.A. Platinum Deposition on Carbon Nanotubes via Chemical Modification. *Chem. Mater.* **1998**, *10*, 718–722.

[115] Li, X.; Ge, S.; Hui, C.L.; Hsing, I.-M. Well-Dispersed Multiwalled Carbon Nanotubes Supported Platinum Nanocatalysts for Oxygen Reduction. *Electrochem. Solid-State Lett.* **2004**, 7, A286–A289.

[116] Saha, M.S.; Kundu, A. Functionalizing Carbon Nanotubes for Proton Exchange Membrane Fuel Cells Electrode. *J. Power Sources* **2010**, *195*, 6255–6261.

[117] Xing, Y. Synthesis and Electrochemical Characterization of Uniformly-Dispersed High Loading Pt Nanoparticles on Sonochemically-Treated Carbon Nanotubes. *J. Phys. Chem. B* **2004**, *108*, 19255–19259.

[118] He, C.; Song, S.; Liu, J.; Maragou, V.; Tsiakaras, P. KOH-Activated Multi-Walled Carbon Nanotubes as Platinum Supports for Oxygen Reduction Reaction. *J. Power Sources* **2010**, *195*, 7409–7414.

[119] Hernández-Fernández, P.; Montiel, M.; Ocón, P.; de la Fuente, J.L.G.; García-Rodríguez, S.; Rojas, S.; Fierro, J.L.G. Functionalization of Multi-Walled Carbon Nanotubes and Application as Supports for Electrocatalysts in Proton-Exchange Membrane Fuel Cell. *Appl. Catal. B: Environ.* **2010**, *99*, 343–352.

[120] Centi, G.; Gangeri, M.; Fiorello, M.; Perathoner, S.; Amadou, J.; Bègin, D.; Ledoux, M.J.; Pham-Huu, C.; Schuster, M.E.; Su, D.S.; Tessonnier, J.P.; Schlögl, R. The Role of Mechanically Induced Defects in Carbon Nanotubes to Modify the Properties of Electrodes for PEM Fuel Cell. *Catal. Today* **2009**, *147*, 287–299.

[121] Xu, Y.; Lin, X. Selectively Attaching Pt-Nano-Clusters to the Open Ends and Defect Sites on Carbon Nanotubes for Electrochemical Catalysis. *Electrochim. Acta* **2007**, *52*, 5140–5149.

[122] Wang, J.-G.; Lv, Y.-A.; Li, X.-N.; Dong, M. Point-Defect Mediated Bonding of Pt Clusters on (5,5) Carbon Nanotubes. *J. Phys. Chem. C* **2008**, *113*, 890–893.

[123] Matsubara, K.; Waki, K. The Effect of O-Functionalities for the Electrochemical Reduction of Oxygen on MWCNTs in Acid Media. *Electrochem. Solid-State Lett.* **2010**, *13*, F7–F9.

[124] Georgakilas, V.; Gournis, D.; Tzitzios, V.; Pasquato, L.; Guldi, D.M.; Prato, M. Decorating Carbon Nanotubes with Metal or Semiconductor Nanoparticles. *J. Mater. Chem.* **2007**, *17*, 2679–2694.

[125] Shao, Y.; Yin, G.; Wang, J.; Gao, Y.; Shi, P. Multi-Walled Carbon Nanotubes Based Pt Electrodes Prepared with in situ Ion Exchange Method for Oxygen Reduction. *J. Power Sources* **2006**, *161*, 47–53.

[126] Wang, J.; Yin, G.; Shao, Y.; Wang, Z.; Gao, Y. Platinum Deposition on Multiwalled Carbon Nanotubes by Ion-Exchange Method as Electrocatalysts for Oxygen Reduction. *J. Electrochem. Soc.* **2007**, *154*, B687–B693.

[127] Lee, K.; Zhang, J.; Wang, H.; Wilkinson, D.P. Progress in the Synthesis of Carbon Nanotube- and Nanofiber-Supported Pt Electrocatalysts for PEM Fuel Cell Catalysis. *J. Appl. Electrochem.* **2006**, *36*, 507–522.

[128] Li, X.; Hsing, I.M. The Effect of the Pt Deposition Method and the Support on Pt Dispersion on Carbon Nanotubes. *Electrochim. Acta* **2006**, *51*, 5250–5258.

[129] Alexeyeva, N.; Tammeveski, K.; Lopez-Cudero, A.; Solla-Gullón, J.; Feliu, J.M. Electroreduction of Oxygen on Pt Nanoparticle/Carbon Nanotube Nanocomposites in Acid and Alkaline Solutions. *Electrochim. Acta* **2010**, *55*, 794–803.

[130] Liu, Z.; Gan, L.M.; Hong, L.; Chen, W.; Lee, J.Y. Carbon-Supported Pt Nanoparticles as Catalysts for Proton Exchange Membrane Fuel Cells. *J. Power Sources* **2005**, *139*, 73–78.

[131] Knupp, S.L.; Li, W.; Paschos, O.; Murray, T.M.; Snyder, J.; Haldar, P. The Effect of Experimental Parameters on the Synthesis of Carbon Nanotube/Nanofiber Supported Platinum by Polyol Processing Techniques. *Carbon* **2008**, *46*, 1276–1284.

[132] Zhang, W.; Chen, J.; Swiegers, G.F.; Ma, Z.-F.; Wallace, G.G. Microwave-Assisted Synthesis of Pt/CNT Nanocomposite Electrocatalysts for PEM Fuel Cells. *Nanoscale* **2010**, *2*, 282–286.

[133] Lin, Y.; Cui, X.; Yen, C.; Wai, C.M. Platinum/Carbon Nanotube Nanocomposite Synthesized in Supercritical Fluid as Electrocatalysts for Low-Temperature Fuel Cells. *J. Phys. Chem. B* **2005**, *109*, 14410–14415.

[134] Bayrakçeken, A.; Smirnova, A.; Kitkamthorn, U.; Aindow, M.; Türker L.; Eroglu, I.; Erkey, C. Pt-Based Electrocatalysts for Polymer Electrolyte Membrane Fuel Cells Prepared by Supercritical Deposition Technique. *J. Power Sources* **2008**, *179*, 532–540.

[135] Liu, C.; Wang, C.-C.; Kei, C.-C.; Hsueh, Y.-C.; Perng, T.-P. Atomic Layer Deposition of Platinum Nanoparticles on Carbon Nanotubes for Application in Proton-Exchange Membrane Fuel Cells. *Small* **2009**, *5*, 1535–1538.

[136] Hasché, F.; Oezaslan, M.; Strasser, P. Activity, Stability and Degradation of Multi Walled Carbon Nanotube (MWCNT) Supported Pt Fuel Cell Electrocatalysts. *Phys. Chem. Chem. Phys.* **2010**, *12*, 15251–15258.

[137] Rajalakshmi, N.; Ryu, H.; Shaijumon, M.M.; Ramaprabhu, S. Performance of Polymer Electrolyte Membrane Fuel Cells with Carbon Nanotubes as Oxygen Reduction Catalyst Support Material. *J. Power Sources* **2005**, *140*, 250–257.

[138] Villers, D.; Sun, S.H.; Serventi, A.M.; Dodelet, J.P.; Désilets, S. Characterization of Pt Nanoparticles Deposited onto Carbon Nanotubes Grown on Carbon Paper and Evaluation of This Electrode for the Reduction of Oxygen. *J. Phys. Chem. B* **2006**, *110*, 25916–25925.

[139] Saha, M.S.; Li, R.; Sun, X. High Loading and Monodispersed Pt Nanoparticles on Multiwalled Carbon Nanotubes for High Performance Proton Exchange Membrane Fuel Cells. *J. Power Sources* **2008**, *177*, 314–322.

[140] Saminathan, K.; Kamavaram, V.; Veedu, V.; Kannan, A.M. Preparation and Evaluation of Electrodeposited Platinum Nanoparticles on in situ Carbon Nanotubes Grown Carbon Paper for Proton Exchange Membrane Fuel Cells. *Int. J. Hydrogen Energy* **2009**, *34*, 3838–3844.

[141] Prehn, K.; Adelung, R.; Heinen, M.; Nunes, S.P.; Schulte, K. Catalytically Active CNT-Polymer-Membrane Assemblies: From Synthesis to Application. *J. Membr. Sci.* **2008**, *321*, 123–130.

[142] Rao, S.M.; Xing, Y. Simulation of Nanostructured Electrodes for Polymer Electrolyte Membrane Fuel Cells. *J. Power Sources* **2008**, *185*, 1094–1100.

[143] Zhang, W.; Chen, J.; Minett, A.I.; Swiegers, G.F.; Too, C.O.; Wallace, G.G. Novel ACNT Arrays Based MEA Structure-Nano-Pt Loaded ACNT/Nafion/ACNT for Fuel Cell Applications. *Chem. Commun*. (Cambridge, U.K.) **2010**, *46*, 4824–4826.

[144] Gasteiger, H.A.; Kocha, S.S.; Sompalli, B.; Wagner, F.T. Activity Benchmarks and Requirements for Pt, Pt-Alloy, and Non-Pt Oxygen Reduction Catalysts for PEMFCs. *Appl. Catal. B: Environ.* **2005**, *56*, 9–35.

[145] Kongkanand, A.; Kuwabata, S.; Girishkumar, G.; Kamat, P. Single-Wall Carbon Nanotubes Supported Platinum Nanoparticles with Improved Electrocatalytic Activity for Oxygen Reduction Reaction. *Langmuir* **2006**, *22*, 2392–2396.

[146] Garsany, Y.; Baturina, O.A.; Swider-Lyons, K.E.; Kocha, S.S. Experimental Methods for Quantifying the Activity of Platinum Electrocatalysts for the Oxygen Reduction Reaction. *Anal. Chem.* **2010**, *82*, 6321–6328.

[147] Tang, Z.; Chua, D.H.C. Investigation of Pt/CNT-Based Electrodes in Proton Exchange Membrane Fuel Cells Using AC Impedance Spectroscopy. *J. Electrochem. Soc.* **2010**, *157*, B868–B873.

[148] Wang, X.; Li, W.; Chen, Z.; Waje, M.; Yan, Y. Durability Investigation of Carbon Nanotube as Catalyst Support for Proton Exchange Membrane Fuel Cell. *J. Power Sources* **2006**, *158*, 154–159.

[149] Shao, Y.; Yin, G.; Gao, Y.; Shi, P. Durability Study of Pt/C and Pt/CNTs Catalysts under Simulated PEM Fuel Cell Conditions. *J. Electrochem. Soc.* **2006**, *153*, A1093–A1097.

[150] Li, L.; Xing, Y. Electrochemical Durability of Carbon Nanotubes in Noncatalyzed and Catalyzed Oxidations. *J. Electrochem. Soc.* **2006**, *153*, A1823–A1828.

[151] Li, L.; Xing, Y. Electrochemical Durability of Carbon Nanotubes at 80°C. *J. Power Sources* **2008**, *178*, 75–79.

[152] Wang, J.; Yin, G.; Shao, Y.; Wang, Z.; Gao, Y. Electrochemical durability Investigation of Single-Walled and Multi-Walled Carbon Nanotubes under Potentiostatic Conditions. *J. Power Sources* **2008**, *176*, 128–131.

[153] Wang, J.; Yin, G.; Shao, Y.; Wang, Z.; Gao, Y. Investigation of Further Improvement of Platinum Catalyst Durability with Highly Graphitized Carbon Nanotubes Support. *J. Phys. Chem. C* **2008**, *112*, 5784–5789.

[154] Tang, Z.; Ng, H.Y.; Lin, J.; Wee, A.T.S.; Chua, D.H.C. Pt/CNT-Based Electrodes with High Electrochemical Activity and Stability for Proton Exchange Membrane Fuel Cells. *J. Electrochem. Soc.* **2010**, *157*, B245–B250.

[155] Novoselov, K.S.; Geim, A.K.; Morozov, S.V.; Jiang, D.; Zhang, Y.; Dubonos, S.V.; Grigorieva, I.V.; Firsov, A.A. Electric Field Effect in Atomically Thin Carbon Films. *Science* **2004**, *306*, 666–669.

[156] Geim, A.K.; Novoselov, K.S. The Rise of Graphene. *Nat. Mater.* **2007**, *6*, 183–191.

[157] Geim, A.K. Graphene: Status and Prospects. *Science* **2009**, *324*, 1530–1534.

[158] Park, S.; Ruoff, R.S. Chemical Methods for the Production of Graphenes. *Nat. Nano.* **2009**, *4*, 217–224.

[159] Qin, W.; Li, X. A Theoretical Study on the Catalytic Synergetic Effects of Pt/Graphene Nanocomposites. *J. Phys. Chem. C* **2010**, *114*, 19009–19015.

[160] Boukhvalov, D.W.; Katsnelson, M.I. Modeling of Graphite Oxide. *J. Am. Chem. Soc.* **2008**, *130*, 10697–10701.

[161] Pumera, M. Graphene-Based Nanomaterials and Their Electrochemistry. *Chem. Soc. Rev.* **2010**, *39*, 4146–4157.

[162] Si, Y.; Samulski, E.T. Exfoliated Graphene Separated by Platinum Nanoparticles. *Chem. Mater.* **2008**, *20*, 6792–6797.

[163] Zhu, C.; Guo, S.; Zhai, Y.; Dong, S. Layer-by-Layer Self-Assembly for Constructing a Graphene/Platinum Nanoparticle Three-Dimensional Hybrid Nanostructure Using Ionic Liquid as a Linker. *Langmuir* **2010**, *26*, 7614–7618.

[164] Gotoh, K.; Kawabata, K.; Fujii, E.; Morishige, K.; Kinumoto, T.; Miyazaki, Y.; Ishida, H. The Use of Graphite Oxide to Produce Mesoporous Carbon Supporting Pt, Ru, or Pd Nanoparticles. *Carbon* **2009**, *47*, 2120–2124.

[165] Seger, B.; Kamat, P.V. Electrocatalytically Active Graphene-Platinum Nanocomposites. Role of 2-D Carbon Support in PEM Fuel Cells. *J. Phys. Chem. C* **2009**, *113*, 7990–7995.

[166] Schniepp, H.C.; Li, J.-L.; McAllister, M.J.; Sai, H.; Herrera-Alonso, M.; Adamson, D.H.; Prud'homme, R.K.; Car, R.; Saville, D.A.; Aksay, I.A. Functionalized Single Graphene Sheets Derived from Splitting Graphite Oxide. *J. Phys. Chem. B* **2006**, *110*, 8535–8539.

[167] McAllister, M.J.; Li, J.-L.; Adamson, D.H.; Schniepp, H.C.; Abdala, A.A.; Liu, J.; Herrera-Alonso, M.; Milius, D.L.; Car, R.; Prud'homme, R.K.; Aksay, I.A. Single Sheet Functionalized Graphene by Oxidation and Thermal Expansion of Graphite. *Chem. Mater.* **2007**, *19*, 4396–4404.

[168] Kou, R.; Shao, Y.; Wang, D.; Engelhard, M.H.; Kwak, J.H.; Wang, J.; Viswanathan, V.V.; Wang, C.; Lin, Y.; Wang, Y.; Aksay, I.A.; Liu, J. Enhanced Activity and Stability of Pt Catalysts on Functionalized Graphene Sheets for Electrocatalytic Oxygen Reduction. *Electrochem. Commun.* **2009**, *11*, 954–957.

[169] Hughes, T.V.; Chambers, C.R. *Manufacture of Carbon Filaments*; U.S. Patent 405, 480, 1989.

[170] De Jong, K.P.; Geus, J.W. Carbon Nanofibers: Catalytic Synthesis and Applications. *Catal. Rev.: Sci. & Eng.* **2000**,.*42*,.481–510.

[171] Bessel, C.A.; Laubernds, K.; Rodriguez, N.M.; Baker, R.T.K. Graphite Nanofibers as an Electrode for Fuel Cell Applications. *J. Phys. Chem. B* **2001**, *105*, 1115–1118.

[172] Zaragoza-Martín F.; Sopeña-Escario, D.; Morallón, E.; de Lecea, C.S.-M. Pt/carbon Nanofibers Electrocatalysts for Fuel Cells: Effect of the Support Oxidizing Treatment. *J. Power Sources* **2007**, *171*, 302–309.

[173] Calvillo, L.; Gangeri, M.; Perathoner, S.; Centi, G.; Moliner, R.; Lázaro, M. J.. Effect of the Support Properties on the Preparation and Performance of Platinum Catalysts Supported on Carbon Nanofibers. *J. Power Sources* **2009**, *192*, 144–150.

[174] Oh, H.-S.; Kim, K.; Ko, Y.-J.; Kim, H. Effect of Chemical Oxidation of CNFs on the Electrochemical Carbon Corrosion in Polymer Electrolyte Membrane Fuel Cells. *Int. J. Hydrogen Energy* **2010**, *35*, 701–708.

[175] Li, W.; Waje, M.; Chen, Z.; Larsen, P.; Yan, Y. Platinum Nanopaticles Supported on Stacked-Cup Carbon Nanofibers as Electrocatalysts for Proton Exchange Membrane Fuel Cell. *Carbon* **2010**, *48*, 995–1003.

[176] Guha, A.; Lu, W.; Zawodzinski Jr, T.A.; Schiraldi, D.A. Surface-Modified Carbons as Platinum Catalyst Support for PEM Fuel Cells. *Carbon* **2007**, *45*, 1506–1517.

[177] Yuan, F.; Yu, H.K.; Ryu, H. Preparation and Characterization of Carbon Nanofibers as Catalyst Support Material for PEMFC. *Electrochim. Acta* **2004**, *50*, 685–691.

[178] Fangli, Y.; Hojin, R. The Synthesis, Characterization, and Performance of Carbon Nanotubes and Carbon Nanofibres with Controlled Size and Morphology as a Catalyst Support Material for a Polymer Electrolyte Membrane Fuel Cell. *Nanotechnology* **2004**, *15*, S596.

[179] Zhang, L.; Cheng, B.; Samulski, E.T. In situ Fabrication of Dispersed, Crystalline Platinum Nanoparticles Embedded in Carbon Nanofibers. *Chem. Phys. Lett.* **2004**, *398*, 505–510.

[180] Caillard, A.; Charles, C.; Boswell, R.; Brault, P. Integrated Plasma Synthesis of Efficient Catalytic Nanostructures for Fuel Cell Electrodes. *Nanotechnology* **2007**, *18*, 305603.

[181] Guha, A.; Zawodzinski Jr, T.A.; Schiraldi, D.A. Evaluation of Electrochemical Performance for Surface-Modified Carbons as Catalyst Support in Polymer Electrolyte Membrane (PEM) Fuel Cells. *J. Power Sources* **2007**, *172*, 530–541.

[182] Wallnöfer, E.; Perchthaler, M.; Hacker, V.; Squadrito, G. Optimisation of Carbon Nanofiber Based Electrodes for Polymer Electrolyte Membrane Fuel Cells Prepared by a Sedimentation Method. *J. Power Sources* **2009**, *188*, 192–198.

[183] Biddinger, E.J.; Ozkan, U.S. Role of Graphitic Edge Plane Exposure in Carbon Nanostructures for Oxygen Reduction Reaction. *J. Phys. Chem. C* **2010**, *114*, 15306–15314.

[184] Ismagilov, Z.R.; Kerzhentsev, M.A.; Shikina, N.V.; Lisitsyn, A.S.; Okhlopkova, L.B.; Barnakov, C.N.; Sakashita, M.; Iijima, T.; Tadokoro, K. Development of Active Catalysts for Low Pt Loading Cathodes of PEMFC by Surface Tailoring of Nanocarbon Materials. *Catal. Today* **2005**, *102–103*, 58–66.

[185] Al-Muhtaseb, S.A.; Ritter, J.A. Preparation and Properties of Resorcinol—Formaldehyde Organic and Carbon Gels. *Adv. Mater.* **2003**, *15*, 101–114.

[186] Job, N.; Thèry, A.; Pirard, R.; Marien, J.; Kocon, L.; Rouzaud, J.-N.; Béguin, F.; Pirard, J.-P. Carbon Aerogels, Cryogels and Xerogels: Influence of the Drying Method on the Textural Properties of Porous Carbon Materials. *Carbon* **2005**, *43*, 2481–2494.

[187] Pekala, R.W. U.S. Patent 4873218, 1989.

[188] Gavalda, S.; Kaneko, K.; Thomson, K.T.; Gubbins, K.E. Molecular Modeling of Carbon Aerogels. *Coll. & Surf. A: Physicochem. Eng. Aspects* **2001**, *187–188*, 531–538.

[189] Moreno-Castilla, C.; Maldonado-Hódar, F. J. Carbon Aerogels for Catalysis Applications: An Overview. *Carbon* **2005**, *43*, 455–465.

[190] Smirnova, A.; Dong, X.; Hara, H.; Vasiliev, A.; Sammes, N. Novel Carbon Aerogel-Supported Catalysts for PEM Fuel Cell Application. *Int. J. Hydrogen Energy* **2005**, *30*, 149–158.

[191] Marie, J.; Chenitz, R.; Chatenet, M.; Berthon-Fabry, S.; Cornet, N.; Achard, P. Highly Porous PEM Fuel Cell Cathodes Based on Low Density Carbon Aerogels as Pt-Support: Experimental Study of the Mass-Transport Losses. *J. Power Sources* **2009**, *190*, 423–434.

[192] Job, N.; Maillard, F.; Marie, J.; Berthon-Fabry, S.; Pirard, J.-P.; Chatenet, M. Electrochemical Characterization of Pt/Carbon Xerogel and Pt/Carbon Aerogel Catalysts: First Insights into the Influence of the Carbon Texture on the Pt Nanoparticle Morphology and Catalytic Activity. *J. Mater. Sci.* **2009**, *44*, 6591–6600.

[193] Job, N.; Marie, J.; Lambert, S.; Berthon-Fabry, S.; Achard, P. Carbon Xerogels as Catalyst Supports for PEM Fuel Cell Cathode. *Energy Convers. Manage.* **2008**, *49*, 2461–2470.

[194] Liu, B.; Creager, S. Carbon Xerogels as Pt Catalyst Supports for Polymer Electrolyte Membrane Fuel-Cell Applications. *J. Power Sources* **2010**, *195*, 1812–1820.

[195] Du, H.; Gan, L.; Li, B.; Wu, P.; Qiu, Y.; Kang, F.; Fu, R.; Zeng, Y. Influences of Mesopore Size on Oxygen Reduction Reaction Catalysis of Pt/Carbon Aerogels. *J. Phys. Chem. C* **2007**, *111*, 2040–2043.

[196] Kimijima, K.I.; Hayashi, A.; Umemura, S.; Miyamoto, J.; Sekizawa, K.; Yoshida, T.; Yagi, I. Oxygen Reduction Reactivity of Precisely Controlled Nanostructured Model Catalysts. *J. Phys. Chem. C* **2010**, *114*, 14675–14683.

[197] Marie, J.; Berthon-Fabry, S.; Achard, P.; Chatenet, M.; Pradourat, A.; Chainet, E. Highly Dispersed Platinum on Carbon Aerogels as Supported Catalysts for PEM Fuel Cell-Electrodes: Comparison of Two Different Synthesis Paths. *J. Non-Cryst. Solids* **2004**, *350*, 88–96.

[198] Yoon, S.B.; Sohn, K.; Kim, J.Y.; Shin, C.H.; Yu, J.S.; Hyeon, T. Fabrication of Carbon Capsules with Hollow Macroporous Core/Mesoporous Shell Structures. *Adv. Mater.* **2002**, *14*, 19–21.

[199] Fang, B.; Kim, M.; Kim, J.H.; Yu, J.-S. Controllable Synthesis of Hierarchical Nanostructured Hollow Core/Mesopore Shell Carbon for Electrochemical Hydrogen Storage. *Langmuir* **2008**, *24*, 12068–12072.

[200] Fang, B.; Kim, J.H.; Lee, C.; Yu, J.-S. Hollow Macroporous Core/Mesoporous Shell Carbon with a Tailored Structure as a Cathode Electrocatalyst Support for Proton Exchange Membrane Fuel Cells. *J. Phys. Chem. C* **2007**, *112*, 639–645.

[201] Fang, B.; Kim, J.H.; Kim, M.; Kim, M.; Yu, J.-S. Hierarchical Nanostructured Hollow Spherical Carbon with Mesoporous Shell as a Unique Cathode Catalyst Support in Proton Exchange Membrane Fuel Cell. *Phys. Chem. Chem. Phys.* **2009**, *11*, 1380–1387.

[202] Kim, J.H.; Yu, J.-S. Erythrocyte-Like Hollow Carbon Capsules and Their Application in Proton Exchange Membrane Fuel Cells. *Phys. Chem. Chem. Phys.* **2010**, *12*, 15301–15308.

[203] Fang, B.; Kim, J.H.; Kim, M.; Yu, J.-S. Ordered Hierarchical Nanostructured Carbon as a Highly Efficient Cathode Catalyst Support in Proton Exchange Membrane Fuel Cell. *Chem. Mater.* **2009**, *21*, 789–796.

[204] FiçIcIlar, B.; Bayrakçeken, A.; Eroglu, I. Pt Incorporated Hollow Core Mesoporous Shell Carbon Nanocomposite Catalyst for Proton Exchange Membrane Fuel Cells. *Int. J. Hydrogen Energy* **2010**, *35*, 9924–9933.

[205] Ryoo, R.; Joo, S.H.; Jun, S. Synthesis of Highly Ordered Carbon Molecular Sieves via Template-Mediated Structural Transformation. *J. Phys. Chem. B* **1999**, *103*, 7743–7746.

[206] Jun, S.; Joo, S.H.; Ryoo, R.; Kruk, M.; Jaroniec, M.; Liu, Z.; Ohsuna, T.; Terasaki, O. Synthesis of New, Nanoporous Carbon with Hexagonally Ordered Mesostructure. *J. Am. Chem. Soc.* **2000**, *122*, 10712–10713.

[207] Lee, J.; Kim, J.; Hyeon, T. Recent Progress in the Synthesis of Porous Carbon Materials. *Adv. Mater.* **2006**, *18*, 2073–2094.

[208] Ryoo, R.; Joo, S.H.; Kruk, M.; Jaroniec, M. Ordered Mesoporous Carbons. *Adv. Mater.* **2001**, *13*, 677–681.

[209] Xia, Y.; Yang, Z.; Mokaya, R. Templated Nanoscale Porous Carbons. *Nanoscale* **2010**, *2*, 639–659.

[210] Meng, Y.; Gu, D.; Zhang, F.; Shi, Y.; Yang, H.; Li, Z.; Yu, C.; Tu, B.; Zhao, D. Ordered Mesoporous Polymers and Homologous Carbon Frameworks: Amphiphilic Surfactant Templating and Direct Transformation. *Angewandte Chemie Intl. Ed.* **2005**, *44*, 7053–7059.

[211] Shrestha, S.; Mustain, W.E. Properties of Nitrogen-Functionalized Ordered Mesoporous Carbon Prepared Using Polypyrrole Precursor. *J. Electrochem. Soc.* **2010**, *157*, B1665–B1672.

[212] Song, S.; Liang, Y.; Li, Z.; Wang, Y.; Fu, R.; Wu, D.; Tsiakaras, P. Effect of Pore Morphology of Mesoporous Carbons on the Electrocatalytic Activity of Pt Nanoparticles for Fuel Cell Reactions. *Appl. Catal. B: Environ.* **2010**, *98*, 132–137.

[213] Du, C.Y.; Yang, T.; Shi, P.F.; Yin, G.P.; Cheng, X.Q. Performance Analysis of the Ordered and The Conventional Catalyst Layers in Proton Exchange Membrane Fuel Cells. *Electrochim. Acta* **2006**, *51*, 4934–4941.

[214] Joo, S.H.; Choi, S.J.; Oh, I.; Kwak, J.; Liu, Z.; Terasaki, O.; Ryoo, R. Ordered Nanoporous Arrays of Carbon Supporting High Dispersions of Platinum Nanoparticles. *Nature* **2001**, *412*, 169–172.

[215] Hayashi, A.; Notsu, H.; Kimijima, K.I.; Miyamoto, J.; Yagi, I. Preparation of Pt/Mesoporous Carbon (MC) Electrode Catalyst and Its Reactivity toward Oxygen Reduction. *Electrochim. Acta* **2008**, *53*, 6117–6125.

[216] Hayashi, A.; Kimijima, K.I.; Miyamoto, J.; Yagi, I. Oxygen Transfer and Storage Processes inside the Mesopores of Platinum-Deposited Mesoporous Carbon Catalyst Thin-Layer Electrode. *J. Phys. Chem. C* **2009**, *113*, 12149–12153.

[217] Ding, J.; Chan, K.-Y.; Ren, J.; Xiao, F.-S. Platinum and Platinum-Ruthenium Nanoparticles Supported on Ordered Mesoporous Carbon and Their Electrocatalytic Performance for Fuel Cell Reactions. *Electrochim. Acta* **2005**, *50*, 3131–3141.

[218] Ambrosio, E.P.; Francia, C.; Manzoli, M.; Penazzi, N.; Spinelli, P. Platinum Catalyst Supported on Mesoporous Carbon for PEMFC. *Int. J. Hydrogen Energy* **2008**, *33*, 3142–3145.

[219] Ambrosio, E.P.; Dumitrescu, M.A.; Francia, C.; Gerbaldi, C.; Spinelli, P. Ordered Mesoporous Carbons as Catalyst Support for PEM Fuel Cells. *Fuel Cells* **2009**, *9*, 197–200.

[220] Ambrosio, E.; Francia, C.; Gerbaldi, C.; Penazzi, N.; Spinelli, P.; Manzoli, M.; Ghiotti, G. Mesoporous Carbons as Low Temperature Fuel Cell Platinum Catalyst Supports. *J. Appl. Electrochem.* **2008**, *38*, 1019–1027.

[221] Wikander, K.; Ekström, H.; Palmqvist, A.E.C.; Lundblad, A.; Holmberg, K.; Lindbergh, G. Alternative Catalysts and Carbon Support Material for PEMFC. *Fuel Cells* **2006**, *6*, 21–25.

[222] Joo, S.H.; Kwon, K.; You, D.J.; Pak, C.; Chang, H.; Kim, J.M. Preparation of High Loading Pt Nanoparticles on Ordered Mesoporous Carbon with a Controlled Pt Size and Its Effects on Oxygen Reduction and Methanol Oxidation Reactions. *Electrochim. Acta* **2009**, *54*, 5746–5753.

[223] Liu, S.-H.; Chiang, C.-C.; Wu, M.-T.; Liu, S.-B. Electrochemical Activity and Durability of Platinum Nanoparticles Supported on Ordered Mesoporous Carbons for Oxygen Reduction Reaction. *Int. J. Hydrogen Energy* **2010**, *35*, 8149–8154.

[224] Gupta, G.; Slanac, D.A.; Kumar, P.; Wiggins-Camacho, J.D.; Kim, J.; Ryoo, R.; Stevenson, K.J.; Johnston, K.P. Highly Stable Pt/Ordered Graphitic Mesoporous Carbon Electrocatalysts for Oxygen Reduction. *J. Phys. Chem. C* **2010**, *114*, 10796–10805.

[225] Shanahan, P.V.; Xu, L.; Liang, C.; Waje, M.; Dai, S.; Yan, Y.S. Graphitic Mesoporous Carbon as a Durable Fuel Cell Catalyst Support. *J. Power Sources* **2008**, *185*, 423–427.

[226] Gong, K.; Du, F.; Xia, Z.; Durstock, M.; Dai, L. Nitrogen-Doped Carbon Nanotube Arrays with High Electrocatalytic Activity for Oxygen Reduction. *Science* **2009**, *323*, 760–764.

[227] Subramanian, N.P.; Li, X.; Nallathambi, V.; Kumaraguru, S.P.; Colon-Mercado, H.; Wu, G.; Lee, J.-W.; Popov, B.N. Nitrogen-Modified Carbon-Based Catalysts for Oxygen Reduction Reaction in Polymer Electrolyte Membrane Fuel Cells. *J. Power Sources* **2009**, *188*, 38–44.

[228] Liu, R.; Wu, D.; Feng, X.; Müllen, K. Nitrogen-Doped Ordered Mesoporous Graphitic Arrays with High Electrocatalytic Activity for Oxygen Reduction. *Angewandte Chemie Intl. Ed.* **2010**, *49*, 2565–2569.

[229] Wang, X.; Lee, J.S.; Zhu, Q.; Liu, J.; Wang, Y.; Dai, S. Ammonia-Treated Ordered Mesoporous Carbons as Catalytic Materials for Oxygen Reduction Reaction. *Chem. Mater.* **2010**, *22*, 2178–2180.

[230] Higgins, D.C.; Meza, D.; Chen, Z. Nitrogen-Doped Carbon Nanotubes as Platinum Catalyst Supports for Oxygen Reduction Reaction in Proton Exchange Membrane Fuel Cells. *J. Phys. Chem. C* **2010**, *114*, 21982–21988.

[231] Lee, K.R.; Lee, K.U.; Lee, J.W.; Ahn, B.T.; Woo, S.I. Electrochemical Oxygen Reduction on Nitrogen Doped Graphene Sheets in Acid Media. *Electrochem. Commun.* **2010**, *12*, 1052–1055.

[232] Rao, C.V.; Cabrera, C.R.; Ishikawa, Y. In Search of the Active Site in Nitrogen-Doped Carbon Nanotube Electrodes for the Oxygen Reduction Reaction. *J. Phys. Chem. Lett.* **2010**, *1*, 2622–2627.

[233] Roy, S.C.; Christensen, P.A.; Hamnett, A.; Thomas, K.M.; Trapp, V. Direct Methanol Fuel Cell Cathodes with Sulfur and Nitrogen-Based Carbon Functionality. *J. Electrochem. Soc.* **1996**, *143*, 3073–3079.

[234] Vijayaraghavan, G.; Stevenson, K.J. Synergistic Assembly of Dendrimer-Templated Platinum Catalysts on Nitrogen-Doped Carbon Nanotube Electrodes for Oxygen Reduction. *Langmuir* **2007**, *23*, 5279–5282.

[235] Imran Jafri, R.; Rajalakshmi, N.; Ramaprabhu, S. Nitrogen Doped Graphene Nanoplatelets as Catalyst Support for Oxygen Reduction Reaction in Proton Exchange Membrane Fuel Cell. *J. Mater. Chem.* **2010**, *20*, 7114–7117.

[236] Jafri, R.I.; Rajalakshmi, N.; Ramaprabhu, S. Nitrogen-Doped Multi-Walled Carbon Nanocoils as Catalyst Support for Oxygen Reduction Reaction in Proton Exchange Membrane Fuel Cell. *J. Power Sources* **2010**, *195*, 8080–8083.

[237] Li, X.; Park, S.; Popov, B.N. Highly Stable Pt and PtPd Hybrid Catalysts Supported on a Nitrogen-Modified Carbon Composite for Fuel Cell Application. *J. Power Sources* **2010**, *195*, 445–452.

[238] Su, F.; Tian, Z.; Poh, C.K.; Wang, Z.; Lim, S.H.; Liu, Z.; Lin, J. Pt Nanoparticles Supported on Nitrogen-Doped Porous Carbon Nanospheres as an Electrocatalyst for Fuel Cells. *Chem. Mater.* **2009**, *22*, 832–839.

[239] Zhou, Y.; Pasquarelli, R.; Holme, T.; Berry, J.; Ginley, D.; O'Hayre, R. Improving PEM Fuel Cell Catalyst Activity and Durability Using Nitrogen-Doped Carbon Supports: Observations from Model Pt/HOPG Systems. *J. Mater. Chem.* **2009**, *19*, 7830–7838.

[240] Holme, T.; Zhou, Y.; Pasquarelli, R.; O'Hayre, R. First Principles Study of Doped Carbon Supports for Enhanced Platinum Catalysts. *Phys. Chem. Chem. Phys.* **2010**, *12*, 9461–9468.

[241] Groves, M.N.; Chan, A.S.W.; Malardier-Jugroot, C.; Jugroot, M. Improving Platinum Catalyst Binding Energy to Graphene through Nitrogen Doping. *Chem. Phys. Lett.* **2009**, *481*, 214–219.

[242] Maldonado, S.; Stevenson, K.J. Influence of Nitrogen Doping on Oxygen Reduction Electrocatalysis at Carbon Nanofiber Electrodes. *J. Phys. Chem. B* **2005**, *109*, 4707–4716.

[243] Baker, W.S.; Long, J.W.; Stroud, R.M.; Rolison, D.R. Sulfur-Functionalized Carbon Aerogels: A New Approach for Loading High-Surface-Area Electrode Nanoarchitectures with Precious Metal Catalysts. *J. Non-Cryst. Solids* **2004**, *350*, 80–87.

[244] Lee, H.I.; Joo, S.H.; Kim, J.H.; You, D.J.; Kim, J.M.; Park, J.-N.; Chang, H.; Pak, C. Ultrastable Pt Nanoparticles Supported on Sulfur-Containing Ordered Mesoporous Carbon via Strong Metal-Support Interaction. *J. Mater. Chem.* **2009**, *19*, 5934–5939.

[245] Acharya, C.K.; Li, W.; Liu, Z.; Kwon, G.; Heath Turner, C.; Lane, A.M.; Nikles, D.; Klein, T.; Weaver, M. Effect of Boron Doping in the Carbon Support on Platinum Nanoparticles and Carbon Corrosion. *J. Power Sources* **2009**, *192*, 324–329.

[246] Shao, Y.; Sui, J.; Yin, G.; Gao, Y. Nitrogen-Doped Carbon Nanostructures and Their Composites as Catalytic Materials for Proton Exchange Membrane Fuel Cell. *Appl. Catal. B: Environ.* **2008**, *79*, 89–99.

[247] Zhou, Y.; Neyerlin, K.; Olson, T.S.; Pylypenko, S.; Bult, J.; Dinh, H.N.; Gennett, T.; Shao, Z.; O'Hayre, R. Enhancement of Pt and Pt-alloy Fuel Cell Catalyst Activity and Durability via Nitrogen-Modified Carbon Supports. *Energy & Environ. Sci.* **2010**, *3*, 1437–1446.

[248] Lei, B.; Xue, J.; Jin, D.; Ni, S.; Sun, H. Fabrication, Annealing, and Electrocatalytic Properties of Platinum Nanoparticles Supported on Self-Organized TiO_2 Nanotubes. *Rare Metals* **2008**, *27*, 445–450.

[249] Shim, J.; Lee, C.-R.; Lee, H.-K.; Lee, J.-S.; Cairns, E.J. Electrochemical Characteristics of Pt-WO_3/C and Pt-TiO_2/C Electrocatalysts in a Polymer Electrolyte Fuel Cell. *J. Power Sources* **2001**, *102*, 172–177.

[250] Wang, M.; Guo, D.-J.; Li, H.-L. High Activity of Novel Pd/TiO_2 Nanotube Catalysts for Methanol Electro-Oxidation. *J. Solid State Chem.* **2005**, *178*, 1996–2000.

[251] Ioroi, T.; Siroma, Z.; Fujiwara, N.; Yamazaki, S.-I.; Yasuda, K. Sub-Stoichiometric Titanium Oxide-Supported Platinum Electrocatalyst for Polymer Electrolyte Fuel Cells. *Electrochem. Commun.* **2005**, *7*, 183–188.

[252] Cui, X.; Shi, J.; Chen, H.; Zhang, L.; Guo, L.; Gao, J.; Li, J. Platinum/Mesoporous WO_3 as a Carbon-Free Electrocatalyst with Enhanced Electrochemical Activity for Methanol Oxidation. *J. Phys. Chem. B* **2008**, *112*, 12024–12031.

[253] Kang, S.H.; Sung, Y.-E.; Smyrl, W.H. The Effectiveness of Sputtered PtCo Catalysts on TiO_2 Nanotube Arrays for the Oxygen Reduction Reaction. *J. Electrochem. Soc.* **2008**, *155*, B1128–B1135.

[254] Lee, K.-S.; Park, I.-S.; Cho, Y.-H.; Jung, D.-S.; Jung, N.; Park, H.-Y.; Sung, Y.-E. Electrocatalytic Activity and Stability of Pt Supported on Sb-Doped SnO_2 Nanoparticles for Direct Alcohol Fuel Cells. *J. Catal.* **2008**, *258*, 143–152.

[255] Baturina, O.A.; Garsany, Y.; Zega, T.J.; Stroud, R.M.; Schull, T.; Swider-Lyons, K.E. Oxygen Reduction Reaction on Platinum/Tantalum Oxide Electrocatalysts for PEM Fuel Cells. *J. Electrochem. Soc.* **2008**, *155*, B1314–B1321.

[256] Sasaki, K.; Zhang, L.; Adzic, R.R. Niobium Oxide-Supported Platinum Ultra-Low Amount Electrocatalysts for Oxygen Reduction. *Phys. Chem. Chem. Phys.* **2008**, *10*, 159–167.

[257] Hayden, B.E.; Malevich, D.V.; Pletcher, D. Electrode Coatings from Sprayed Titanium Dioxide Nanoparticles—Behaviour in NaOH Solutions. *Electrochem. Commun.* **2001**, *3*, 390–394.

[258] Chhina, H.; Campbell, S.; Kesler, O. An Oxidation-Resistant Indium Tin Oxide Catalyst Support for Proton Exchange Membrane Fuel Cells. *J. Power Sources* **2006**, *161*, 893–900.

[259] Smith, J.R.; Walsh, F.C.; Clarke, R.L. Electrodes Based on Magnéli Phase Titanium Oxides: The Properties and Applications of Ebonex® Materials. *J. Appl. Electrochem.* **1998**, *28*, 1021–1033.

[260] Bartholomew, R.F.; Frankl, D.R. Electrical Properties of Some Titanium Oxides. *Phys. Rev.* **1969**, *187*, 828.

[261] Bavykin, D.V.; Friedrich, J.M.; Walsh, F.C. Protonated Titanates and TiO_2 Nanostructured Materials: Synthesis, Properties, and Applications. *Adv. Mater.* **2006**, *18*, 2807–2824.

[262] Gustavsson, M.; Ekström, H.; Hanarp, P.; Eurenius, L.; Lindbergh, G.; Olsson, E.; Kasemo, B. Thin Film Pt/TiO_2 Catalysts for the Polymer Electrolyte Fuel Cell. *J. Power Sources* **2007**, *163*, 671–678.

[263] Ekström, H.; Wickman, B.; Gustavsson, M.; Hanarp, P.; Eurenius, L.; Olsson, E.; Lindbergh, G. Nanometer-Thick Films of Titanium Oxide Acting as Electrolyte in the Polymer Electrolyte Fuel Cell. *Electrochim. Acta* **2007**, *52*, 4239–4245.

[264] Graves, J.E.; Pletcher, D.; Clarke, R.L.; Walsh, F.C. The Electrochemistry of Magnéli Phase Titanium Oxide Ceramic Electrodes Part I. The Deposition and Properties of Metal Coatings. *J. Appl. Electrochem.* **1991**, *21*, 848–857.

[265] Hu, F.; Ding, F.; Song, S.; Shen, P.K. Pd Electrocatalyst Supported on Carbonized TiO_2 Nanotube for Ethanol Oxidation. *J. Power Sources* **2006**, *163*, 415–419.

[266] Shanmugam, S.; Gedanken, A. Carbon-Coated Anatase TiO_2 Nanocomposite as a High-Performance Electrocatalyst Support. *Small* **2007**, *3*, 1189–1193.

[267] Xiong, L.; Manthiram, A. Synthesis and Characterization of Methanol Tolerant Pt/TiO_x/C Nanocomposites for Oxygen Reduction in Direct Methanol Fuel Cells. *Electrochim. Acta* **2004**, *49*, 4163–4170.

[268] Macak, J.M.; Barczuk, P.J.; Tsuchiya, H.; Nowakowska, M.Z.; Ghicov, A.; Chojak, M.; Bauer, S.; Virtanen, S.; Kulesza, P.J.; Schmuki, P. Self-Organized Nanotubular TiO_2 Matrix as Support for Dispersed Pt/Ru Nanoparticles: Enhancement of the Electrocatalytic Oxidation of Methanol. *Electrochem. Commun.* **2005**, *7*, 1417–1422.

[269] Kang, S.H.; Jeon, T.-Y.; Kim, H.-S.; Sung, Y.-E.; Smyrl, W.H. Effect of Annealing PtNi Nanophases on Extended TiO_2 Nanotubes for the Electrochemical Oxygen Reduction Reaction. *J. Electrochem. Soc.* **2008**, *155*, B1058–B1065.

[270] Song, H.; Qiu, X.; Li, F.; Zhu, W.; Chen, L. Ethanol Electro-Oxidation on Catalysts with TiO_2 Coated Carbon Nanotubes as Support. *Electrochem. Commun.* **2007**, *9*, 1416–1421.

[271] Chen, J.-M.; Sarma, L.S.; Chen, C.-H.; Cheng, M.-Y.; Shih, S.-C.; Wang, G.-R.; Liu, D.-G.; Lee, J.-F.; Tang, M.-T.; Hwang, B.-J. Multi-Scale Dispersion in Fuel Cell Anode Catalysts: Role of TiO_2 towards Achieving Nanostructured Materials. *J. Power Sources* **2006**, *159*, 29–33.

[272] Chen, S.Y.; Han, C.C.; Tsai, C.H.; Huang, J.; Chen-Yang, Y.W. Effect of Morphological Properties of Ionic Liquid-Templated Mesoporous Anatase TiO_2 on Performance of PEMFC with Nafion/TiO_2 Composite Membrane at Elevated Temperature and Low Relative Humidity. *J. Power Sources* **2007**, *171*, 363–372.

[273] Chhina, H. *Oxidation Resistant Catalyst Support for Proton Exchange Membrane Fuel Cells, Mechanical and Industrial Engineering*. Ph.D. thesis, University of Toronto, 2010.

[274] Morris, D.; Dou, Y.; Rebane, J.; Mitchell, C.E.J.; Egdell, R.G.; Law, D.S.L.; Vittadini, A.; Casarin, M. Photoemission and STM Study of the Electronic Structure of Nb-Doped TiO_2. *Phys. Rev. B* **2000**, *61*, 13445.

[275] Rüdorff, W.; Luginsland, H.-H. Studies of Ternary Oxides of the Transition Metals. II. The Systems of TiO_2-NbO_2 and TiO_2-$TiTaO_4$. *Z. Anorg. Allg. Chem.* **1964**, *334*, 125–141 (in German).

[276] Arbiol, J.; Cerda, J.; Dezanneau, G.; Cirera, A.; Peiro, F.; Cornet, A.; Morante, J.R. Effects of Nb Doping on the TiO_2 Anatase-to-Rutile Phase Transition. *J. Appl. Phys.* **2002**, *92*, 853–861.

[277] Garcia, B.L.; Fuentes, R.; Weidner, J.W. Low-Temperature Synthesis of a PtRu/$Nb_{0.1}Ti_{0.9}O_2$ Electrocatalyst for Methanol Oxidation. *Electrochem. Solid-State Lett.* **2007**, *10*, B108–B110.

[278] Chen, G.; Bare, S.R.; Mallouk, T.E. Development of Supported Bifunctional Electrocatalysts for Unitized Regenerative Fuel Cells. *J. Electrochem. Soc.* **2002**, *149*, A1092–A1099.

[279] Park, K.-W.; Seol, K.-S. Nb-TiO_2 Supported Pt Cathode Catalyst for Polymer Electrolyte Membrane Fuel Cells. *Electrochem. Commun.* **2007**, *9*, 2256–2260.

[280] Lee, S.H.; Deshpande, R.; Parilla, P.A.; Jones, K.M.; To, B.; Mahan, A.H.; Dillon, A.C. Crystalline WO_3 Nanoparticles for Highly Improved Electrochromic Applications. *Adv. Mater.* **2006**, *18*, 763–766.

[281] Supothina, S.; Seeharaj, P.; Yoriya, S.; Sriyudthsak, M. Synthesis of Tungsten Oxide Nanoparticles by Acid Precipitation Method. *Ceram. Int.* **2007**, *33*, 931–936.

[282] Shukla, A.K.; Ravikumar, M.K.; Roy, A.; Barman, S.R.; Sarma, D.D.; Arico, A.S.; Antonucci, V.; Pino, L.; Giordano, N. Electro-Oxidation of Methanol in Sulfuric Acid Electrolyte on Platinized-Carbon Electrodes with Several Functional-Group Characteristics. *J. Electrochem. Soc.* **1994**, *141*, 1517–1522.

[283] Shukla, A.K.; Ravikumar, M.K.; Aricò, S.; Candiano, G.; Antonucci, V.; Giordano, N.; Hamnett, A. Methanol Electrooxidation on Carbon-Supported Pt-WO_{3-x} Electrodes in Sulphuric Acid Electrolyte. *J. Appl. Electrochem.* **1995**, *25*, 528–532.

[284] Ganesan, R.; Lee, J.S. An Electrocatalyst for Methanol Oxidation Based on Tungsten Trioxide Microspheres and Platinum. *J. Power Sources* **2006**, *157*, 217–221.

[285] Nagel, T.; Bogolowski, N.; Samjeske, G.; Baltruschat, H. On the Effect of Tungsten on CO Oxidation at Pt Electrodes. *J. Solid State Electrochem.* **2003**, *7*, 614–618.

[286] Roth, C.; Goetz, M.; Fuess, H. Synthesis and Characterization of Carbon-Supported Pt–Ru–WO_x Catalysts by Spectroscopic and Diffraction Methods. *J. Appl. Electrochem.* **2001**, *31*, 793–798.

[287] Chiu, H.C.; Tseung, A.C.C. The Performance of a Pt/C Oxygen Electrode in the Presence of Dissolved Tungsten in Sulfuric Acid. *Electrochem. Solid-State Lett.* **1999**, *2*, 379–381.

[288] Chen, K.Y.; Sun, Z.; Tseung, A.C.C. Preparation and Characterization of High-Performance Pt-Ru/WO_3-C Anode Catalysts for the Oxidation of Impure Hydrogen. *Electrochem. Solid-State Lett.* **2000**, *3*, 10–12.

[289] Kulesza, P.J.; Grzybowska, B.; Malik, M.A.; Galkowski, M.T. Tungsten Oxides as Active Supports for Highly Dispersed Platinum Microcenters: Electrocatalytic Reactivity Toward Reduction of Hydrogen Peroxide and Oxygen. *J. Electrochem. Soc.* **1997**, *144*, 1911–1917.

[290] Kulesza, P.; Miecznikowski, K.; Baranowska, B.; Skunik, M.; Kolary-Zurowska, A.; Lewera, A.; Karnicka, K.; Chojak, M.; Rutkowska, I.; Fiechter, S.; Bogdanoff, P.; Dorbandt, I.; Zehl, G.; Hiesgen, R.; Dirk, E.; Nagabhushana, K.; Boennemann, H. Electroreduction of Oxygen at Tungsten Oxide Modified Carbon-Supported $RuSe_x$ Nanoparticles. *J. Appl. Electrochem.* **2007**, *37*, 1439–1446.

[291] Barczuk, P.J.; Tsuchiya, H.; Macak, J.M.; Schmuki, P.; Szymanska, D.; Makowski, O.; Miecznikowski, K.; Kulesza, P.J. Enhancement of the Electrocatalytic Oxidation of Methanol at Pt/Ru Nanoparticles Immobilized in Different WO_3 Matrices. *Electrochem. Solid-State Lett.* **2006**, *9*, E13–E16.

[292] Rajesh, B.; Karthik, V.; Karthikeyan, S.; Ravindranathan Thampi, K.; Bonard, J.M.; Viswanathan, B. Pt-WO3 Supported on Carbon Nanotubes as Possible Anodes for Direct Methanol Fuel Cells. *Fuel* **2002**, *81*, 2177–2190.

[293] Cui, X.; Guo, L.; Cui, F.; He, Q.; Shi, J. Electrocatalytic Activity and CO Tolerance Properties of Mesostructured Pt/WO_3 Composite as an Anode Catalyst for PEMFCs. *J. Phys. Chem. C* **2009**, *113*, 4134–4138.

[294] Li, Y.; Bando, Y.; Golberg, D. Quasi-Aligned Single-Crystalline $W_{18}O_{49}$ Nanotubes and Nanowires. *Adv. Mater.* **2003**, *15*, 1294–1296.

[295] Saha, M.S.; Banis, M.N.; Zhang, Y.; Li, R.; Sun, X.; Cai, M.; Wagner, F.T. Tungsten Oxide Nanowires Grown on Carbon Paper as Pt Electrocatalyst Support for High Performance Proton Exchange Membrane Fuel Cells. *J. Power Sources* **2009**, *192*, 330–335.

[296] Wang, S.-J.; Chen, C.-H.; Ko, R.-M.; Kuo, Y.-C.; Wong, C.-H.; Wu, C.-H.; Uang, K.-M.; Chen, T.-M.; Liou, B.-W. Preparation of Tungsten Oxide Nanowires from Sputter-Deposited WC_x Films Using an Annealing/Oxidation Process. *Appl. Phys. Lett.* **2005**, *86*, 263103–263103.

[297] Shi, S.; Xue, X.; Feng, P.; Liu, Y.; Zhao, H.; Wang, T. Low-Temperature Synthesis and Electrical Transport Properties of $W_{18}O_{49}$ Nanowires. *J. Cryst. Growth* **2008**, *310*, 462–466.

[298] Salje, E.; Güttler, B. Anderson Transition and Intermediate Polaron Formation in WO_{3-x} Transport Properties and Optical Absorption. *Philosophical Maga. Part B* **1984**, *50*, 607–620.

[299] Patzke, G.R.; Krumeich, F.; Nesper, R. Oxidic Nanotubes and Nanorods—Anisotropic Modules for a Future Nanotechnology. *Angewandte Chemie Intl. Ed.* **2002**, *41*, 2446–2461.

[300] Maiyalagan, T.; Viswanathan, B. Catalytic Activity of Platinum/Tungsten Oxide Nanorod Electrodes towards Electro-Oxidation of Methanol. *J. Power Sources* **2008**, *175*, 789–793.

[301] Chhina, H.; Campbell, S.; Kesler, O. Ex Situ Evaluation of Tungsten Oxide as a Catalyst Support for PEMFCs. *J. Electrochem. Soc.* **2007**, *154*, B533–B539.

[302] Liu, Y.; Mustain, W.E. Structural and Electrochemical Studies of Pt Clusters Supported on High-Surface-Area Tungsten Carbide for Oxygen Reduction. *ACS Catal.* **2011**, *1*, 212–220.

[303] Reichman, B.; Bard, A.J. The Electrochromic Process at WO_3 Electrodes Prepared by Vacuum Evaporation and Anodic Oxidation of W. *J. Electrochem. Soc.* **1979**, *126*, 583–591.

[304] Chen, K.Y.; Tseung, A.C.C. Effect of Nafion Dispersion on the Stability of Pt/WO_3 Electrodes. *J. Electrochem. Soc.* **1996**, *143*, 2703–2707.

[305] Raghuveer, V.; Viswanathan, B. Synthesis, Characterization and Electrochemical Studies of Ti-Incorporated Tungsten Trioxides as Platinum Support for Methanol Oxidation. *J. Power Sources* **2005**, *144*, 1–10.

[306] Gadgil, M.M.; Sasikala, R.; Kulshreshtha, S.K. CO Oxidation over Pd/SnO_2 Catalyst. *J. Mol. Catal.* **1994**, *87*, 297–309.

[307] Schryer, D.R.; Upchurch, B.T.; Van Norman, J.D.; Brown, K.G.; Schryer, J. Effects of Pretreatment Conditions on a Pt/SnO_2 Catalyst for the Oxidation of CO in CO_2 Lasers. *J. Catal.* **1990**, *122*, 193–197.

[308] Sekizawa, K.; Widjaja, H.; Maeda, S.; Ozawa, Y.; Eguchi, K. Low Temperature Oxidation of Methane over Pd Catalyst Supported on Metal Oxides. *Catal. Today* **2000**, *59*, 69–74.

[309] Amalric-Popescu, D.; Bozon-Verduraz, F. SnO_2-Supported Palladium Catalysts: Activity in deNOx at Low Temperature. *Catal. Lett.* **2000**, *64*, 125–128.

[310] Liberková, K.; Touroude, R. Performance of Pt/SnO_2 Catalyst in the Gas Phase Hydrogenation of Crotonaldehyde. *J. Mol. Catal. A: Chem.* **2002**, *180*, 221–230.

[311] Okanishi, T.; Matsui, T.; Takeguchi, T.; Kikuchi, R.; Eguchi, K. Chemical Interaction between Pt and SnO_2 and Influence on Adsorptive Properties of Carbon Monoxide. *Applied Catalysis A: Gen.* **2006**, *298*, 181–187.

[312] Liu, Z.; Guo, B.; Hong, L.; Lim, T.H. Microwave Heated Polyol Synthesis of Carbon-Supported PtSn Nanoparticles for Methanol Electrooxidation. *Electrochem. Commun.* **2006**, *8*, 83–90.

[313] Jiang, L.; Colmenares, L.; Jusys, Z.; Sun, G.Q.; Behm, R.J. Ethanol Electrooxidation on Novel Carbon Supported Pt/SnO_x/C Catalysts with Caried Pt:Sn Ratio. *Electrochim. Acta* **2007**, *53*, 377–389.

[314] Nakada, M.; Ishihara, A.; Mitsushima, S.; Kamiya, N.; Ota, K.-I. Effect of Tin Oxides on Oxide Formation and Reduction of Platinum Particles. *Electrochem. Solid-State Lett.* **2007**, *10*, F1–F4.

[315] Ota, K.I.; Ishihara, A.; Mitsushima, S.; Lee, K.; Suzuki, Y.; Horibe, N.; Nakagawa, T.; Kamiya, N. Improvement of Cathode Materials for Polymer Electrolyte Fuel Cell. *J. New Mater. Electrochem. Sys.* **2005**, *8*, 25–35.

[316] Saha, M.S.; Li, R.; Cai, M.; Sun, X. High Electrocatalytic Activity of Platinum Nanoparticles on SnO_2 Nanowire-Based Electrodes. *Electrochem. Solid-State Lett.* **2007**, *10*, B130–B133.

[317] Kohnke, E.E. Electrical and Optical Properties of Natural Stannic Oxide Crystals. *J. Phys. Chem. Solids* **1962**, *23*, 1557–1562.

[318] Saadeddin, I.; Pecquenard, B.; Manaud, J.P.; Decourt, R.; Labrugère, C.; Buffeteau, T.; Campet, G. Synthesis and Characterization of Single- and Co-Doped SnO_2 Thin Films for Optoelectronic Applications. *Appl. Surf. Sci.* **2007**, *253*, 5240–5249.

[319] Pang, H.L.; Zhang, X.H.; Zhong, X.X.; Liu, B.; Wei, X.G.; Kuang, Y.F.; Chen, J.H. Preparation of Ru-Doped SnO_2-Supported Pt Catalysts and Their Electrocatalytic Properties for Methanol Oxidation. *J. Colloid Interface Sci.* **2008**, *319*, 193–198.

[320] Pang, H.L.; Lu, J.P.; Chen, J.H.; Huang, C.T.; Liu, B.; Zhang, X.H. Preparation of SnO_2-CNTs Supported Pt Catalysts and Their Electrocatalytic Properties for Ethanol Oxidation. *Electrochim. Acta* **2009**, *54*, 2610–2615.

[321] Hsu, R.S.; Higgins, D.; Chen, Z. Tin-Oxide-Coated Single-Walled Carbon Nanotube Bundles Supporting Platinum Electrocatalysts for Direct Ethanol Fuel Cells. *Nanotechnology* **2010**, *21*, 165705.

[322] Du, C.; Chen, M.; Cao, X.; Yin, G.; Shi, P. A Novel CNT@SnO_2 Core-Sheath Nanocomposite as a Stabilizing Support for Catalysts of Proton Exchange Membrane Fuel Cells. *Electrochem. Commun.* **2009**, *11*, 496–498.

[323] Parrondo, J.; Mijangos, F.; Rambabu, B. Platinum/Tin Oxide/Carbon Cathode Catalyst for High Temperature PEM Fuel Cell. *J. Power Sources* **2010**, *195*, 3977–3983.

[324] Safonova, O.V.; Delabouglise, G.; Chenevier, B.; Gaskov, A.M.; Labeau, M. CO and NO_2 Gas Sensitivity of Nanocrystalline Tin Dioxide Thin Films Doped with Pd, Ru and Rh. *Mater. Sci. & Eng.: C* **2002**, *21*, 105–111.

[325] Santos, A.L.; Profeti, D.; Olivi, P. Electrooxidation of Methanol on Pt Microparticles Dispersed on SnO_2 Thin Films. *Electrochim. Acta* **2005**, *50*, 2615–2621.

[326] Zhou, W.J.; Zhou, B.; Li, W.Z.; Zhou, Z.H.; Song, S.Q.; Sun, G.Q.; Xin, Q.; Douvartzides, S.; Goula, M.; Tsiakaras, P. Performance Comparison of Low-Temperature Direct Alcohol Fuel Cells with Different Anode Catalysts. *J. Power Sources* **2004**, *126*, 16–22.

[327] Chang, G.; Oyama, M.; Hirao, K. In Situ Chemical Reductive Growth of Platinum Nanoparticles on Indium Tin Oxide Surfaces and Their Electrochemical Applications. *J. Phys. Chem. B* **2006**, *110*, 1860–1865.

[328] Chang, G.; Oyama, M.; Hirao, K. Seed-Mediated Growth of Palladium Nanocrystals on Indium Tin Oxide Surfaces and Their Applicability as Modified Electrodes. *J. Phys. Chem. B* **2006**, *110*, 20362–20368.

[329] Wang, Y.; Viswanathan, V.V.; Liu, J.; Lin, Y.; Park, S.; Shao, Y.; Wan, H. Development of Alternative and Durable High Performance Cathode Supports for PEM Fuel Cells. In *U.S. Department of Energy Hydrogen Program FY 2010 Annual Progress Report*, 2010, p. 805.

[330] Garsany, Y.; Epshteyn, A.; Purdy, A.P.; More, K.L.; Swider-Lyons, K.E. High-Activity, Durable Oxygen Reduction Electrocatalyst: Nanoscale Composite of Platinum-Tantalum Oxyphosphate on Vulcan Carbon. *J. Phys. Chem. Lett.* **2010**, *1*, 1977–1981.

[331] Alexander, A.-M.; Hargreaves, J.S.J. Alternative Catalytic Materials: Carbides, Nitrides, Phosphides and Amorphous Boron Alloys. *Chem. Soc. Rev.* **2010**, *39*, 4388–4401.

[332] Levy, R.B.; Boudart, M. Platinum-Like Behavior of Tungsten Carbide in Surface Catalysis. *Science* **1973**, *181*, 547–549.

[333] Hwu, H.H.; Chen, J.G. Potential Application of Tungsten Carbides as Electrocatalysts. *J. Vacuum Sci. & Tech. A: Vacuum, Surf., and Films* **2003**, *21*, 1488–1493.

[334] Weigert, E.C.; Stottlemyer, A.L.; Zellner, M.B.; Chen, J.G. Tungsten Monocarbide as Potential Replacement of Platinum for Methanol Electrooxidation. *J. Phys. Chem. C* **2007**, *111*, 14617–14620.

[335] Wu, M.; Shen, P.K.; Wei, Z.; Song, S.; Nie, M. High Activity PtPd-WC/C Electrocatalyst for Hydrogen Evolution Reaction. *J. Power Sources* **2007**, *166*, 310–316.

[336] Zhong, H.; Zhang, H.; Liang, Y.; Zhang, J.; Wang, M.; Wang, X. A Novel Non-Noble Electrocatalyst for Oxygen Reduction in Proton Exchange Membrane Fuel Cells. *J. Power Sources* **2007**, *164*, 572–577.

[337] Jeon, M.K.; Daimon, H.; Lee, K.R.; Nakahara, A.; Woo, S.I. CO tolerant Pt/WC Methanol Electro-Oxidation Catalyst. *Electrochem. Commun.* **2007**, *9*, 2692–2695.

[338] Ganesan, R.; Ham, D.J.; Lee, J.S. Platinized Mesoporous Tungsten Carbide for Electrochemical Methanol Oxidation. *Electrochem. Commun.* **2007**, *9*, 2576–2579.

[339] Nie, M.; Shen, P.K.; Wei, Z. Nanocrystaline Tungsten Carbide Supported Au-Pd Electrocatalyst for Oxygen Reduction. *J. Power Sources* **2007**, *167*, 69–73.

[340] Xiao, T.; Hanif, A.; York, A.P.E.; Sloan, J.; Green, M.L.H. Study on Preparation of High Surface Area Tungsten Carbides and Phase Transition during the Carburisation. *Phys. Chem. Chem. Phys.* **2002**, *4*, 3522–3529.

[341] Yang, X.G.; Wang, C.Y. Nanostructured Tungsten Carbide Catalysts for Polymer Electrolyte Fuel Cells. *Appl. Phys. Lett.* **2005**, *86*, 224104–224103.

[342] Chhina, H.; Campbell, S.; Kesler, O. Thermal and Electrochemical Stability of Tungsten Carbide Catalyst Supports. *J. Power Sources* **2007**, *164*, 431–440.

[343] Hwu, H.H.; Chen, J.G. Potential Application of Tungsten Carbides as Electrocatalysts: 4. Reactions of Methanol, Water, and Carbon Monoxide over Carbide-Modified W(110). *J. Phys. Chem. B* **2003**, *107*, 2029–2039.

[344] Ganesan, R.; Lee, J.S. Tungsten Carbide Microspheres as a Noble-Metal-Economic Electrocatalyst for Methanol Oxidation. *Angewandte Chemie Intl. Ed.* **2005**, *44*, 6557–6560.

[345] Zellner, M.B.; Chen, J.G. Surface Science and Electrochemical Studies of WC and W_2C PVD Films as Potential Electrocatalysts. *Catal. Today* **2005**, *99*, 299–307.

[346] Chhina, H.; Campbell, S.; Kesler, O. High Surface Area Synthesis, Electrochemical Activity, and Stability of Tungsten Carbide Supported Pt during Oxygen Reduction in Proton Exchange Membrane Fuel Cells. *J. Power Sources* **2008**, *179*, 50–59.

[347] Li, G.; Ma, C.A.; Zheng, Y.; Zhang, W. Preparation and Electrocatalytic Activity of Hollow Global Tungsten Carbide with Mesoporosity. *Microporous Mesoporous Mater.* **2005**, *85*, 234–240.

[348] Hara, Y.; Minami, N.; Matsumoto, H.; Itagaki, H. New Synthesis of Tungsten Carbide Particles and the Synergistic Effect with Pt Metal as a Hydrogen

Oxidation Catalyst for Fuel Cell Applications. *Appl. Catal. A: Gen.* **2007**, *332*, 289–296.

[349] Li, G.; Ma, C.A.; Tang, J.; Zheng, Y. Preparation of Tungsten Carbide Porous Sphere Core Wrapped by Porous Multiwall. *Mater. Lett.* **2007**, *61*, 991–993.

[350] Wang, Y.; Song, S.; Maragou, V.; Shen, P.K.; Tsiakaras, P. High Surface Area Tungsten Carbide Microspheres as Effective Pt Catalyst Support for Oxygen Reduction Reaction. *Appl. Catal. B: Environ.* **2009**, *89*, 223–228.

[351] Liang, C.; Ding, L.; Li, C.; Pang, M.; Su, D.; Li, W.; Wang, Y. Nanostructured WC_x/CNTs as Highly Efficient Support of Electrocatalysts with Low Pt Loading for Oxygen Reduction Reaction/CNTs as Highly Efficient Support of Electrocatalysts with Low Pt Loading for Oxygen Reduction Reaction. *Energy & Environ. Sci.* **2010**, *3*, 1121–1127.

[352] Rodriguez, J.A.; Dvorak, J.; Jirsak, T. Chemistry of SO_2, H_2S, and CH_3SH on Carbide-Modified Mo(110) and Mo2C Powders: Photoemission and XANES Studies. *J. Phys. Chem. B* **2000**, *104*, 11515–11521.

[353] Oyama, S.T. Preparation and Catalytic Properties of Transition Metal Carbides and Nitrides. *Catal. Today* **1992**, *15*, 179–200.

[354] Yeh, E.B.; Schwartz, L.H.; Butt, J.B. Silica-Supported Iron Nitride in Fischer-Tropsch Reactions : II. Comparison of the Promotion Effects of Potassium and Nitrogen on Activity and Selectivity. *J. Catal.* **1985**, *91*, 241–253.

[355] Kojima, R.; Aika, K.-I. Molybdenum Nitride and Carbide Catalysts for Ammonia Synthesis. *Appl. Catal. A: Gen.* **2001**, *219*, 141–147.

[356] Chen, J.G.; Eng, J.; Kelty, S.P. NEXAFS Determination of Electronic and Catalytic Properties of Transition Metal Carbides and Nitrides: From Single Crystal Surfaces to Powder Catalysts. *Catal. Today* **1998**, *43*, 147–158.

[357] Frapper, G.; Pélissier, M.; Hafner, J. CO Adsorption on Molybdenum Nitride's γ-Mo_2N(100) Surface: Formation of NCO Species? A Density Functional Study. *J. Phys. Chem. B* **2000**, *104*, 11972–11976.

[358] Pang, M.; Li, C.; Ding, L.; Zhang, J.; Su, D.; Li, W.; Liang, C. Microwave-Assisted Preparation of Mo2C/CNTs Nanocomposites as Efficient Electrocatalyst Supports for Oxygen Reduction Reaction. *Ind. Eng. Chem. Res.* **2010**, *49*, 4169–4174.

[359] Chen, J.G. Carbide and Nitride Overlayers on Early Transition Metal Surfaces: Preparation, Characterization, and Reactivities. *Chem. Rev. (Washington, DC, U.S.)* **1996**, *96*, 1477–1498.

[360] Bensebaa, F.; Farah, A.A.; Wang, D.; Bock, C.; Du, X.; Kung, J.; Le Page, Y. Microwave Synthesis of Polymer-Embedded Pt-Ru Catalyst for Direct Methanol Fuel Cell. *J. Phys. Chem. B* **2005**, *109*, 15339–15344.

[361] Li, Q.; He, R.; Jensen, J.O.; Bjerrum, N.J. Approaches and Recent Development of Polymer Electrolyte Membranes for Fuel Cells Operating above 100°C. *Chem. Mater.* **2003**, *15*, 4896–4915.

[362] Alberti, G.; Casciola, M. Composite Membranes for Medium-Temperature PEM Fuel Cells. *Annu. Rev. Mater. Res.* **2003**, *33*, 129–154.

[363] Liu, H.; Song, C.; Zhang, L.; Zhang, J.; Wang, H.; Wilkinson, D.P. A Review of Anode Catalysis in the Direct Methanol Fuel Cell. *J. Power Sources* **2006**, *155*, 95–110.

[364] Musthafa, O.T.M.; Sampath, S. High Performance Platinized Titanium Nitride Catalyst for Methanoloxidation. *Chem. Commun. (Cambridge, U.K.)* **2008**, 67–69.

[365] Smotkin, E.S.; Diaz-Morales, R.R. New Electrocatalysts by Combinatorial Methods. *Annu. Rev. Mater. Res.* **2003**, *33*, 557–579.

[366] Avasarala, B.; Murray, T.; Li, W.; Haldar, P. Titanium Nitride Nanoparticles Based Electrocatalysts for Proton Exchange Membrane Fuel Cells. *J. Mater. Chem.* **2009**, *19*, 1803–1805.

[367] Xia, D.; Liu, S.; Wang, Z.; Chen, G.; Zhang, L.; Zhang, L.; Hui, S.; Zhang, J. Methanol-Tolerant MoN Electrocatalyst Synthesized through Heat Treatment of Molybdenum Tetraphenylporphyrin for Four-Electron Oxygen Reduction Reaction. *J. Power Sources* **2008**, *177*, 296–302.

[368] Zhong, H.; Zhang, H.; Liu, G.; Liang, Y.; Hu, J.; Yi, B. A Novel Non-Noble Electrocatalyst for PEM Fuel Cell Based on Molybdenum Nitride. *Electrochem. Commun.* **2006**, *8*, 707–712.

[369] Adzic, R.; Zhang, J.; Sasaki, K.; Vukmirovic, M.; Shao, M.; Wang, J.; Nilekar, A.; Mavrikakis, M.; Valerio, J.; Uribe, F. Platinum Monolayer Fuel Cell Electrocatalysts. *Top. Catal.* **2007**, *46*, 249–262.

[370] Inoue, H.; Brankovic, S.R.; Wang, J.X.; Adzic, R.R. Oxygen Reduction on Bare and Pt Monolayer-Modified Ru(0001), Ru(100) and Ru Nanostructured Surfaces. *Electrochim. Acta* **2002**, *47*, 3777–3785.

[371] Brankovic, S.R.; Wang, J.X.; Adzic, R.R. Metal Monolayer Deposition by Replacement of Metal Adlayers on Electrode Surfaces. *Surf. Sci.* **2001**, *474*, L173–L179.

[372] Sasaki, K.; Mo, Y.; Wang, J.X.; Balasubramanian, M.; Uribe, F.; McBreen, J.; Adzic, R.R. Pt Submonolayers on Metal Nanoparticles—Novel Electrocatalysts for H_2 Oxidation and O_2 Reduction. *Electrochim. Acta* **2003**, *48*, 3841–3849.

[373] Zhang, J.V., Vukmirovic, M.B.; Sasaki, K.; Uribe, F.; Adžić, R. R.. Platinum Monolayer Electrocatalysts for Oxygen Reduction: Effect of Substrates, and Long-term Stability. *J. Serb. Chem. Soc.* **2005**, *70*, 513–525.

[374] Lima, F.H.B.; Zhang, J.; Shao, M.H.; Sasaki, K.; Vukmirovic, M.B.; Ticianelli, E.A.; Adzic, R.R. Catalytic Activity-d-Band Center Correlation for the O_2 Reduction Reaction on Platinum in Alkaline Solutions. *J. Phys. Chem. C* **2006**, *111*, 404–410.

[375] Vukmirovic, M.B.; Zhang, J.; Sasaki, K.; Nilekar, A.U.; Uribe, F.; Mavrikakis, M.; Adzic, R.R. Platinum Monolayer Electrocatalysts for Oxygen Reduction. *Electrochim. Acta* **2007**, *52*, 2257–2263.

[376] Kongkanand, A.; Kuwabata, S. Oxygen Reduction at Platinum Monolayer Islands Deposited on Au(111). *J. Phys. Chem. B* **2005**, *109*, 23190–23195.

[377] Mun, B.S.; Lee, C.; Stamenkovic, V.; Markovic, N.M.; Ross, P.N. Electronic Structure of Pd Thin Films on Re(0001) Studied by High-Resolution Core-Level and Valence-Band Photoemission. *Physical Review B* **2005**, *71*, 115420.

[378] Stamenkovic, V.R.; Mun, B.S.; Arenz, M.; Mayrhofer, K.J.J.; Lucas, C.A.; Wang, G.; Ross, P.N.; Markovic, N.M. Trends in Electrocatalysis on Extended and Nanoscale Pt-Bimetallic Alloy Surfaces. *Nat. Mater.* **2007**, *6*, 241–247.

[379] Stamenkovic, V.R.; Fowler, B.; Mun, B.S.; Wang, G.; Ross, P.N.; Lucas, C.A.; Markovic, N.M. Improved Oxygen Reduction Activity on Pt3Ni(111) via Increased Surface Site Availability. *Science* **2007**, *315*, 493–497.

[380] Zhang, J.; Lima, F.H.B.; Shao, M.H.; Sasaki, K.; Wang, J.X.; Hanson, J.; Adzic, R.R. Platinum Monolayer on Nonnoble Metal-Noble Metal Core-Shell Nanoparticle Electrocatalysts for O_2 Reduction. *J. Phys. Chem. B* **2005**, *109*, 22701–22704.

[381] Shao, M.; Sasaki, K.; Marinkovic, N.S.; Zhang, L.; Adzic, R.R. Synthesis and Characterization of Platinum Monolayer Oxygen-Reduction Electrocatalysts with Co-Pd Core-Shell Nanoparticle Supports. *Electrochem. Commun.* **2007**, *9*, 2848–2853.

[382] Zhou, W.-P.; Yang, X.; Vukmirovic, M.B.; Koel, B.E.; Jiao, J.; Peng, G.; Mavrikakis, M.; Adzic, R.R. Improving Electrocatalysts for O_2 Reduction by Fine-Tuning the Pt-Support Interaction: Pt Monolayer on the Surfaces of a $Pd_3Fe(111)$ Single-Crystal Alloy. *J. Am. Chem. Soc.* **2009**, *131*, 12755–12762.

[383] Shao, M.; Shoemaker, K.; Peles, A.; Kaneko, K.; Protsailo, L. Pt Monolayer on Porous Pd-Cu Alloys as Oxygen Reduction Electrocatalysts. *J. Am. Chem. Soc.* **2010**, *132*, 9253–9255.

[384] Zhou, W.-P.; Sasaki, K.; Su, D.; Zhu, Y.; Wang, J.X.; Adzic, R.R. Gram-Scale-Synthesized Pd_2Co-Supported Pt Monolayer Electrocatalysts for Oxygen Reduction Reaction. *J. Phys. Chem. C* **2010**, *114*, 8950–8957.

[385] Ghosh, T.; Vukmirovic, M.B.; DiSalvo, F.J.; Adzic, R.R. Intermetallics as Novel Supports for Pt Monolayer O_2 Reduction Electrocatalysts: Potential for Significantly Improving Properties. *J. Am. Chem. Soc.* **2009**, *132*, 906–907.

[386] Gong, K.; Su, D.; Adzic, R.R. Platinum-Monolayer Shell on AuNi0.5Fe Nanoparticle Core Electrocatalyst with High Activity and Stability for the Oxygen Reduction Reaction. *J. Am. Chem. Soc.* **2010**, *132*, 14364–14366.

[387] Gong, K.; Chen, W.-F.; Sasaki, K.; Su, D.; Vukmirovic, M.B.; Zhou, W.; Izzo, E.L.; Perez-Acosta, C.; Hirunsit, P.; Balbuena, P.B.; Adzic, R.R. Platinum-Monolayer Electrocatalysts: Palladium Interlayer on IrCo Alloy Core Improves Activity in Oxygen-Reduction Reaction. *J. Electroanal. Chem.* **2010**, *649*, 232–237.

[388] Xing, Y.; Cai, Y.; Vukmirovic, M.B.; Zhou, W.-P.; Karan, H.; Wang, J.X.; Adzic, R.R. Enhancing Oxygen Reduction Reaction Activity via Pd-Au Alloy Sublayer Mediation of Pt Monolayer Electrocatalysts. *J. Phys. Chem. Lett.* **2010**, *1*, 3238–3242.

[389] Zhai, J.; Huang, M.; Dong, S. Electrochemical Designing of Au/Pt Core Shell Nanoparticles as Nanostructured Catalyst with Tunable Activity for Oxygen Reduction. *Electroanalysis* **2007**, *19*, 506–509.

[390] Mani, P.; Srivastava, R.; Strasser, P. Dealloyed Pt-Cu Core-Shell Nanoparticle Electrocatalysts for Use in PEM Fuel Cell Cathodes. *J. Phys. Chem. C* **2008**, *112*, 2770–2778.

[391] Luo, J.; Wang, L.; Mott, D.; Njoki, P.N.; Lin, Y.; He, T.; Xu, Z.; Wanjana, B.N.; Lim, I.I.S.; Zhong, C.-J. Core/Shell Nanoparticles as Electrocatalysts for Fuel Cell Reactions. *Adv. Mater.* **2008**, *20*, 4342–4347.

[392] Wu, Y.-N.; Liao, S.-J.; Liang, Z.-X.; Yang, L.-J.; Wang, R.-F. High-Performance Core-Shell PdPt@Pt/C Catalysts via Decorating PdPt Alloy Cores with Pt. *J. Power Sources* **2009**, *194*, 805–810.

[393] Beard, K.D.; Borrelli, D.; Cramer, A.M.; Blom, D.; Van Zee, J.W.; Monnier, J.R. Preparation and Structural Analysis of Carbon-Supported Co Core/Pt Shell Electrocatalysts Using Electroless Deposition Methods. *ACS Nano* **2009**, *3*, 2841–2853.

[394] Zhang, H.; Yin, Y.; Hu, Y.; Li, C.; Wu, P.; Wei, S.; Cai, C. Pd@Pt Core-Shell Nanostructures with Controllable Composition Synthesized by a Microwave Method and Their Enhanced Electrocatalytic Activity toward Oxygen Reduction and Methanol Oxidation. *J. Phys. Chem. C* **2010**, *114*, 11861–11867.

[395] Zhang, W.; Wang, R.; Wang, H.; Lei, Z. High Performance Carbon-Supported Core@Shell PdSn@Pt Electrocatalysts for Oxygen Reduction Reaction. *Fuel Cells* **2010**, *10*, 734–739.

[396] Hartl, K.; Mayrhofer, K.J.J.; Lopez, M.; Goia, D.; Arenz, M. AuPt Core-Shell Nanocatalysts with Bulk Pt Activity. *Electrochem. Commun.* **2010**, *12*, 1487–1489.

[397] Kulp, C.; Chen, X.; Puschhof, A.; Schwamborn, S.; Somsen, C.; Schuhmann, W.; Bron, M. Electrochemical Synthesis of Core–Shell Catalysts for Electrocatalytic Applications. *Chem. Phys. Chem.* **2010**, *11*, 2854–2861.

[398] Li, X.; Liu, J.; He, W.; Huang, Q.; Yang, H. Influence of the Composition of Core-Shell Au-Pt Nanoparticle Electrocatalysts for the Oxygen Reduction Reaction. *J. Colloid Interface Sci.* **2010**, *344*, 132–136.

[399] Sarkar, A.; Manthiram, A. Synthesis of Pt@Cu Core-Shell Nanoparticles by Galvanic Displacement of Cu by Pt^{4+} Ions and Their Application as Electrocatalysts for Oxygen Reduction Reaction in Fuel Cells. *J. Phys. Chem. C* **2010**, *114*, 4725–4732.

[400] Wang, W.; Wang, R.; Ji, S.; Feng, H.; Wang, H.; Lei, Z. Pt Overgrowth on Carbon Supported PdFe Seeds in the Preparation of Core-Shell Electrocatalysts for the Oxygen Reduction Reaction. *J. Power Sources* **2010**, *195*, 3498–3503.

[401] Malheiro, A.R.; Perez, J.; Santiago, E.I.; Villullas, H.M. The Extent on the Nanoscale of Pt-Skin Effects on Oxygen Reduction and Its Influence on Fuel Cell Power. *J. Phys. Chem. C* **2010**, *114*, 20267–20271.

[402] Wang, J.X.; Inada, H.; Wu, L.; Zhu, Y.; Choi, Y.; Liu, P.; Zhou, W.-P.; Adzic, R.R. Oxygen Reduction on Well-Defined Core-Shell Nanocatalysts: Particle Size, Facet, and Pt Shell Thickness Effects. *J. Am. Chem. Soc.* **2009**, *131*, 17298–17302.

[403] Schlapka, A.; Lischka, M.; Grob; A.; Käsberger, U.; Jakob, P. Surface Strain versus Substrate Interaction in Heteroepitaxial Metal Layers: Pt on Ru(0001). *Phys. Rev. Lett.* **2003**, *91*, 016101.

[404] Zhang, J.; Sasaki, K.; Sutter, E.; Adzic, R.R. Stabilization of Platinum Oxygen-Reduction Electrocatalysts Using Gold Clusters. *Science* **2007**, *315*, 220–222.

[405] Sasaki, K.; Naohara, H.; Cai, Y.; Choi, Y.M.; Liu, P.; Vukmirovic, M.B.; Wang, J.X.; Adzic, R.R. Core-Protected Platinum Monolayer Shell High-Stability Electrocatalysts for Fuel-Cell Cathodes. *Angewandte Chemie Intl. Ed.* **2010**, *49*, 8602–8607.

[406] Ramírez-Caballero, G. E.; Ma, Y.; Callejas-Tovar, R.; Balbuena, P.B. Surface Segregation and Stability of Core-Shell Alloy Catalysts for Oxygen Reduction in Acid Medium. *Phys. Chem. Chem. Phys.* **2010**, *12*, 2209–2218.

[407] Hirunsit, P.; Balbuena, P.B. Stability of Pt Monolayers on Ir-Co Cores with and without a Pd Interlayer. *J. Phys. Chem. C* **2010**, *114*, 13055–13060.

[408] Ramírez-Caballero, G. E.; Hirunsit, P.; Balbuena, P.B. Shell-Anchor-Core Structures for Enhanced Stability and Catalytic Oxygen Reduction Activity. *J. Chem. Phys.* **2010**, *133*, 134705–134708.

[409] Debe, M.K.; Poirier, R.J. Postdeposition Growth of a Uniquely Nanostructured Organic Film by Vacuum Annealing. *J. Vacuum Sci. & Tech.—Vacuum Surf. & Films* **1994**, *12*, 2017–2022.

[410] Debe, M.K.; Drube, A.R. Structural Characteristics of a Uniquely Nanostructured Organic Thin-Film. *J. Vacuum Sci. & Tech. B* **1995**, *13*, 1236–1241.

[411] Debe, M.K. Nanostructured Thin Film Catalysts (NSTFC) for Next Generation PEM Fuel Cells. *Northern Nano Workshop*, University of Minnesota, November 9, 2006.

[412] Gancs, L.; Kobayashi, T.; Debe, M.K.; Atanasoski, R.; Wieckowski, A. Crystallographic Characteristics of Nanostructured Thin-Film Fuel Cell Electrocatalysts: A HRTEM Study. *Chem. Mater.* **2008**, *20*, 2444–2454.

[413] Debe, M.K.; Schmoeckel, A.K.; Vernstrom, G.D.; Atanasoski, R. High voltage stability of nanostructured thin film catalysts for PEM fuel cells. *J. Power Sources* **2006**, *161*, 1002–1011.

[414] Kongkanand, A.; Sinha, P.K. Load Transients of Nanostructured Thin Film Electrodes in Polymer Electrolyte Fuel Cells. *J. Electrochem. Soc.* **2011**, *158*, B703–B711.